

Preparation, Characterization and Applications of Nanoparticles from Chitosan



Ph. D Thesis

Submitted by

Fatema Tuj Jahura

Registration Number: 112

Session: 2016-2017

**Department of Chemistry
University of Dhaka**

08 September, 2022

Preparation, Characterization and Applications of Nanoparticles from Chitosan



Ph. D Thesis

Submitted by

Fatema Tuj Jahura

Registration Number: 112

Session: 2016-2017

Supervisor

Dr. Mohammad Abul Hossain

Professor

Department of Chemistry

University of Dhaka

Joint-supervisor

Dr. Md. Qamrul Ehsan

Professor

Department of Chemistry

University of Dhaka

Acknowledgements

First of all, I would like to express my sincere and full thanks to my creator, Allah for giving me the full ability to complete my doctoral research works smoothly and successfully.

Then I would like to express my sincere gratitude and cordial thanks to my supervisor Professor Dr. Mohammad Abul Hossain, Ph. D (Env. Sci. & Chem. Technol., Kanazawa University, Japan), MS (Chem. Engr., Kanazawa University, Japan), M. Sc. (Phy. Chem., Dhaka University, Bangladesh), Department of Chemistry, University of Dhaka for giving me the opportunity to do work in his laboratory and his efficient guidance through the entire path of research.

I would also like to express my deep gratitude and heartfelt thanks to my joint-supervisor, Professor Dr. Md. Qamrul Ehsan, D. Sc. (Phy. Chem., Tohoku University, Japan), M. Sc. (Phy.-Inorg. Chem., Dhaka University, Bangladesh), Department of Chemistry, University of Dhaka for his suggestions, encouragement and valuable discussions throughout my research period.

I sincerely thank all the respected teachers of the Department of Chemistry at University of Dhaka for their support in many ways during my Ph. D study.

I am also very much thankful to the Bangabandhu Science and Technology Fellowship Trust, Ministry of Science and Technology, Bangladesh for providing me with a prestigious scholarship for the study of doctoral course.

I am also very grateful to the Bangladesh Atomic Energy Commission for the opportunity to conduct my research by granting leave with financial support.

I would like to thank to Dr. Anwar Ul-Hamid, King Fahd University of Petroleum and Minerals, Kingdom of Saudi Arabia for providing instrumental support for sample analysis.

I am immensely grateful to Abu Hena Mostofa Kamal, Senior Scientific Officer, IFRB, AERE, Bangladesh Atomic Energy Commission for his support in microbiological activity testing.

Finally, I wish to express my heartfelt gratitude to my parents, parents-in-law, brother and sister for their prayers, emotional support and encouragement.

My final thanks goes to my beloved husband Dr. Mohammad Shahid Ullah for his continuous mental support with endless inspiration.

Fatema Tuj Jahura

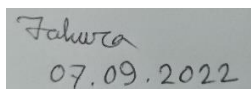
Ruqayyah Hall

University of Dhaka, Bangladesh

07 September, 2022

Declaration

I hereby declare that this Ph. D thesis entitled “*Preparation, Characterization and Applications of Nanoparticles from Chitosan*” is based on my original research work which has been carried out between March, 2018 to August, 2022 under the joint supervision of Professor Dr. Mohammad Abul Hossain and Professor Dr. Md. Qamrul Ehsan in the Department of Chemistry, University of Dhaka. I also declare that it has not been previously and concurrently submitted anywhere for the award of any degree or diploma at this or any other university.



Fahura
07.09.2022

Fatema Tuj Jahura

Registration No.: 112

Session: 2016-2017

Date: 07 September, 2022

Abstract

Chitosan is a naturally occurring amino polysaccharide and largely applicable in biomedical field as it is biodegradable, biocompatible and nontoxic. The nanoparticles of chitosan have gained more focus in the delivery of drugs and also in sustaining drug release for increasing drug bioavailability. The main source of chitosan are the discarded exoskeleton of crustaceans. Thus, the aim of the present research was to extract chitosan from wasted shrimp shell and to formulate and evaluate chitosan based nanoparticles of different types of drugs in enhancement of residence time and bioavailability of drugs in the human body. First, chitosan was extracted from shrimp shell by demineralization, deproteination and deacetylation. Then it was characterized by various methods, mainly solubility, molecular weight (MW), degree of deacetylation (DDA) determination and elemental analysis, FTIR analysis and XRD pattern analysis. The outcomes of the study represents that, the solubility of extracted chitosan was about 83%, while the MW was 2.3×10^5 Da and DDA was 70%. Based on these results, the extracted chitosan was considered to have the qualities to be used in biomedical field. Thus the extracted chitosan was used to formulate a novel drug delivery system for different types of drugs. In this regard, three antibiotic drugs and one antihypertensive drug was loaded to this drug delivery system individually with improved association efficiency to enhance the drug bioavailability within the body and also for the enhancement of the antibacterial activity for the antibiotic drugs. The drug delivery systems of chitosan nanoparticles (CSNPs) was prepared by ionic gelation method and the drugs were loaded to this delivery system during the nanoparticle formation. The conditions applied and the results obtained were different from previous studies. After drug loading on CSNPs, the physicochemical properties were investigated by SEM and TEM analysis for morphology study and particle size observation, FTIR and XRD analysis. The association efficiencies of the different drug loaded CSNPs were found to be in the range of 88-93%. The TEM analysis confirms the formation of nano sized particles as well as the adsorption of drug molecules on the surface of the nanoparticles. All of the drug loaded nanoparticles prepared in this study shows sustained release of drugs after initial rapid release in the case of in vitro release studies. Thus, the adsorption of drugs on the surface of nanoparticles results the sustained release of drugs from nanoparticles without encapsulation. This sustained release properties of these drug delivery systems improve the drug bioavailability in the body. Besides, the antibacterial activities of antibiotic drug loaded CSNPs against both gram (+) and gram (-) bacteria shows that they could inhibit the bacterial growth. The value of minimum inhibitory concentration (MIC) and minimum bactericidal concentration (MBC) showed that the inhibitory effect of prepared antibiotic loaded nanoparticles on specific bacterial strain was similar to that of the corresponding antibiotic in the in vitro cases. Thus the drug delivery system from CSNPs prepared in this study can be a promising drug delivery system.

Contents

Chapter 1	Introduction	1-22
1.1	General Introduction	1
1.1.1	Background	2
1.1.2	Chitin and chitosan	2
1.1.3	Properties of chitosan	3
1.1.4	Sources of chitosan	5
1.1.5	Nanoparticles	6
1.1.6	Chitosan nanoparticles (CSNPs)	7
1.1.7	Drug delivery	10
1.1.8	Mechanism of drug release from particulate systems	11
1.2	Objective of Research	13
1.3	Present Work	14
1.4	Review of Literature	18
Chapter 2	Experimental	23-40
2.1	Materials	23
2.2	Instrumentation	23
2.3	Extraction of Chitosan	24
2.3.1	Demineralization of Shrimp Shell	24
2.3.2	Deproteination of Shrimp Shell	24
2.3.3	Conversion of Chitin into Chitosan	25
2.4	Characterization of Chitosan	26
2.4.1	Solubility	26
2.4.2	Molecular Weight (MW) Determination	26
2.4.3	Fourier Transform Infrared (FT-IR) Spectroscopic Analysis	27
2.4.4	Elemental Analysis	28
2.4.5	Degree of Deacetylation (DDA)	28
2.4.6	X-ray diffraction (XRD) Analysis	29
2.5	Preparation of Chitosan Nanoparticles (CSNPs)	30
2.6	Drug Loading into/on Nanoparticles of Chitosan	31
2.6.1	Ciprofloxacin (CP) Loading into/on Chitosan Nanoparticles (CSNPs)	32
2.6.1.1	Evaluation of CP loading within CSNPs	33
2.6.2	Erythromycin (ER) Loading into/on Chitosan Nanoparticles (CSNPs)	33
2.6.2.1	Evaluation of ER loading within CSNPs	34
2.6.3	Metronidazole (MTZ) Loading into/on Chitosan Nanoparticles (CSNPs)	34
2.6.3.1	Evaluation of MTZ loading within CSNPs	34

2.6.4	Perindopril Erbumine (PE) Loading into/on Chitosan Nanoparticles (CSNPs)	35
2.6.4.1	Evaluation of PE loading within CSNPs	35
2.7	Characterization of Drug Loaded Chitosan Nanoparticles (CSNPs)	35
2.7.1	SEM Analysis	35
2.7.2	TEM Analysis	36
2.7.3	EDX Analysis	36
2.7.4	FT-IR Analysis	37
2.7.5	XRD Analysis	37
2.8	Biomedical Application of Drug Loaded Chitosan Nanoparticles	37
2.8.1	In Vitro Release of Drugs from Chitosan Nanoparticles (CSNPs)	37
2.8.2	Antibacterial Activity Analysis	38
Chapter 3	Results and Discussion	41-107
3.1	Chitosan Yield and Efficiency of Method	41
3.2	Characterization of Chitosan	42
3.2.1	Solubility	42
3.2.2	Viscosity Average Molecular Weight	43
3.2.3	Elemental Analysis of Extracted Chitosan	45
3.2.4	Fourier Transform Infrared (FTIR) Spectroscopy Analysis	45
3.2.5	Degree of Deacetylation (DDA) using FTIR Method	47
3.2.6	X-ray Diffraction (XRD) Analysis	48
3.3	Formation of Chitosan Nanoparticles (CSNPs)	50
3.4	Characterization of Chitosan Nanoparticles (CSNPs)	52
3.4.1	SEM and TEM Analysis	52
3.4.2	EDX Analysis	54
3.4.3	FT-IR Analysis of Chitosan Nanoparticles (CSNPs)	55
3.4.4	XRD Analysis of Chitosan Nanoparticles (CSNPs)	57
3.5	Ciprofloxacin Loading on Chitosan Nanoparticles (CSNPs)	58
3.5.1	Association Efficiency (AE) of Ciprofloxacin (CP)	58
3.5.2	Characterization of Ciprofloxacin Loaded Chitosan Nanoparticles (CP-CSNPs)	59
3.5.2.1	SEM analysis	59
3.5.2.2	EDX analysis	60
3.5.3.3	TEM analysis	61
3.5.4.4	FT-IR analysis	62
3.5.5.5	XRD analysis	65
3.5.3	Biomedical Application of Ciprofloxacin Loaded Chitosan Nanoparticles (CP-CSNPs)	66
3.5.3.1	In vitro release study of ciprofloxacin (CP) from chitosan nanoparticles (CSNPs)	66

3.5.3.2	Release kinetics of ciprofloxacin (CP) from the nanoparticles	68
3.5.3.3	Antibacterial activity analysis	73
3.6	Erythromycin Loading on Chitosan Nanoparticles (CSNPs)	76
3.6.1	Characterization of Erythromycin Loaded Chitosan Nanoparticles (ER-CSNPs)	76
3.6.1.1	SEM analysis	76
3.6.1.2	EDX analysis	76
3.6.1.3	Association efficiency (AE)	77
3.6.1.4	FT-IR analysis	78
3.6.1.5	XRD analysis	80
3.6.2	Biomedical Application of Erythromycin Loaded Chitosan Nanoparticle (ER-CSNPs)	81
3.6.2.1	Antibacterial activity analysis	81
3.6.2.2	In vitro release study of erythromycin (ER) from chitosan nanoparticles (CSNPs)	83
3.6.2.3	Release kinetics of erythromycin (ER) from the nanoparticles	84
3.7	Metronidazole (MTZ) Loading on Chitosan Nanoparticles (CSNPs)	86
3.7.1	Characterization of Metronidazole Loaded Chitosan Nanoparticles (MTZ-CSNPs)	86
3.7.1.1	SEM analysis	86
3.7.1.2	EDX analysis	87
3.7.1.3	TEM analysis	88
3.7.1.4	Association efficiency (AE)	90
3.7.1.5	FTIR analysis	90
3.7.1.6	XRD analysis	92
3.7.2	Biomedical Application of Metronidazole Loaded Chitosan Nanoparticles (MTZ-CSNPs)	93
3.7.2.1	In vitro release study of metronidazole (MTZ) from chitosan nanoparticles (CSNPs)	93
3.7.2.2	Release kinetics of metronidazole (MTZ) from the nanoparticles	94
3.8	Perindopril Erbumine (PE) Loading on Chitosan Nanoparticles (CSNPs)	97
3.8.1	Characterization of Perindopril Erbumine Loaded Chitosan Nanoparticles (PE-CSNPs)	97
3.8.1.1	SEM analysis	97
3.8.1.2	EDX analysis	98
3.8.1.3	TEM analysis	99
3.8.1.4	Association efficiency (AE)	100
3.8.1.5	FT-IR analysis	100
3.8.1.6	XRD analysis	102

3.8.2	Biomedical Application of Perindopril Erbumine Loaded Chitosan Nanoparticles (PE-CSNPs)	103
3.8.2.1	In vitro release study of perindopril erbumine (PE) from the nanoparticles	104
3.8.2.2	Release kinetics of perindopril erbumine (PE) from the nanoparticles	105
3.9	Proposed Model for Controlled Release Drug Delivery System in This Study	107
	Conclusion	108-109
	References	110-117

List of Figures

Figure 1.1	Structure of cellulose, chitin and chitosan	3
Figure 1.2	Sources of chitin and chitosan and its uses	5
Figure 1.3	Dry shrimp shell	
Figure 1.4	Protonation of chitosan (a), sodium tripolyphosphate (Na-TPP) (b) and ionic crosslinking of positive amino group of chitosan with negative phosphate group TPP to form nanoparticles, (c)	8
Figure 1.5	Mechanism of drug release from a particulate system	11
Figure 1.6	Diagram representing the mechanism of drug release from CSNPs	12
Figure 1.7	Outline of the present study	14
Figure 1.8	Structure of ciprofloxacin	15
Figure 1.9	Structure of metronidazole	16
Figure 1.10	Structure of erythromycin	16
Figure 1.11	Structure of perindopril erbumine	17
Figure 2.1:	Flow diagram of extraction of chitosan from shrimp shell	25
Figure 2.2:	Procedure for chitosan nanoparticles preparation	31
Figure 3.1	Extraction of chitosan from shrimp shell	42
Figure 3.2	Plot of Reduced viscosity against Chitosan concentration	44
Figure 3.3	FT-IR spectra of extracted chitin and chitosan	46
Figure 3.4	Structure of chitin and chitosan	48
Figure 3.5	XRD pattern of extracted chitosan	49
Figure 3.6	Formation of chitosan nanoparticles	51
Figure 3.7	SEM micrographs of prepared chitosan nanoparticles for (a) CS03 and (b) CS04 formulations	52
Figure 3.8	TEM micrographs of prepared chitosan nanoparticles for (a) CS03 and (b) CS04 formulations	52
Figure 3.9	The particle size of prepared chitosan nanoparticles observed in different studies using 0.1% chitosan and 0.25% TPP and (b) using Chitosan: TPP mass ratio of 12:1	54
Figure 3.10	EDS spectrum of chitosan nanoparticles	54
Figure 3.11	FTIR spectra of extracted chitosan and chitosan nanoparticles (CSNPs)	56
Figure 3.12	X-ray diffraction pattern of chitosan and CSNPs	57
Figure 3.13	The effect of chitosan: CP (w:w) on association efficiency of ciprofloxacin loading on CSNPs. Data are represented as means \pm standard deviation (n = 3)	59
Figure 3.14	SEM micrograph of ciprofloxacin loaded chitosan nanoparticles at (a) $\times 2,000$ and (b) $\times 1,00,000$ magnification.	60

Figure 3.15	EDX spectra of Ciprofloxacin loaded chitosan nanoparticle	61
Figure 3.16	TEM micrographs of ciprofloxacin loaded chitosan nanoparticles of CS4 formulation at different magnifications	62
Figure 3.17	FTIR spectra of ciprofloxacin (CP), chitosan, and ciprofloxacin loaded chitosan nanoparticles (CP-CSNPs).	64
Figure 3.18	The XRD pattern of ciprofloxacin (CP), chitosan and ciprofloxacin loaded chitosan nanoparticles (CP-CSNPs)	65
Figure 3.19	Ciprofloxacin release profile from CSNPs in PBS of pH=7.4.	67
Figure 3.20	Zero order kinetic release of ciprofloxacin.	69
Figure 3.21	First order kinetic release of ciprofloxacin	70
Figure 3.22	Higuchi model kinetic release of ciprofloxacin	71
Figure 3.23	Hixson-Crowell model kinetic release of ciprofloxacin	72
Figure 3.24	Photographic representation of zone of inhibition of free ciprofloxacin (CP) and ciprofloxacin loaded nanoparticles (CP-CSNPs) against <i>Staphylococcus aureus</i> .	74
Figure 3.25	SEM micrograph of erythromycin loaded chitosan nanoparticles at (a) $\times 50,000$ and (b) $100,000$ magnification	76
Figure 3.26	EDX spectra of erythromycin loaded chitosan nanoparticles	77
Figure 3.27	FT-IR spectra of pure erythromycin (ER), chitosan and erythromycin loaded Chitosan nanoparticles (ER-CSNPs)	79
Figure 3.28	Powder XRD pattern of free erythromycin (ER), pure chitosan and erythromycin loaded chitosan nanoparticles (ER-CSNPs).	80
Figure 3.29	MBC of (a) erythromycin (ER) and (b) erythromycin loaded chitosan nanoparticles (ER-CSNPs) against <i>S. aureus</i>	82
Figure 3.30	MBC of (a) erythromycin (ER) and (b) erythromycin loaded chitosan nanoparticles (ER-CSNPs) against <i>E. coli</i>	82
Figure 3.31	In vitro release of ER from CSNPs in PBS of 7.4	83
Figure 3.32	Study of release kinetics of ER release from CSNPs into PBS at pH 7.4 using four different kinetic models	84
Figure 3.33	SEM micrograph of metronidazole loaded chitosan nanoparticles at (a) $\times 50,000$ and (b) $\times 150,000$ magnification	86
Figure 3.34	EDX spectra of metronidazole loaded chitosan nanoparticles	87
Figure 3.35	(a, b) TEM images of MTZ-CSNPs at two different magnification and (c) the SAED pattern of MTZ-CSNPs	89
Figure 3.36	FTIR spectra of pure metronidazole (MTZ), chitosan and metronidazole loaded chitosan nanoparticles (MTZ-CSNPs)	91
Figure 3.37	Powder XRD pattern of free metronidazole (MTZ), pure chitosan and metronidazole loaded chitosan nanoparticles (MTZ-CSNPs).	92
Figure 3.38	Metronidazole release profile from CSNPs in PBS of pH=7.4.	93

Figure 3.39	Release kinetics study of MTZ release from CSNPs into PBS at pH 7.4 using four different kinetic models.	95
Figure 3.40	SEM micrographs of perindopril erbumine loaded chitosan nanoparticles at (a) x 100000 magnification and (b) ×150000 magnification	97
Figure 3.41	Elemental analysis of PE-CSNPs from EDX spectra	98
Figure 3.42	TEM micrographs of PE-CSNPs with different magnifications (a and b), and (c) SAED pattern of PE-CSNPs	99
Figure 3.43	FTIR spectra of pure perindopril erbumine, chitosan and perindopril erbumine loaded chitosan nanoparticle.	101
Figure 3.44	Powder XRD pattern of free perindopril erbumine, pure chitosan, and perindopril erbumine-loaded chitosan nanoparticles	103
Figure 3.45	Perindopril erbumine release profile from chitosan nanoparticles in phosphate buffered saline of pH=7.4.	104
Figure 3.46	Release kinetics study by fitting the data of perindopril erbumine release from chitosan nanoparticles into phosphate-buffered saline at pH 7.4 using four different kinetics model.	105
Figure 3.47	Proposed model for drug delivery system	107

List of Tables

Table-2.1	Different composition of chitosan and TPP used in chitosan nanoparticle preparation	30
Table 2.2	Designed formulations for CP-CSNPs formation varying the ratio of CP and chitosan	32
Table-3.1	Percent yield of products during the extraction of chitosan from shrimp shell.	42
Table 3.2	Percentage of carbon, hydrogen, and nitrogen and the C/N ratio for chitin and chitosan	45
Table 3.3	Tentative assessment of IR band of chitin and chitosan	46
Table 3.4	Crystallinity index calculation in refer to 020 reflection for extracted chitosan (I_{am} represents the amorphous diffraction at $2\theta = 16^\circ$)	49
Table 3.5	Effect of concentration of chitosan and TPP o chitosan nanoparticles formation	50
Table 3.6	Distribution of elements in blank chitosan nanoparticles	55
Table 3.7	Tentative assessment of IR band of chitosan nanoparticles (CSNPs)	56
Table 3.8	Distribution of elements in ciprofloxacin loaded chitosan nanoparticles	62
Table 3.9	Tentative assessment of IR band of ciprofloxacin loaded chitosan nanoparticles	64
Table 3.10	The correlation coefficients (R^2) obtained by fitting the ciprofoxacin release data from the ciprofloxacin loaded chitosan nanoparticles (CP-CSNPs) in PBS solutions at pH 7.4	73
Table 3.11	Results of the antibacterial activity of free CP and CP-CSNPs	74
Table 3.12	Distribution of elements in erythromycin loaded chitosan nanoparticles	77
Table 3.13	Tentative assessment of IR band of chitosan and ER-CSNPs	79
Table 3.14	MIC and MBC of erythromycin and ER-CSNPs against two microorganisms	81
Table 3.15	The correlation coefficients (R^2) obtained after data of ER release from ER-CSNPs in PBS of pH 7.4 fitted to different kinetic equations	85
Table 3.16	Distribution of elements in metronidazole loaded chitosan nanoparticles	87
Table 3.17	Tentative assessment of IR band of metronidazole loaded chitosan nanoparticles	91

Table 3.18	The correlation coefficients (R^2) obtained after data of MTZ release from MTZ-CSNPs in PBS of pH fitted to different kinetic equations	95
Table 3.19	Distribution of elements in perindopril erbumine loaded chitosan nanoparticles	98
Table 3.20	Tentative assessment of IR band of PE-loaded chitosan nanoparticles	101
Table 3.21	The correlation coefficients (R^2) obtained by fitting the perindopril erbumine release data from the perindopril erbumine loaded chitosan nanoparticles (PE-CSNPs) in PBS solutions at pH 7.4	106

Abbreviations and Symbols

Da	:	Dalton
CSNPs	:	Chitosan nanoparticles
MIC	:	Minimum Inhibitory concentration
MBC	:	Minimum bactericidal concentration
AE	:	Association efficiency
nm	:	Nano meter
mV	:	Mili volt
ml	:	Mili liter
RT	:	Room temperature
MW	:	Molecular weight
DDA	:	Degree of deacetylation
FTIR	:	Fourier transform infrared
uv	:	Ultra violet
TEM	:	Transmission electron microscopy
SEM	:	Scanning electron microscopy
EDX	:	Energy dispersive X-ray
XRD	:	X-ray diffraction
CP	:	Ciprofloxacin
ER	:	Erythromycin
Na-TPP	:	Sodium tripolyphosphate
MTZ	:	Metronidazole
PE	:	Perindopril erbumine
CP-CSNPs	:	Ciprofloxacin loaded chitosan nanoparticles
ER-CSNPs	:	Erythromycin loaded chitosan nanoparticles
MTZ-CSNPs	:	Metronidazole loaded chitosan nanoparticles
PE-CSNPs	:	Perindopril erbumine loaded chitosan nanoparticles
%	:	Percentage
α	:	Alpha
β	:	Beta
$^{\circ}\text{C}$:	Degree celsius

Chapter 1: Introduction

1.1 General Introduction

The importance of naturally occurring biopolymers known as polysaccharides (chitin, starch and cellulose) has grown enormously as a result of its renewable resource. It has a large variety of applications in nature. Chitosan, a polysaccharide that can easily be obtained from crab, shrimp and shrimp shells. Chitosan is a deacetylated form of chitin. Moreover, this is an environmentally friendly compound and related to the green chemistry. Recently, the purpose of chitosan and its derivatives has recently been the subject of much research. Chitosan is used as the component of waste water treatment, and also biosensors, artificial muscles, environmentally friendly membranes, the component of highly efficient batteries like electrolyte (*I*) etc.

Chitosan has a variety of properties such as it is occurring in large amounts on the earth, it is a linear polymer that is made of β -(1-4)-2-amino-2-deoxy-D-glucopyranose units. It's a white, hard, inelastic and nitrogenous polysaccharide. Because of its properties of biodegradability, biocompatibility, non-toxicity, antibacterial activity and its versatile physico-chemical properties, it has more field of purposes. Chitosan has many uses in our daily-life productions such as the pharmaceutical industry, textiles, paper production, biotechnology, wastewater treatment, cosmetics, agriculture and agribusiness. Chitosan is an excellent cellular transfectant due to the presence of the primary amine group. Chitosan has a 'Proton sponge' effect, which point out the swelling property of the polymer that encounter the pH (acidic) inside the cell's endosome. Due to this property, chitosan itself an efficient transporter for therapeutic molecules. The application of chitosan significantly increased due to its macromolecular property. Fabrication of chitosan as nano or submicron form is also effective. In recent years, preparation of drug carriers is so significant by applying nanotechnology process. For the immobilization of drug, the magnetism and surface area properties of nano and nanomaterial have significant role. Several reported works for chitosan nanoparticles (CSNPs) preparation and their applications in drug transporter and other pharmaceutical applications have been found. Researchers have been trying to prepare CSNPs using different methods. The main objective of this researches to prepare chitosan from shrimp shells and the preparation of different drug-loaded CSNPs. For this purpose, we are using simple yet effective methods in addition to their optimization

by observing shape of particles and its morphology, surface charge, size distribution and drug loading capacity and final study of their biomedical applications.

1.1.1 Background

Shrimp processing industry is rapidly growing concern in Bangladesh. Seafood processing industry does packaging and processing after culture or capture of shellfishes. Peeling of shrimps/prawns gives required product meat and generates waste. The shells of shrimp consist large amount of raw shrimp weight that is discarded as waste. By this way, a huge amount of raw shrimp wastes are generated from the shellfish industry that is prominent in all costal countries. These wastes are responsible for the surface pollution in coastal areas. Because shrimp shells are not naturally soluble, they occupy much of the physical space and ccreates pollution. Due to the dumping off a large quantities of wastes, it makes degradation process slow and increasing the waste process time that is a vital environmental concern, though the wastes are also biodegradable. Recycling shellfish waste and extracting commercially viable substances such as chitin are a quick and effective way to alleviate this problem. Chitin has various applications, but due to the insolubility in water that has many uses. As a results, chitosan extraction from the shrimp shells has therefore become increasingly popular over the last few years.

1.1.2 Chitin and Chitosan

Chitin and chitosan are similarly chemically structured. Chitin has a linear chain of acetyl glucosamine groups and chitosan is got by removing enough acetyl groups ($\text{CH}_3\text{-CO-}$) from chitin and both are soluble in the most diluted acids. The actual difference between chitin and chitosan is the acetylene part of the polymer. Chitosan with an amino-free group is the most valuable derivative of chitin. It is a biodegradable, non-toxic polymer of high molecular weight, and is very near to cellulose, a plant fiber ([Figure 1.1](#)).

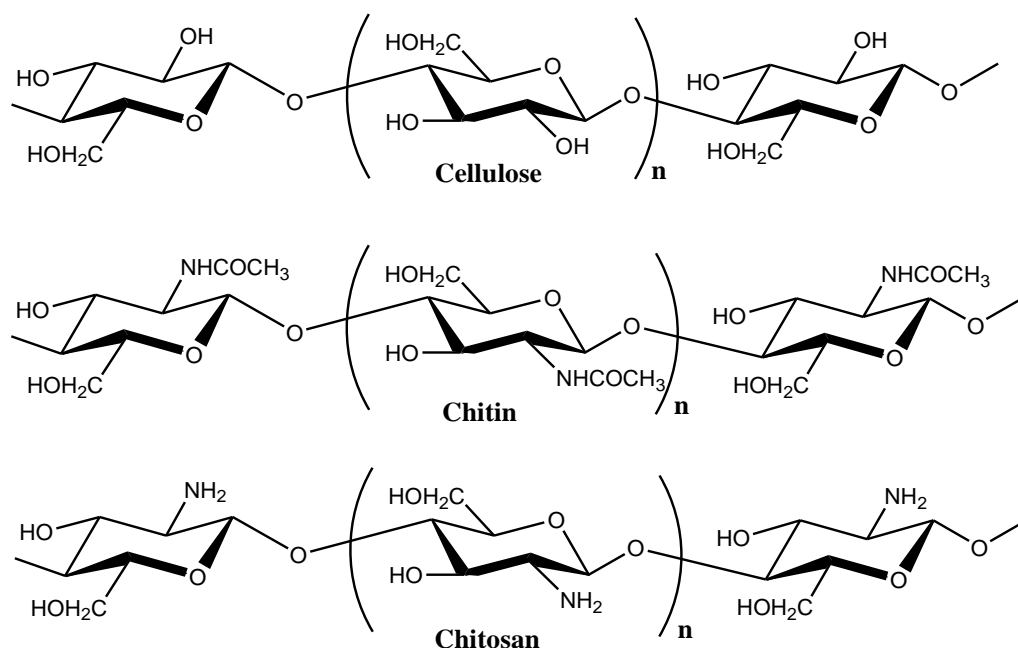


Figure 1.1: Structure of cellulose, chitin and chitosan

Chitosan, a polysaccharide that is available in large quantities on earth. It is a polymer that is linearly shaped containing B-(1-4)-2-amino-2-deoxy-D-glucopyranose unit. It has a white color, rigid, non-elastic material and nitrogenous containing polysaccharide which has a wide range of uses due to its biocompatibility, biodegradability, antibacterial activity, non-toxicity and multifunctional physical and chemical properties. The pharmaceutical industry, paper production, textiles, sewage treatment, biotechnology, agro-food and agriculture, cosmetics are just a few of the many areas in which chitosan is helpful. Chitosan is an excellent cellular transfectant due to the presence of primary amino groups. However, chitosan is a macromolecule, which has a significant impact on its application. Over the last few years, nanotechnology has demonstrated a strong trend towards preparing the drug transporters. Below the Nano scale, nanomaterials have features such as magnetic property and huge surface area, which are conducive to the immobilization of medicines. Numerous studies have dealt with the preparation of CSNPs and their versatile applications in the transport of drugs and other pharmaceutical applications.

1.1.3 Properties of Chitosan

Chitosan is a high molecular weight polycaternal heteropolysaccharide with two monosaccharides units: *N*-acetyl-glucosamine and *D*-glucosamine. The comparative

quantity of the two monosaccharides in chitosan varies significantly, giving of different degrees of deacetylation, molecular weight, different viscosities and pKa values. Moreover, chitosan has three functionality; the amino functional group on C2, the primary and secondary hydroxyl groups on the C3 position and also C6 position respectively. These three functional groups play an important role in its different functions. Among the three groups, the amino group is the most important particularly in acid conditions, because of the protonation phenomenon. Furthermore, the chitosan polymer interacts with metallic cations via amino groups, hydroxyl ions and coordination bonds.

Based on the extent of deacetylation, chitin contains 5 to 8 percent (w/v) of nitrogen, which is mainly in the form of primary aliphatic amino groups as found in chitosan. Chitosan is subjected to normal amino reactions, of which *N*-acylation and Schiff reactions are the most significant. Chitosan glucans are easy to get under soft conditions, but it is difficult to get cellulosic glucans. The biological characteristics of chitosan include; (i) biocompatible, (ii) capable to bind with mammalian and microbial cells, (iii) regenerative effect on connective gum tissue, (iv) accelerates the development of osteoblast which is responsible for the buildup of bone, (v) hemostatic, (vi) fungistatic, (vii) spermicidal, (viii) antitumor, (ix) anticholesteremic, (x) the central nervous system depressant.

Biodegradability of chitosan: Biodegradation refers to the decomposition of a substance aided by a biological host after encountering physiochemical conditions (2). The metabolic process of chitosan in the organism is largely dependent on its biodegradability (3). Lysozyme applies an important role in the biodegradation of chitosan and produces glucosamine and *N*-acetylglucosamine (4). The two glucosamine and *N*-acetylglucosamine are again degraded by the glycoprotein to form carbon dioxide (5). The greater the amount of chitosan crosslinking, the slower the biodegradation, so that the biodegradation can be controlled by crosslinking. The degree of molecular weight and deacetylation also have an effect on the biodegradation process of chitosan in the living organisms. Higher levels of deacetylation and molecular weight lead to lower rate of degradation (4). This is due to the fact that lysozyme disturb the areas of the chitosan chain that is built in more than three units of *N*-acetyl-D-glucosamine. Chitosan with a greater level of deacetylation will be more stable since it will have more units of *N*-acetyl-D-glucosamine in order.

Biocompatibility of chitosan: Chitosan is naturally occurring polymer that is considered as highly biocompatible in numerous biomedical applications because of the non-allergic

properties of it (6). The entire polymeric structure is similar to hyaluronic acid, which is situated in the connective, epithelial and neural tissues. It is gradually degraded to the product of amino sugars that are completely absorbed by the human body (6) and the degradation products are the natural metabolites (7).

1.1.4 Sources of Chitosan

The availability of Chitosan in nature is not so high, as it is found in Mucoral species, in mainly Mucor, Absidia and Rhizopus (8). The most significant source of commercially available chitosan is the process of deacetylation of its original chitin polymer.

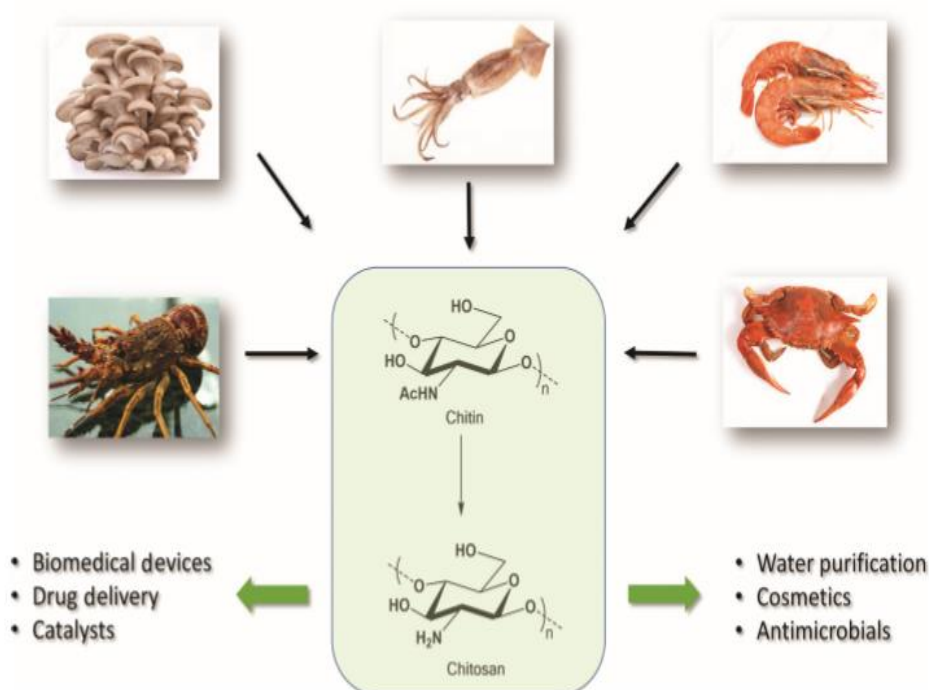


Figure 1.2: Sources of chitin and chitosan and its uses

Chitin is found on this earth as the polysaccharide and also in the cell walls or fungi, green algae, the cuticles of arachnids and insects and in the exoskeleton of crustaceans. On an industrial purposes, the main sources of chitin are leftovers from crustacean processing plants (crabs, shrimps and lobsters). The main ingredients of crustacean shells are 15-40% of chitin, 20-40% of protein and 20-50% of CaCO₃/MgCO₃ (9). In nature, shrimp carapace is the major or common sources of chitosan (Figure 1.2). Bangladesh has a huge shrimp industry at Khulna, Shatkhira, Chottogram and Cox's Bazar. So the chitosan raw material is so much available in Bangladesh.



Figure 1.3: Dry shrimp shell

1.1.5 Nanoparticles

The particles having the size of 100 nm or less in at least one dimension are considered as nanoparticles. After forming nanoparticles, the surface chemistry and various properties is noticeably changed from the original material which increases their field of applications. The most widely used application of nanoparticles is in the biomedical field. The higher surface area to volume ratio of nanoparticles as compared to that of larger ones results in increasing the reactivity to other molecules and the high carrier capacity that allows it to be integrated with drugs. Nanoparticles can be more easily and readily taken up by human body, tissue and organs as well as cross biological membranes and enter cells than larger particles owing to their small size (10). The nanoparticles consisting the size of 100nm shows 2.5 fold and 6 fold greater uptake than microparticles of 1 μ m and 10 μ m respectively (11).

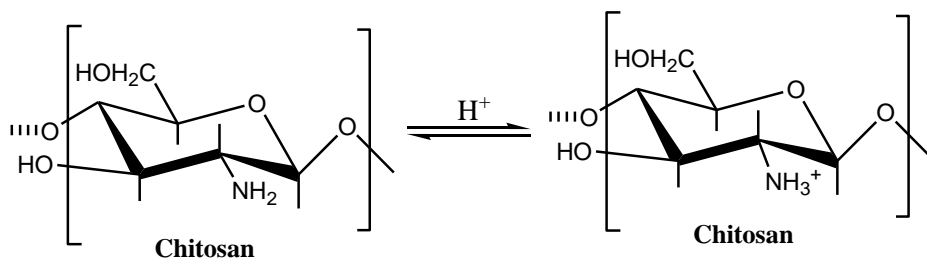
Nanotechnology and its uses: Nanotechnology means the investigation and use of structures from 1-100 nm. Nanotechnology is a incorporation of chemical engineering, microelectronics, mechanics, material science, electricity and biological detection. Nanotechnologies are the combination of idea, production, categorization and the application of device, structure, and system by controlling the size and shape at the nano level (12). Nanoparticles would be illustrate as the particles under the diameter of 100 nm that have new of developed properties as a function of size, unlike larger particles of similar

materials. Nanoparticles are widely present in natural world (13). Nanotechnology offers immense visions for a developed, individualized management of the disease.

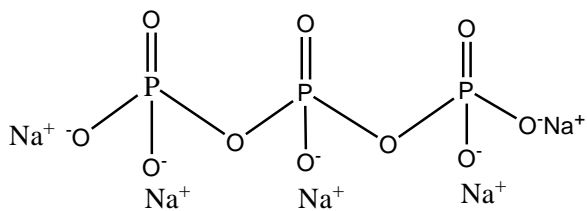
Nano drugs are becoming significant-valued in the recent times due to the use of nanostructures as administration agents by encapsulation of drugs and targeted administration in particular tissues. Nanoparticle containing medicines have been developed both for the purposes of cancer diagnosis and also for pharmacotherapeutic treatment (14). The first generation of nanoparticle products including lipid systems such as micelles and liposomes, which have been accepted as satisfactory level for use in the manufacture of edible items and medical products (15). These liposome and micelles are the inorganic nanoparticles like magnetic or gold nanoparticles (15). Nano compounds persist in the bloodstream for an extended time frame and to be easy the long time release of the drug being transported.

1.1.6 Chitosan Nanoparticles (CSNPs)

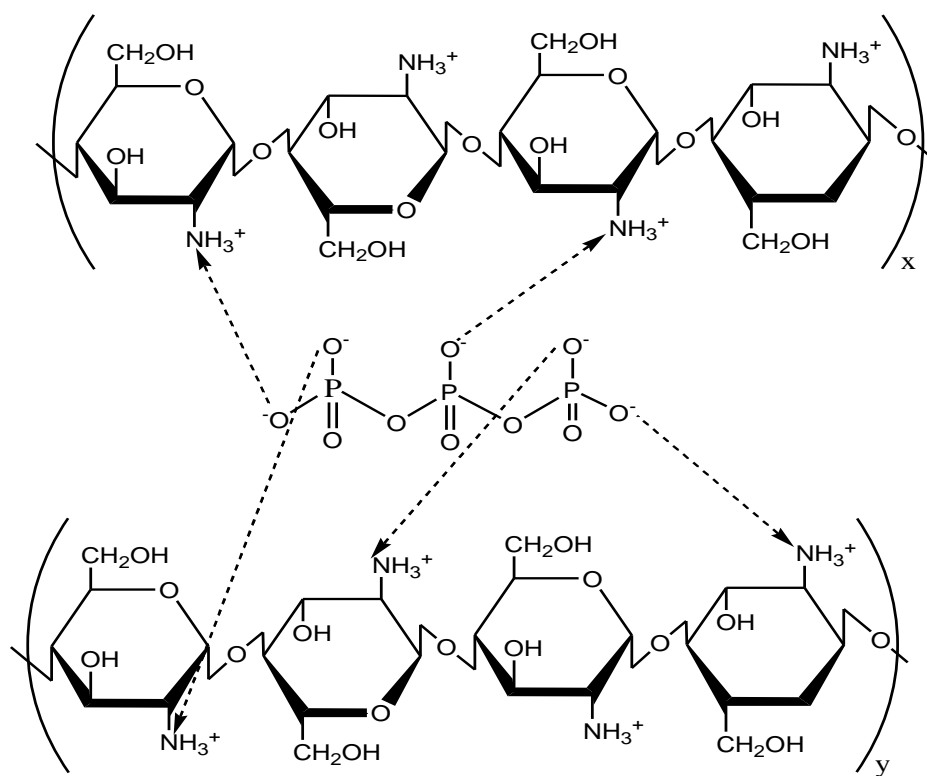
Chitosan nanoparticles (CSNPs) have very good physiochemical characteristics. These are environmentally benign and biodegradable. It is often used as a vector for drugs with controlled release for drugs with controlled release for genetic convey in artificial organs and for immune prophylaxis. Moreover, this nanoparticles have been used to increase the strength and washing ability of textile products and to confer anti biological (anti-bacterial) effects. CSNPs are usually prepared by micro-emulsion, auto-assembly and ionotropic gelation processes. The micro emulsion process may give nanoparticles with a small size distribution to the detriment of large quantities of organic solvent. Self-assembly is a simple procedure, but in this case chitosan must be altered by the introduction of new chemical groups. Ionotropic gelation is a light reparative method in an aqueous environment, without incorporating the chemical groups into the chitosan structure. Nanoparticle size is affected by the two terms: molecular weight and concentration of chitosan. Moreover, suspension of CSNPs is a thermodynamically unstable system and changes in particle size during storage as well (16).



(a)



(b)



(c)

Figure 1.4: protonation of chitosan (a) sodium triphosphate (Na-TPP) (b) and ionic crosslinking of positive amino group of chitosan with negative phosphate group TPP to form nanoparticles, (c)

Biomedical Applications of Chitosan Nanoparticles (CSNPs): The effectiveness of more medicines is frequently limited by their ability to go to the site of therapeutic function. In the case of normal dosage volume, only a very little amount of ejected dose go to the target site, on the other side the maximum portion of dose disperses in every part of the rest of the body according to its biochemical and physicochemical properties. Therefore, it is difficult to develop a drug administration system that optimizes the pharmaceutical performance of a drug, thereby reducing its toxic side effects. One such approach is the applying of colloidal drug transporters. Liposomes and nano-particles are the most important transporters. Nanoparticles have attracted much attention from pharmaceutical scientists in the case of drug administration system due to the different functions of targeted tissues, access to deep molecular targets, and control of drug release. Polymeric materials like chitosan and poly-d,l-lactide-co-glycolide (PLGA) are used to synthesize bio-degrading nanoparticles. Chitosan is a naturally occurring polysaccharide that has the properties like biodegradability, non-toxic properties and good biocompatibility turn it to the suitable component for the use in biomedical and pharmaceutical applications.

The general properties of CSNPs are small size effect, surface effect, and quantum size effect. These CSNPs have been extensively studied for the administration system of antibiotics (such as ampicillin, doxycycline and ceftriaxone), anti-cancer drugs such as 5-fluorouracil, paclitaxel, doxorubicin, letrozole and saponin. These are also widely used for the treatment of Parkinson's disease, such as selegiline and drugs for the central nervous system such as thiocolchicoside. Insulin-loaded CSNPs have the potential to increase insulin's intestinal absorption capacity and increase its relative pharmacological bioavailability. CSNPs were also used as a genetic vector to effectively improve the transfer of genes into cells and also have been used for delivery of gastric drugs. However, the antibacterial activity of CSNPs has rarely been reported anywhere else. In terms of the small-scale and quantum-scale effect of nanoparticles, the CSNPs have the superior activities.

CSNPs are more biocompatible, stable, biodegradable, less toxic, simple and easy to produce. These are made from a natural chitosan polymer which is completely biodegradable, biocompatible and gain the capacity to control the release of active ingredients. Nanoparticles manufactured from chitosan and its derivatives usually have a positively charged surface area. CSNPs have several active applications via the delivery of

ocular drug, parenteral drug, per-oral drug, mucosal drug, vaccine, gene, pulmonary drug, intranasal drug, cancer therapy, etc. A plethora of clinical studies are currently under way to study the biocompatibility, safety and efficacy of CSNPs as a dosage form.

1.1.7 Drug Delivery

Many drugs fail to achieve positive clinical outcomes at the clinical stage, often because they are unable to reach the target site of action. In addition, a significant part of a drug is distributed not specifically to healthy tissues and organs in the body, resulting in serious side effects. Developing targeted drug distribution systems can help to overcome this serious problem by releasing drugs or bioactive agents specifically to the targeted site of action. Drug delivery systems are designed to maintain a drug that has been used for therapeutic periods for a specific period of time. It means that the concentration of the targeted drug must remain in between the highest blood level value and a lowest value (where the drug is inactive) (17). Conventional drug delivery systems may have large fluctuations in serum levels. This is because most drugs are released shortly after administration and the strength of the drug increases rapidly, goes to peak, and then decreases. Controlling the delivery of controlled-release drugs synchronize the rate of drug release to eliminate lower and higher doses and reduce frequent doses to enhance patient compliance.

Controlled drug delivery: Controlled drug delivery increases the availability of the administered doses of drugs within the therapeutic window or at the target site for a sustained period of time which is difficult to obtain in the case of traditional drug delivery systems. In a controlled drug delivery systems, drugs can be protected from degradation in vivo, which improves its half-life and also the therapeutic effect. To establish a controlled drug delivery system, drug is incorporated into the carrier first. Then, after administration, it can release drug over a sustained period of time, ranging from days to months (18). Drugs are associated into the carrier in such a way that the release of drugs from these carrier may be the results of i) diffusion of drugs from carrier matrix, ii) erosion of carrier matrix, iii) release from surface of carrier (19) or, iv) a combination of all of these.

Use of chitosan as a drug delivery system: Chitosan is an example of a drug conveyance or transport system. Because of its ability to target certain tissues and control drug release, chitosan has been formulated with hydrogels, nano fibers, membranes and nanoparticles. Many studies have focused on the development of CSNPs and their applications in drug

transportation and other pharmaceutical applications. CSNPs have been prepared as drug vectors, as reported in a variety of studies. Chitosan microspheres were used in the delivery of gastric drugs. Since chitosan is biologically safe and inexpensive, it can be used in the preparation of dosage forms for commercial medicines. The most important merit is to create a desirable environment with optimum response, minimal side effect and long-term effectiveness. It is a comparatively new technology that demands an interdisciplinary scientific research. Chitosan-controlled distribution systems are being developed and are used for a wide range of reagents in multiple environments. Chitosan and CSNPs have immense applications in the pharmaceutical, food, agricultural and cosmetic fields (20, 21).

1.1.8 Mechanism of Drug Release from Particulate Systems

The mechanism of drug release depends on the quantity of molecules that are engaged in nanoparticles, either on the surface or trapped in the matrix (Figure 1.5). Drugs that are adsorbed onto the surface will suddenly dissolve when they enter into a contact with the release medium creating a bursting effect of drug release (3). Drug release because of the diffusion phenomena through a porous matrix begins when the matrix swells the water entering the particulate system and the pores expand leading to increased bumping (3, 22). If the matrix is very good reticulated this enlargement may be delayed and then the shower scatter can still be taken. The drug will then begin to diffuse from the inflated matrix.

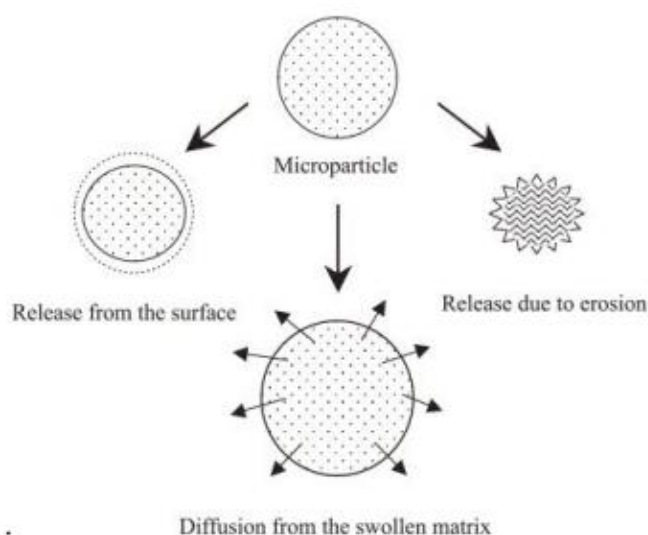


Figure 1.5: Mechanism of drug release from a particulate system (6)

The drug release mechanism shows that the release of the drug from nanoparticles occurs initially quickly and then slowly over time. The delivery of drugs depend on the type of polymer and bonding pattern of inner side, addition of any additives (chitosan derivatives). It also depends on the shape and size of the nanoparticles as this presents the surface area and free energy (23).

Drug release from chitosan nanoparticles (CSNPs): The well-known mechanisms which are related to release of drug from CSNPs such as: spread out of the adsorbed drug by diffusion, drug spreading through the chitosan matrix, that is, swelling, erosion of chitosan chains and a combination of both erosion and swelling as represented in Figure 1.6. CSNPs also show the release of pH-dependent medications because of the solubility of chitosan. The drug release mechanism is characterized by the solubility of the CSNPs in the surrounding water or biological environment. When the CSNPs meets the surrounding medium and the swelling starts, the chitosan chain untangles. This can be followed by the release of medicines from this part of the chitosan matrix.

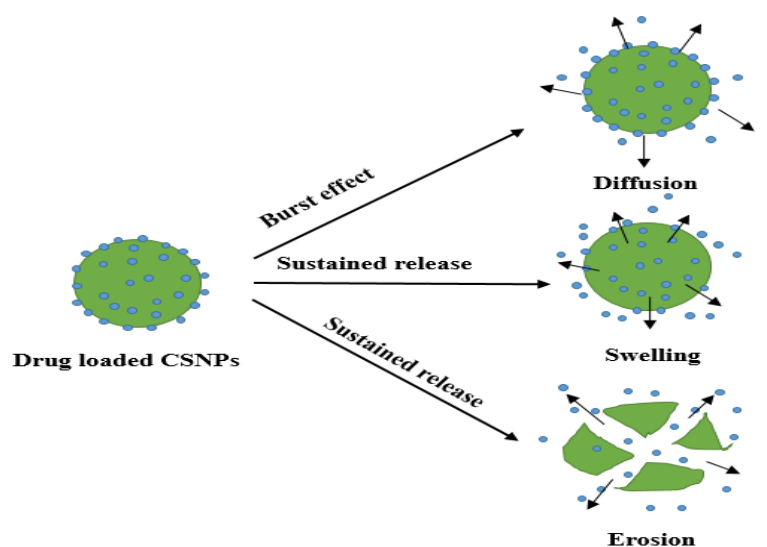


Figure 1.6: Diagram representing the mechanism of drug release from CSNPs

Erosion and swelling may result sustained release as the chitosan chains can act as a rate limiting membrane for drug release. Erosion is associated with diffusion, swelling and dissolution. There are two ways of erosion: homogeneous and heterogeneous. Homogeneous erosion is a process where the erosion occurs at the same rate whole over the matrix, but heterogeneous erosion is a process where the erosion may occur towards the inner site.

1.2 Objective of Research

Chitosan has played an essential role as a carrier in the formulation of an effective drug delivery system through the ability of drug loading. It is the natural cationic polymer that has received growing attention mainly due to their various advantages and providing versatile routes of administration. It has many medicinal properties as mentioned earlier which improve its activity in various biomedical applications. Shrimp shells are a major source of chitosan polymer. In Bangladesh, different types of shrimp are cultivated and the shells of those shrimp are dumped directly into the environment like garbage. As a result, in this research project, used shrimp shells are used as raw material for chitosan production. The chitosan produced has been used to prepare drug-loaded nanoparticles. The preparation and characterization of CSNPs would be very significant and have a lot of applications for various commercial and medical purposes, as described in the previous sections. So the specific objectives of my research works are as follows:

- (i) Extraction of chitosan from shrimp shell.
- (ii) Characterization of extracted chitosan by solubility test, molecular weight determination, FT-IR, XRD and elemental analysis.
- (iii) Synthesis of drug loaded chitosan nanoparticles using different types of drugs (Ciprofloxacin, Metronidazole, Erythromycin and Perindopril erbumine).
- (iv) Characterization of synthesized drug-loaded chitosan nanoparticles by various methods like FT-IR, XRD, SEM, EDX and TEM analysis.
- (v) Study of biomedical application of these nanoparticles through in vitro drug release profile study and antibacterial activity analysis.

1.3 Present Work

Chitosan and CSPNs have diverse applications in the pharmaceutical, food, agricultural, cosmetic and medicinal fields. As an agricultural product, more than 96% of Bangladeshi shrimp is cultivated in the Khulna region. Most shrimp shells are used as garbage and are dumped into the environment. In this context, my research focuses on the extraction of chitosan from the shrimp shell and the preparation of CSNPs loaded with different medications.

The outline of present research is presented below:

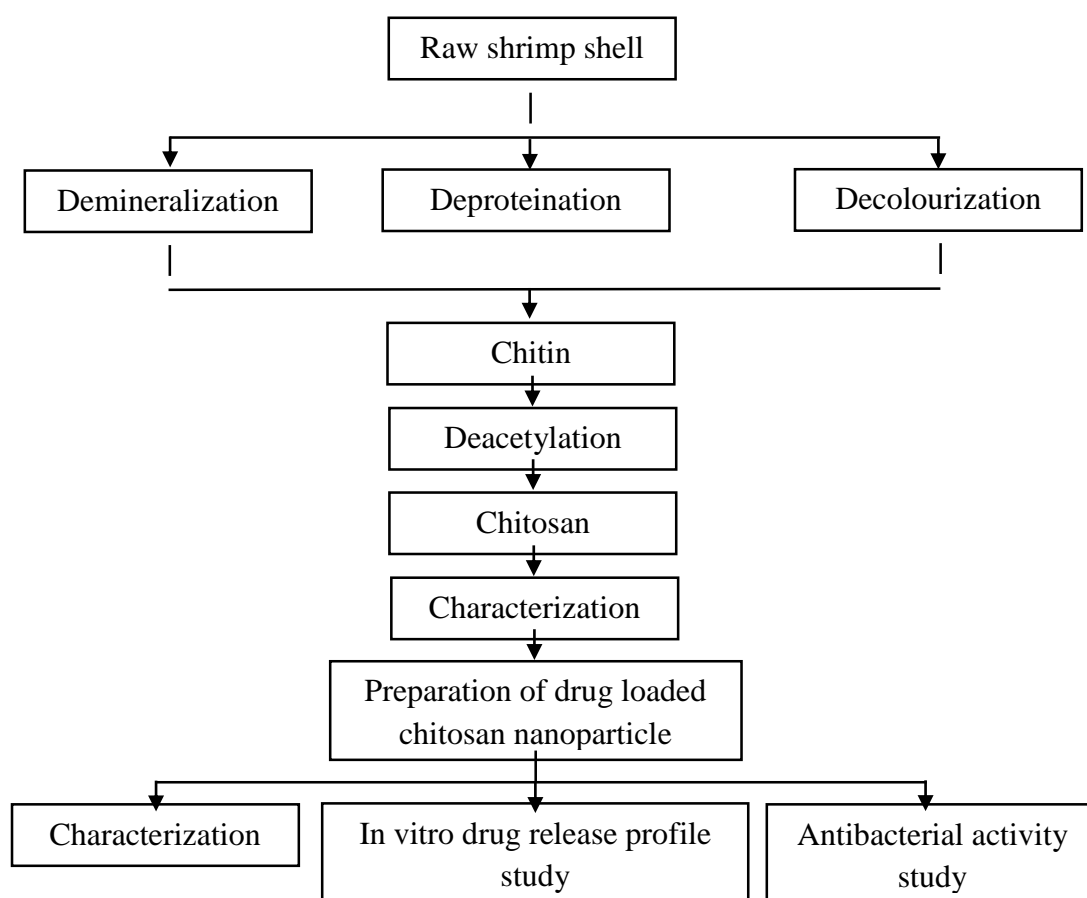


Figure 1.7: Outline of the present study

Figure 1.7 represents the present study. In this study, the shrimp shells were collected from coastal areas. The shells were then processed. Next, the shrimp shells were treated by acid and base for demineralization, Deproteination, decolouration and *N*-deacetylation. Then the product obtained from these processes were characterized using solubility test, X-ray diffraction (XRD), fourier transform infrared spectroscopy (FTIR) and determining the

molecular weight. Lastly, the characterized chitosan was used to prepare drug loaded chitosan nanoparticle by ionotropic gelation technique. *Calvo et. al., 1997* were the first to describe the ionotropic gelation method used to prepare CSNPs (24). This procedure is based on electrostatic interactions between the chitosan amine groups and a variety of negatively charged polyanions, such as tri-polyphosphate. Preparation of drug loaded CSNPs was carried out using three antibiotics; ciprofloxacin, erythromycin, metronidazole and an antihypertensive drug; perindopril erbumine.

Ciprofloxacin is an oral synthetic chemotherapeutic antimicrobial drug whose broad spectrum of activity may treat serious infections caused by Gram-negative and Gram-positive bacteria. Ciprofloxacin is almost not soluble in aqueous medium, very slightly soluble in organic solvents such as ethanol and methylene chloride (25). *Figure 1.8* shows the structural formula of ciprofloxacin. The problem of lower drug solubility can be avoided by formulating the drug in systems containing colloidal drugs transporters, such as liposomes, microparticles, micelles, polymeric nanoparticles or nanosuspensions. The bioavailability of ciprofloxacin can be improved by the formulation in a suitable distribution vehicle such as CSNPs.

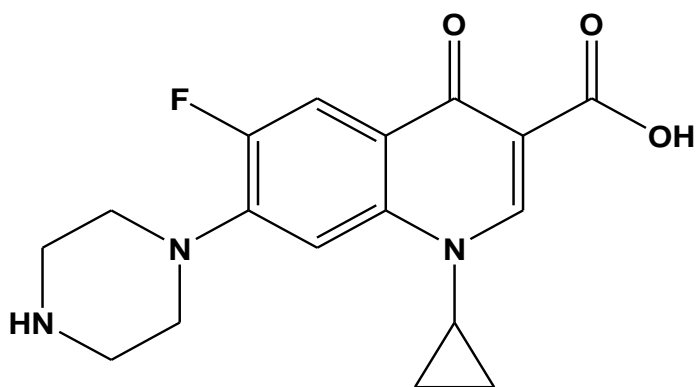


Figure 1.8: Structure of ciprofloxacin

Metronidazole is an amoebicide, antiprotozoan and antibiotic effective against anaerobic bowel amoebiasis, giardiasis, trichomoniasis, bacterial vaginosis, and surgical infections. *Figure 1.9* shows the structural formula of metronidazole. The medication must be delivered to the colon for their effective effect against *E. histolytica*. Administration of this drug as a classic tablet provides a minimum amount of metronidazole for local action in the colon.

(26, 27). Furthermore, the distribution system of drugs targeted by the metronidazole colon is associated with the following additional benefits:

- (i) 98-100% bioavailability with hepatic metabolism and half-living metronidazole during 7-8 hours.
- (ii) High physiochemical stability of metronidazole
- (iii) Feasible method of analysis (UV spectrophotometer) for in vitro studies of the developed delivery system.

So the development of colon targeted metronidazole loaded nanoparticles has gained attention in recent years.

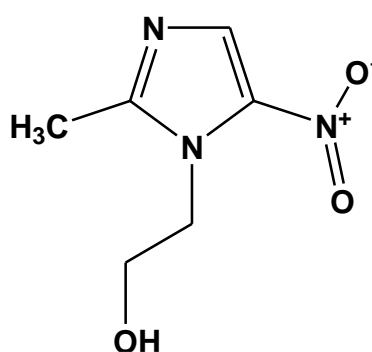


Figure 1.9: Structure of metronidazole

Erythromycin is used as an antibiotic for the treatment of several bacterial diseases like respiratory tract infections, skin related diseases, chlamydia infections, pelvic inflammatory conditions and syphilis. Eye ointment is usually recommended are used to treat conditions such as dry eyes or eye infections (such as conjunctivitis) in newborn babies. Figure 1.10 shows the structural formula of erythromycin.

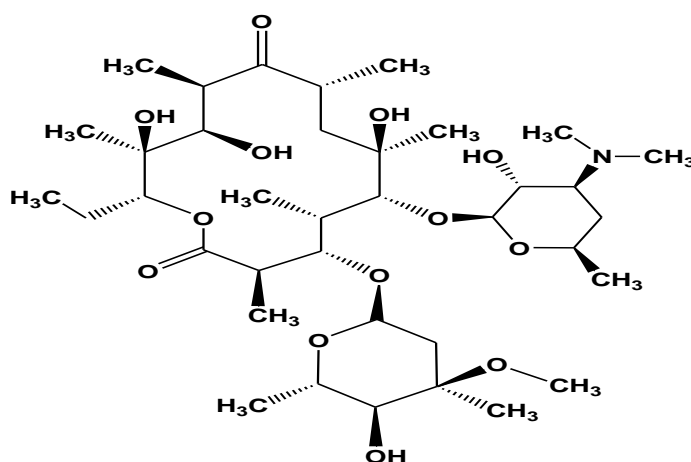


Figure 1.10: Structure of erythromycin

Perindopril is a *tert*-butylamine salt of 1-[(2*S*)-2-[(1*S*)-1-carbethoxybutyl]amino]-1-oxopropyl)-(2*S*, 3*A*s, 7*A*s)-perhydroindole-2-carboxylic acid. It belongs to the class of antihypertensive drugs, which is used in the treatment and prevention of many medical conditions such as a med of mild-to-moderate hypertension (5), congestive heart failure, diabetic nephropathy and post-myocardial infarction (28). It is given orally in tablet form at a 1:1 ratio of perindopril salt to erbumine (*tert*-butylamine). Figure 1.11 shows the structural formula of perindopril.

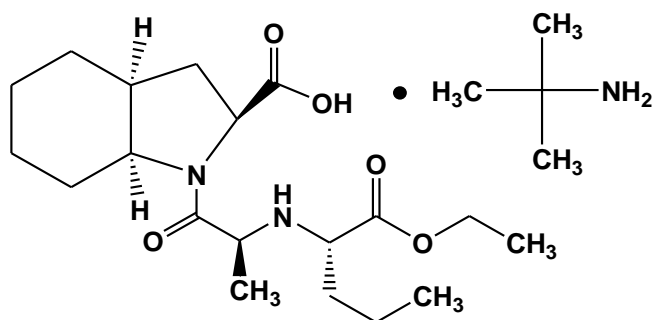


Figure 1.11: Structure of perindopril erbumine

Thus the drug loaded CSNPs are characterized by various techniques such as FT-IR analysis, XRD analysis, and morphology and particle size confirmation by SEM and TEM analysis, quantitative elemental analysis by EDS. In vitro dissolution study was performed in a buffered saline phosphate solution at pH 7.4. The dissolution test measures the amount and rate of solution formation from a dosage form, such as a tablet, capsule, ointment, etc. The dissolution of a medicine is essential to its bioavailability and therapeutic effectiveness.

1.4 Review of Literature

CSNPs were first described in 1994, when Ohya and colleagues proposed the intravenous administration of 5-fluorouracil, a cancer-fighting drug transported by CSNPs derived from emulsification and cross-linking process. Since then, these systems have been thoroughly studied in preparation for drug administration. CNSPs are extensively used as nanocarrier for the delivery of protein, drug and gene (29, 30). Many researchers have developed novel formulations of CSNPs which included secondary materials forming matrices. In particular, various methods have been developed, principally involving emulsification, different types of coacervation, diffusion of emulsion solvents, micellar inverse method, ionic gelation, polyelectrolytic complexation and desolvation. Of these, ionotropic gelation is the most studied formulation method for the preparation of NP chitosans. It is based on electrostatic interaction between the positively-charged aminosugar monomeric units of chitosan and negatively-charged polyanions, e.g., tripolyphosphate or hexametaphosphate or dextran sulfate (31, 32).

Vitali *et. al.*, (2022) investigated the preparation of CSNPs charged with phenolic monoterpene-carvacrol (33). After the completion of optimization process, the best NPs formulation process was the characterization of nanoparticles structurally by different spectroscopic and microscopy techniques like SEM. This described the functional features of NPs such as loading capacity, encapsulation efficiency and release kinetics. The antifungal activity of this formulation was studied with the different *Candida* spp., represented among the most known pathogenic species. CSNPs loaded with antifungal carvacrol showed a better antifungal effect than free carvacrol being more efficient against *C. albicans* strain with a MIC of 24 ug/mL, and were also able to affect the viability of the pre-formed cells as well as the formation of biofilm.

Protein-peptide-based drug delivery system was developed by Yadav and Yadav, (2021) using the bovine serum albumin (BSA) loaded CSNPs which can effectively transport the therapeutic molecules to the lung by pulmonary delivery (34). CSNPs were prepared by ionic freezing, and bovine serum albumen was used as a model protein. The size and zeta potential of BSA nanoparticles ranged from 193.53 ± 44.97 to 336.36 ± 94.63 with PDI values of 0.35-0.45. BSA-charged nanoparticles showed good uptake with no significant cytotoxicity observed in cell line A549. In this research, it was also found that during nanoparticle synthesis, the structure and integrity of proteins are not compromised. In the

TEM pictures, it was shown that the distribution of nanoparticles is uniform in the nanometer range. Thus, nanoparticles prepared by this method was suitable for delivering the peptide/protein into the cells without any protein degradation during the nanoparticle making process.

The antileishmanial efficacies of amphotericin B-loaded CSNPs were studied by Sohail *et. al.*, (2021) under in vitro conditions (35). CSNPs were prepared using ionic gelation method with negatively charged tripolyphosphate and the nanoparticles were analyzed for their size and surface structure, drug loading content, encapsulation efficacy different techniques. The prepared amphotericin B-loaded CSNPs showed spherical shape with a mean particle size of 118 nm, an encapsulation efficacy of 88% and a positive zeta potential. Free amphotericin B presented very low efficacy than amphotericin B-loaded CSNPs against parasite after 72h incubation. In conclusion, CSNPs loaded with amphotericin B can be a suitable alternative treatment to eliminate drug-resistant Leishmania parasites.

Tetracycline, gentamycin and ciprofloxacin loaded CSNPs were synthesized by Ekhlas *et. al.*, (2020) (36). It has been used as a new drug administration system to improve the antibacterial properties of cellulose-containing tissues. The CSPNs have been prepared from the solution of chitosan using tripolyphosphate (TPP) using the ionic gel method. Next, the prepared nano-composite used as superior antibacterial materials with minimal toxicity. The results showed that tissue treated with nanoparticles of chitosan and its nanocomposite with different antibiotics inhibited the growth of Gram-positive and Gram-negative bacteria.

Ampicillin-CSNPs were produced by Ciro *et. al.*, (2019) using ionic gelation method (37). The antimicrobial effect was determined by the method of micro-dilution of the broth using susceptible and resistant strains of *S. aureus*, giving a potential application in medical purposes. Thus, the results obtained in this study demonstrate the application of synthetic nanoparticles to treat infections caused by the pathogenic *S. aureus* strains.

Alqahtani F.Y. *et. al.*, (2019) reported the antimicrobial activity of diclofenac (DIC) loaded CSNPs (38). They prepared no-antibiotic DIC-loaded CSNPs (DIC.CNPs) and characterized them in vitro antibacterial activity. DIC-loaded CSNPs were prepared from low molecular weight (LMW) and high molecular weight (HMW) chitosan using an ionic gelation method. Particle size, poly-dispersity index (PDI) and encapsulation efficiency of the formulated DIC-CSNPs increased with the increasing of MW of chitosan. The prepared

CSNPs showed a narrow size distribution with low PDI values (0.18 and 0.24) and encapsulation efficiency (29.3% and 31.1%) for LMW.DIC.CNPs and HMW.DIC.CNPs, respectively. The DIC.CSNPs showed significantly better antibacterial activity against *S. aureus* and *B. subtilis* than DIC alone did. The antibacterial activity has been affected by pH and MW of chitosan. Collectively, these findings can suggest the potential usefulness of DIC.CSNPs as a non-antibiotic antibacterial agent requiring further study to assess the stability of prepared DIC.CNPs.

Duceac L.D. *et al.*, (2020) conducted a research on the preparation of a chitosan nanoparticle which was encapsulated by ceftriaxone (39). These nanoparticles have undergone structural and morphological testing to reduce bacterial resistance and improve the effectiveness of antibiotics against certain dangerous pathogens. Their work is based on improving the antimicrobial effectiveness of ceftriaxone against gram (+) and gram (-) bacteria by antibiotic encapsulation into CSNPs. Physicochemical properties of ceftriaxone-loaded polymer nanoparticles were investigated by particle size distribution and zeta potential, FTIR, TGA, SEM characteristics techniques. It showed an average particle size of 250 nm and a zeta potential of 38.5 mV. The release profile shows a nascent drug delivery of almost 15%, after 2 hours of about 83%, followed by a delayed drug release of up to 24 hours. Because of the small size CSNPs, the nano-hybrids obtained are capable of better penetrating the bacterial cell, thus increasing antimicrobial activity by inhibiting the multiplication of gram (+) and gram (-) microorganisms.

Clarithromycin-loaded CSNPs were synthesized by Bin-Jumah *et al.*, (2020) to demonstrate the efficacy against microorganisms (40). Based on the study. Clarithromycin-loaded CSNPs exhibit the particle size less than 200 nm, which is good for ocular delivery. The prepared formulation has shown a positive zeta potential that indicates that the particles are not aggregated and spherical. The drug release study confirmed a sustained drug release model. It showed approximately 2.7 times as much corneal permeation than the clarithromycin solution. It has also shown a significantly higher antibacterial sensitivity than clarithromycin solution. The results concluded that clarithromycin-loaded CSNPs can be used as a delivery system for antibacterial drugs with a higher precorneal residence time and increased patient adherence by reducing the dose frequency.

Ashvini *et al.*, (2019) also prepared clarithromycin-loaded CSNPs of various formulations and investigated the antibacterial activity against *Streptococcus pneumoniae* (41). The

formulations were prepared through ionic gelation and it was found that the percent entrapment efficiency of the formulations ranged between 12.1 to 60%, particle size was between 155.31 ± 23.36 to 360.05 ± 26.06 nm. The in vitro drug release was found to be good with 65 to 76% release of drug. Antibacterial activity was conducted in vitro for streptococcal pneumonia. Their minimum inhibition concentration values were below the minimum concentration of inhibition of clarithromycin, indicating that clarithromycin-loaded CSNPs have more antibacterial properties than the undisturbed drug.

Abdel Moneim *et. al.*, (2020) investigated on the development of a new oral formulation of polydatin-loaded CSNPs to increase polydatin therapeutic potential against type 2 diabetes (42). The mechanism of interaction between polydatin and CSNPs has been investigated via Monte Carlo and molecular dynamics simulations. The formula has been developed and characterized by FTIR, XRD, TEM, and dynamic light diffusion. The cytotoxicity study confirmed that the formulation was safe at both low and high doses. In addition, an in vivo study found that polydatin-loaded CSNPs had very significant anti-diabetic efficacy in diabetic rats compared with free polydatin. Finally, their study demonstrated that CSNPs hold promise for non-toxic and effective polydatin nanocarrier for type 2 diabetes.

Patel and Yadav, (2020) conducted a research on the formulation and in-vitro cytotoxicity of 5-Fluorouracil based on CSNPs for the medical uses of skin cancer diseases (43). In their study, nanoparticles were synthesized using a simple ionic gelation method using different concentrations of chitosan and sodium tripolyphosphate (Na-TPP). According to their study, the optimized 5-fluorouracil charged nanoparticles were found with particle size of about 320 nm, entrapment efficiency of about 85% and Zeta potential of 29 mv. The uniform spherical particle size of prepared nanoparticles were examined by SEM and dynamic light diffusion technique. In vitro release profile indicated in controlled drug release until 24 h.

Razei *et. al.*, (2019) studied on the efficacy of gentamicin loaded CSNPs on *Brucella* infected J774A. 1 murine cells in vitro (44). CSNPS were prepared using ionic gelation technique. The effects of gentamicin-loaded CSNPs and free gentamicin on J774A. 1 murine cells infected with these bacteria were tested. The average size and charge of the nanoparticles were calculated at 100 nm and 28 mV respectively. The loading capacity of nanoparticles was 22%. Approximately 70 percent of the drug was released from nanoparticles within the first 8 hours. Antibacterial activity showed that the MIC (minimal inhibitory concentration) of gentamicin-charged CSNPS was lower than the free drug.

Based on these results, we can conclude that nanoparticles containing the drug have a great chance for optimizing the treatment of intracellular infections.

Kirimlioglu and Ozturk, (2020) formulate CSNPs loaded with levocetirizine hydrochloride (LCD) with high entrapment efficiency and a prolonged effect to optimize the concentration of the plasma drug enhancing bioavailability (45). In their study, LCD was used as a model drug to be trapped in biodegradable natural matter (chitosan) by spray drying. The analytical results demonstrated that nano-sized spherical nanoparticles were performed using this technique. In addition, the nanoparticles had a narrow, characteristic cationic distribution and relatively high encapsulation efficiency. It was shown that all nanoparticles showed an extended release model without a bursting effect compared to the pure drug. In vitro studies have shown that cationic CSNPs containing LCD are efficient carrier candidates.

El-Assal and El Menofy (2019) investigated the potential improvement of cephalexin-based antimicrobial treatments by loading them into CSNPs, then evaluated their antibacterial and anti-biofilm activities and studied their cytotoxicity (46). The CSNPs were prepared by ion gelation process. CSNPs and its charged antibiotics have proven a combination compatible with small Zeta size, proper Zeta potential, maximum encapsulation efficiency and drug loading capacity. The drug release profile of the cephalexin-loaded CSNPs followed the diffusion kinetic model. Chitosan-loaded cephalexin nanoparticles demonstrated better antimicrobial activity than single CSNPs. In addition, CSNPs loaded with cephalexin showed anti-biofilm activity against *E. faecalis* clinical isolate. Although cephalexin-loaded CSNPs exhibited significant antibacterial activity, they were less toxic against mammalian cells. No cytotoxicity was observed against WI-38 fibroblast cells at 23.4 ug/ml. Thus, CSNPs loaded with cephalexin had good stability and a sustained release effect in addition to its anti-biofilm, antimicrobial activities and reduced cytotoxicity.

Chapter 2: Experimental

2.1 Materials

The raw shrimp shell waste as a source of chitosan was collected from local shrimp hatchery in Cox's bazar, Bangladesh. Sodium hydroxide (NaOH), hydrochloric acid (HCl) having purity of 37%, ethanol, (CH₃CH₂OH), sodium tripolyphosphate (Na₅P₃O₁₀), dimethyl sulfoxide [(CH₃)₂SO], di-sodium hydrogen phosphate, (Na₂HPO₄) were of Merck KGaA, Darmstadt, Germany. Glacial acetic acid (CH₃COOH) was from Daejung Chemicals & Metals Co. Ltd, Korea and sodium acetate (CH₃COONa.3H₂O) was of Merck Specialities Private Limited, India. In order to load drugs within chitosan nanoparticles, ciprofloxacin and perindopril erbumine were collected from Reneta Pharmaceuticals Ltd., Bangladesh. Metronidazole and erythromycin was provided by ACI Pharmaceuticals Ltd. and Square Pharmaceuticals Ltd. respectively with potency of 99%. The bacterial strains for antimicrobial study were collected from Veterinary Drug Residue Analysis Division (VDRAD), IFRB, AERE, Savar, Dhaka, Bangladesh.

All the above chemicals used in this study were of analytical grade and were used without further purification.

2.2 Instrumentation

For investigation of the crystalline state of the nanoparticles, powder X-ray diffraction (XRD) patterns were obtained within a range of 5°-70° on an XRD-6000 diffractometer (Shimadzu, Tokyo, Japan) using CuK α radiation having the wavelength of 1.5406 Å at 40 kV and 30 mA. Fourier transform infrared (FTIR) spectra of the materials were recorded in the range of 4000-400 cm⁻¹ on a IR Prestige-21 (Shimadzu, Japan) with 4 cm⁻¹ resolution by using the potassium bromide (KBr) disk method. The percentage of elements in chitosan was determined by elemental analyzer (varioMICRO CHNS). Freeze Drier (LABCONCO, USA) was used to lyophilize the nanoparticles. Morphological characterization and particle size determination of the nanoparticles were done by a transmission electron microscope (TEM) (Hitachi, H-7100) and scanning electron microscope (SEM) equipped with energy dispersive X-ray (EDX), FESEM (JEOL JSM-7600 F, Field Emission Scanning Electron Microscope). The uv-vis spectrophotometer (UV-1800 UV Spectrophotometer, Shimadzu, Japan) was used to determine the association efficiency and the release properties of drugs

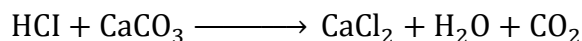
from nanoparticles. Besides, pH Meter (HANNA instruments, pH 210 Microprocessor pH Meter), shaker (NTS-4000A, Japan), sonicator (Powersonic 603) and magnetic stirrer (AGE Magnetic stirrer, VELP scientifica) were used also at different stages of the present research.

2.3 Extraction of Chitosan

Chitosan was extracted from dried waste shrimp shell. For this purpose, the collected, dried shrimp shell was scraped free of loose tissues, washed with water and dried. In this study, to extract chitosan from shrimp shell, the process developed by Rhazi *et al.*, (2000) was followed (47). This process mainly involved the following steps.

2.3.1 Demineralization of Shrimp Shell

Demineralization involves the elimination of minerals from source, mainly calcium carbonate. This process is carried out by hydrochloric acid treatment where demineralization is achieved by decomposing calcium carbonate into the water soluble chloride and releasing carbon dioxide.



Demineralization was performed at room temperature (RT) using 3% HCl for 4 h at a shrimp shell: HCl ratio of 1:10 and this process was repeated. The end of the acid treatment was indicated by the persistence of the acidity in the reaction medium. Most of the minerals present in the shrimp shell react in the same way and produce soluble salt. The soluble salt was then easily separated by filtering the de-mineralized shell and washing it with distilled water until neutral pH was achieved. The demineralized shell was then dried at room temperature (RT) until the weight was found to be constant.

2.3.2 Deproteination of Shrimp Shell

The deproteination step consists of the breakdown of chemical bonds between protein and chitin. Because of the allergic reaction of shellfish in human body in some cases is due to the presence of this protein, the complete removal of protein from shrimp shell is very important. Deproteination was carried out using alkaline treatment with 4% NaOH solutions at 65°-70°C for 2 h at a demineralized shell: NaOH ratio of 1:20. This treatment was

repeated a number of times for the complete removal of protein. The absence of the color of the reaction medium indicates the absence of protein. Then the de-proteinized solid was filtrated and washed in running tap water repeatedly to obtain neutral pH and then rinsed with distilled water.

Then it was bleached by soaking in ethanol for 45 min and then washed with water and dried. The resulting product is known as chitin.

2.3.3 Conversion from Chitin to Chitosan

The chitin derived from the above processes was subsequently deacetylated using 50% NaOH at a chitin to NaOH ratio of 1:20 for 72 h at room temperature (RT) under occasional stirring. The product obtained was filtered and washed to neutrality with distilled water and dried. The dried product is the chitosan after the first deacetylation process. The deacetylation process was repeated with this chitosan using the same concentration of NaOH for 48 h at RT to get higher degree of deacetylation in chitosan.

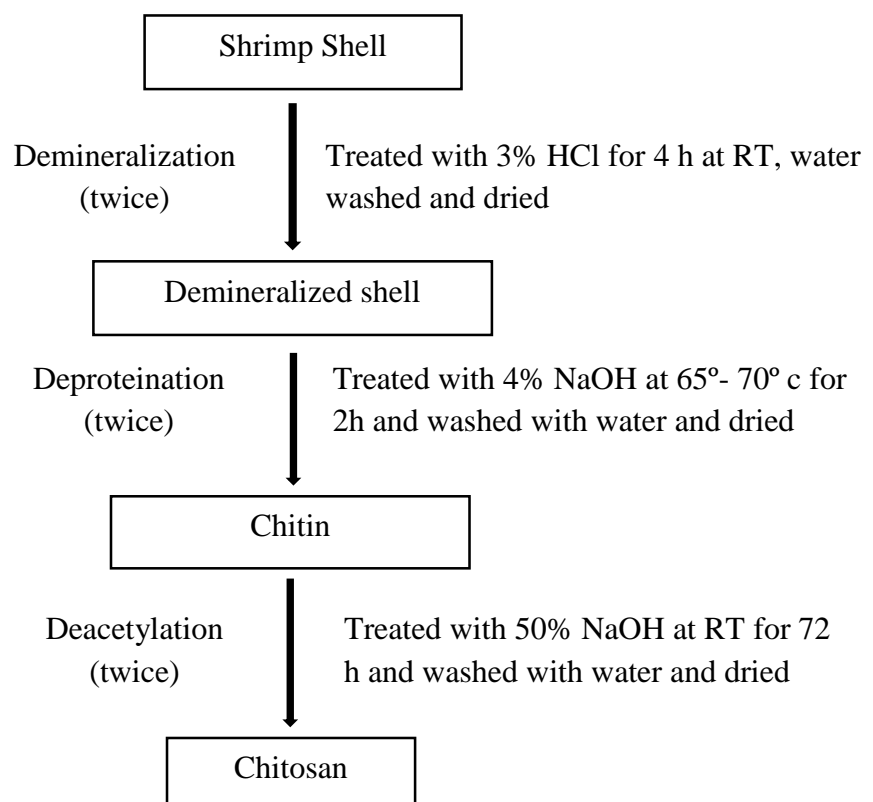


Figure 2.1: Flow diagram of extraction of chitosan from shrimp shell

2.4 Characterization of Chitosan

The effectiveness of the method to extract chitosan depends to a large extent on the quality of the product produced. Therefore, certain characterization techniques were used to substantiate the efficacy of the method. A detailed characterization test may enable us to identify the compound and p a pre-justification about the product. The following characterization tests of chitosan was done to find a brief idea about the quality of the product produced from the method.

2.4.1 Solubility

For solubility test, 1.0 gram of extracted chitosan was dissolved in 50 ml of 1% acetic acid at room temperature. After forming a homogeneous solution, this acidic solution of chitosan was filtered and the solubility percentage was obtained by the following equations (48):

$$\text{Insoluble chitosan, g} = \text{Final weight of dried filter paper, g} - \text{Initial weight of filter paper, g} \quad (2.1)$$

$$\text{Insolubility, \%} = [\text{Insoluble chitosan, g} / \text{Sample taken, g}] \times 100\% \quad (2.2)$$

$$\text{Solubilty, \%} = 100 - \text{Insolubility} \quad (2.3)$$

2.4.2 Molecular Weight (MW) Determination

Molecular weight (MW) is one of the most fundamental parameters to characterize chitosan. There are different techniques to determine the molecular weight of chitosan such as static light scattering (SLS), gel permeation chromatography (GPC) and intrinsic viscosity measurement. Among them, intrinsic viscosity measurement is the rapid and simplest for determination of MW of chitosan. In the present work, intrinsic viscosity measurement was used to determine the MW of chitosan. The intrinsic viscosity (η) of chitosan was determined using Oswald viscometer. First, the chitosan samples, was dissolved in the buffer solution containing acetic acid and sodium acetate (0.2 M CH_3COOH /0.1 M CH_3COONa) to obtain a chitosan solution of concentration of 0.02g/ml. The solutions were then filtered through Whatman no. 40 filter paper. The viscometric parameters were obtained at $25 \pm 0.05^\circ \text{c}$ in a temperature controlled water bath. The measurement was started with the solvent flow time and then the flow time of the five different dilutions from the

initial stock solution of chitosan. For each chitosan concentration, the values of the flow time were used to determine the following viscosities using equations (2.4), (2.5) and (2.6).

$$\text{Relative viscosity, } \eta_{rel} = t/t_0 \quad (2.4)$$

$$\text{Specific viscosity, } \eta_{sp} = \eta_{rel} - 1 \quad (2.5)$$

$$\text{Reduced viscosity, } \eta_{red} = \eta_{sp}/C \quad (2.6)$$

where, t is the flow time of the chitosan solutions, t_0 is the flow time of the solvent and C is chitosan concentration in the solution. Then the intrinsic viscosity (η) was obtained from the plot of reduced viscosity (η_{red}) vs. chitosan concentration (C). The intercept obtained from the extrapolation of this plot to zero concentration represents the intrinsic viscosity. By using this intrinsic viscosity (η), the MW of chitosan was calculated using the equation below known as Mark-Houwink equation.

$$\eta = KM_v^\alpha \quad (2.7)$$

where, M_v is viscosity average molecular weight, K and α are constants, The value of which depend on the polymer type and the chosen solvent.

2.4.3 Fourier Transform Infrared (FTIR) Spectroscopy Analysis

Among the various characterization techniques of a sample, Fourier transform infrared (FTIR) spectroscopy is commonly used as it is very simple and non-destructive analysis. In IR spectroscopy, the IR radiation of different wavelength interacts with matter which is absorbed, emitted or reflected. It can be used in identifying the functional groups or chemical substance in liquid, solid or gaseous forms. The infrared spectrophotometer produces IR spectrum in this method. An IR spectrum is a graph which is obtained from the plot of the absorbance of infrared light against its wavelength or wavenumber. The spectrum of a material is unique and no compound can produce similar spectrum with another. So, IR spectroscopy gives qualitative analysis of different materials.

Infrared spectra for the samples of chitin and chitosan were recorded from FTIR spectrophotometer (IR Prestige-21, Shimadzu) in the range of 400-4000 cm^{-1} at the Department of chemistry, University of Dhaka, Bangladesh. The samples were taken in a mortar, thoroughly grinded with potassium bromide (KBr) in a ratio of 1:100 and then the mixture was pressed in an automatic hydraulic press to form a translucent pellet. This was

placed in the sample cavity of the IR spectrometer for the IR beam to pass through. The tentative band in IR spectra due to various functional groups have been tabulated on the basis of some standard books.

2.4.4 Elemental Analysis

The analysis of a material to determine its elemental or isotopic composition is known as elemental analysis. It can be qualitative (determining the elements present in the sample), and also can be quantitative (determining the mass of the elements). The CHNS analysis, the most common form of elemental analysis, was performed by combustion analysis. The determination of sulfur along with carbon, hydrogen and nitrogen in the same measurement run is also possible in modern elemental analyzers.

The carbon, hydrogen and nitrogen contents in chitosan were determined through elemental analysis using varioMICRO CHNS elemental analyzer.

2.4.5 Degree of Deacetylation (DDA)

The degree deacetylation (DDA) of chitosan indicates the molar fraction of *N*-glucosamine in chitosan which is composed of *N*-glucosamine and *N*-acetylglucosamine that means deacetylated monomer units present in chitosan. It can be represented as:

$$DDA = \frac{n_{GlcN}}{(n_{GlcN} + n_{GlcNAc})} \times 100) \quad (2.8)$$

where, n_{GlcN} and n_{GlcNAc} represents the average number of *N*-glucosamine and *N*-acetylglucosamine units within the polymer chain respectively. The DDA of the extracted chitosan samples was calculated by using data obtained from FT-IR spectrum of chitosan. Measurements were performed by using KBr pellet containing chitosan sample which was prepared by mixing chitosan with KBr in the mass ratio of 1:100 (2 mg chitosan and 200 mg KBr). The spectra of chitosan samples were obtained within a frequency range of 400 - 4000 cm^{-1} . Thus DDA of chitosan was calculated from the produced IR spectra of extracted chitosan sample. Several equations and procedures were used in different literatures for calculation of DDA using FT-IR method. In this study, DDA was calculated from the absorption bands at 1320 which is the characteristic of amide that means the acetylated amine and the band at 1420 cm^{-1} is chosen as the reference band. Finally, the DDA of chitosan was calculated using the following equation (49):

$$\%DDA = 100 - \frac{(A_{1320}/A_{1420})-0.3822}{0.03133} \quad (2.9)$$

2.4.6 X-ray Diffraction (XRD) Analysis

The crystalline phase identification of a material and determination of the unit cell dimension, the analytical technique that is used preliminary is the X-ray powder diffraction. It is also a characterization technique that provide information about sample purity and atomic spacing. In X-ray diffraction method, the cathode tube produces X-ray which is then filtered and generate monochromatic radiation and directed towards the sample. The constructive interference is produced when the condition of the interaction of monochromatic incident rays with the sample satisfy the Bragg's Law ($n\lambda = 2d \sin \theta$) which relates the lattice spacing in a sample and wavelength of electromagnetic radiation to diffraction angle. This constructive interaction produces diffracted ray which is recorded, processed and counted. All possible diffraction directions is attained by scanning the sample through a range of 2θ angles. These signals is then converted to a count rate and the resulting data is then output to a device like computer monitor. In this study, crystallinity of the samples was investigated from X-ray diffraction analysis by using XRD 7000 (Shimadzu, Kyoto, Japan) diffractometer equipped with Ni-filtered Cu- α radiation of wavelength 1.5406 Å). XRD measurements were carried out at 2θ range of $5^\circ - 70^\circ$ with a step size of 0.02 in continuous mode. The diffractometer was operated at 40 mA and 40 kV. The intensity of the peak around 20° which corresponds to maximum intensity and the peak intensity at 16° , considered as amorphous diffraction were used to calculate the crystallinity index (CrI_{020}) with respect to 020 plane. CrI_{020} was calculated using Equation 2.10 based on the data obtained from the diffractogram (50).

$$CrI_{020} \% = (I_{020} - I_{am}) \times 100 / I_{020} \quad (2.10)$$

where, CrI_{020} is the crystallinity index at 020 phase, I_{020} is the maximum intensity at around 20° and I_{am} is the amorphous diffraction at 16° .

2.5 Preparation of Chitosan Nanoparticles (CSNPs)

There are various methods to prepare chitosan nanoparticles (CSNPs) such as, ionotropic gelation, emulsion based solvent evaporation, emulsification, solvent diffusion as well as the microemulsion method (51, 52, 53). Among these methods, ionotropic gelation is most common and widely used. In the present study, the methodology that was followed to prepare CSNPs by inducing the gelation of chitosan solution to Na-TPP (24). The mechanism involves the electrostatic interactions between the positively charged amine groups of chitosan and a negatively charged polyanion, such as sodium tri-polyphosphate (Na-TPP) (54). In brief, specific weight of chitosan was dissolved in 1% acetic acid to prepare chitosan solutions of different concentrations. An aqueous solution of Na-TPP was also prepared at a concentration of 0.25% (w/v), 1% (w/v) and 2% (w/v).

The Na-TPP solution was added dropwise to the chitosan solution and the chitosan-TPP nanoparticles was started to form spontaneously by ionic crosslinking of TPP and chitosan. The Na-TPP was added to the chitosan solution in the chitosan to TPP ratio of 5:1. This procedure was carried out under mild constant magnetic stirring for 30 minutes at RT. The preparation procedure was optimized by varying the chitosan and TPP concentration. Table 2.1 shows the five different formulations varying the chitosan and TPP concentration for observation of nanoparticle formation and also study of optimal condition.

Table-2.1: Different composition of chitosan and TPP used in chitosan nanoparticle preparation

Formulation code	Chitosan concentration (%)	Na-TPP (%)	Ratio (Chitosan:TPP)
CS01	0.5	0.25	5:1
CS02	0.5	1	5:1
CS03	2	0.25	5:1
CS04	2	1	5:1
CS05	2	2	5:1

The results were confirmed visually. Upon addition of Na-TPP into chitosan solution, an opalescent suspension was formed due to the nanoparticle formation. After the formation of nanoparticle suspensions, it was centrifuged for 15 min. The supernatants were discarded and the CSNPs were repeatedly rinsed with distilled water. The CSNPs were then frozen

and lyophilized by freeze drier. The nanoparticles were freeze dried at a maximum temperature of - 50° c and maximum vacuum of 0.340 mbar to obtain dried CSNPs.

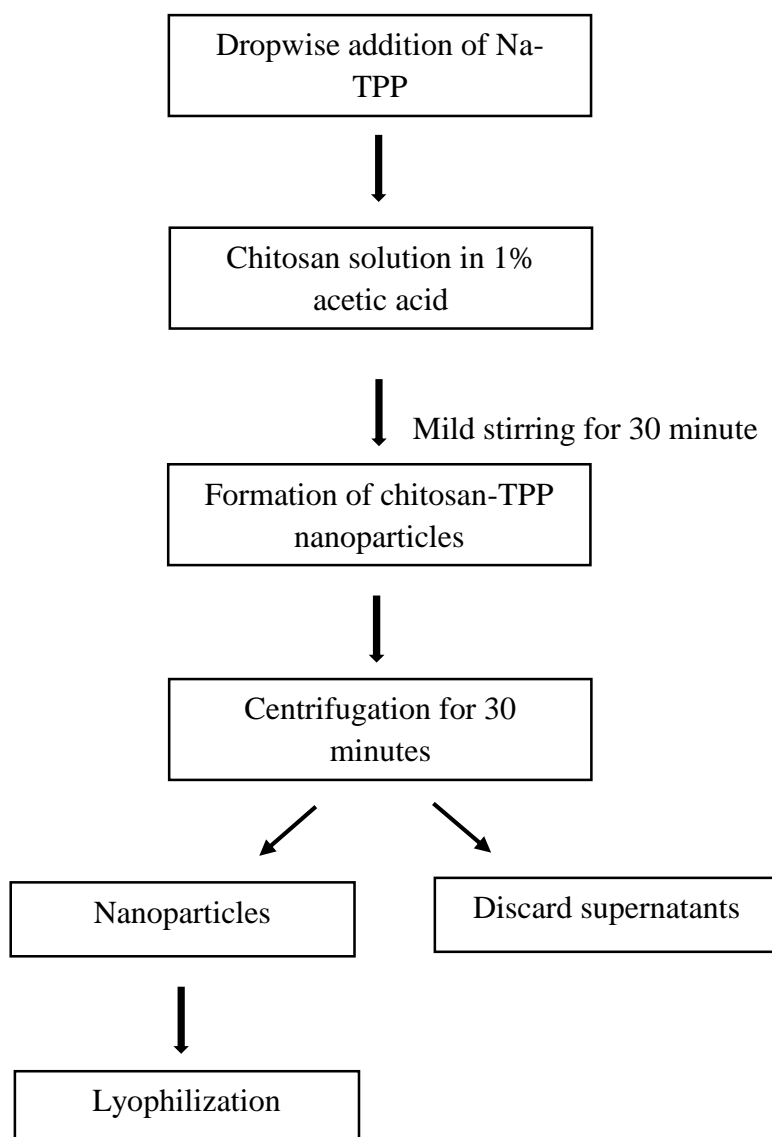


Figure 2.2.: Procedure for chitosan nanoparticles preparation

2.6 Drug Loading into/on Nanoparticles of Chitosan

The drugs were loaded to chitosan nanoparticles systems during the preparation of the particles. For this purpose, four different types of drugs were selected for loading into/on CSNPs system. Three of these were antibiotics. Ciprofloxacin (CP) is one of them which is an oral antimicrobial drug. Bioavailability of CP can be increased by formulating ciprofloxacin with CSNPs. Metronidazole (MTZ) is another one which is an antiprotozoal,

amoebicide and antibiotic effective against various anaerobic bacteria and certain parasites. It is one of the most used drugs for giardiasis, intestinal amoebiasis, bacterial vaginosis, trichomoniasis, surgical infections as well as duodenal ulcer which is associated with helicobacter pylori infections, etc. Another antibiotic used was erythromycin (ER) which is used to treat certain infections of the respiratory tract, including bronchitis, pneumonia, diphtheria, syphilis etc. The last one is perindopril erbumine (PE) which is an antihypertensive drug and acts by inhibiting the angiotensin-converting enzyme (ACE) (55).

2.6.1 Ciprofloxacin (CP) Loading into/on Chitosan Nanoparticles (CSNPs)

For the association of ciprofloxacin (CP) with chitosan nanoparticles (CSNPs), CP was added to the chitosan solution before adding the TPP solution in it. It is theorized that CP will be loaded to the CSNPs during the ionotropic gelation process. Briefly, ciprofloxacin (CP) powder was dissolved in 2% (w/v) chitosan solution in a CP and chitosan ratio of 0.5:1, 0.65:1, 0.8:1 and 1:1. Finally, Na-TPP solution having a concentration of 1% was added to the above mixture in a chitosan to TPP weight ratio of 5:1 under continuous magnetic stirring. The reaction was kept for 30 minutes at RT and an opalescent suspension of ciprofloxacin loaded chitosan nanoparticles (CP-CSNPs) were formed. Then the CP-CSNPs were separated from the suspension by using centrifugation process and were freeze dried. The effect of concentration of CP in chitosan solution on the efficiency of CP to load into/on CSNPs were also investigated by changing the ratio of CP to chitosan ratio as shown in [Table 2.2](#).

Table 2.2: Designed formulations for CP-CSNPs formation varying the ratio of CP and chitosan

Formulation	Chitosan concentration (%)	TPP concentration (%)	Ratio (chitosan:TPP)	Ratio (chitosan: CP)
CS1	2	1	5:1	1:0.05
CS2	2	1	5:1	1:0.65
CS3	2	1	5:1	1:0.8
CS4	2	1	5:1	1:1

2.6.1.1 Evaluation of CP loading within CSNPs

UV- spectrophotometry was used to determine the amount of ciprofloxacin (CP) loaded to chitosan nanoparticles (CSNPs) (56, 57). Absorbance of the samples were determined using UV-1800 Shimadzu UV Spectrophotometer. All of the spectrophotometric measurements were conducted at $\lambda = 316$ nm. The operating wavelength was chosen on the basis of the wavelength scans of CP, chitosan and TPP. At 316 nm, the wavelength peaks of chitosan and TPP do not interfere with the peak of CP. Thus, after separating the CP-CSNPs from the suspension by centrifugation, the amount of free CP in the supernatant was measured using a UV spectrophotometer at 316 nm. The amount of CP loaded or associated was evaluated from the difference between the total quantity of CP added to the loading solution and the quantity of non-entrapped CP remaining in the supernatant. Finally, association efficiencies (AE) of the nanoparticles were calculated as follows:

$$AE \% = \frac{T_c - T_f}{T_c} \times 100 \quad (2.11)$$

where, T_c is the total CP used to prepare the nanoparticles and T_f is the free CP in the supernatant.

Association efficiency (AE) indicates the efficiency of the preparation method as it express the total amount of drug within the nanoparticles. Drug release is the reverse process of drug loading which involves the release of drugs from solid phase for pharmacological action. So, AE indicates the performance of a drug delivery system as it impacts the rate and extent of drug release from that system.

2.6.2 Erythromycin (ER) Loading into/on Chitosan Nanoparticles (CSNPs)

Chitosan solution was prepared by dissolving it in 1% acetic acid to make 2% chitosan solution. Then erythromycin (ER) was added to chitosan solution in the ER to chitosan ratio of 1:2. Then 12 ml of 1% Na-TPP was added drop wise to 30 ml chitosan solution under constant magnetic stirring at RT. An opalescent suspension was formed. The suspension was kept at rest for 3 h to obtain erythromycin loaded chitosan nanoparticles (ER-CSNPs). These ER-CSNPs were separated from the suspension using centrifugation method for 20 min. Then the separated ER-CSNPS were lyophilized at -50° c and stored for further analysis

2.6.2.1 Evaluation of ER loading within CSNPs

The loading of ER on CSNPs, that is, the association efficiency (AE) of ER was evaluated using uv-spectrophotometry. The actual ER loading amount was calculated from the difference between the initial amount of ER dissolved in chitosan solution and the free ER in the supernatants. The absorbance of the clear supernatant was measured using a uv-visible spectrophotometer (UV-1800 Shimadzu UV Spectrophotometer, Kyoto, Japan) at 275 nm. The amount of ER which were not loaded or associated with CSNPs was obtained by comparing the uv absorbance of the supernatant with a concentration versus absorbance calibration curve of ER in chitosan solution. The AE was calculated using the formula,

$$AE \% = \frac{T_{ER} - T_f}{T_{ER}} \times 100 \quad (2.12)$$

where, T_{ER} is the initial amount of ER dissolved in chitosan solution and T_f is the amount of ER in the supernatants.

2.6.3 Metronidazole (MTZ) Loading into/on Chitosan Nanoparticles (CSNPs)

Metronidazole loaded chitosan nanoparticles (MTZ-CSNPs) was also prepared by ionic gelation method. At first 2% chitosan solution was prepared in 1% glacial acetic acid. Then aqueous solution of 1% Na-TPP was prepared in distilled water. For the preparation of MTZ-CSNPs, MTZ was added to chitosan solution in a MTZ to chitosan ratio of 0.5:1 before adding Na-TPP. Then Na-TPP was added drop wise into the chitosan solution containing MTZ in a chitosan to TPP ratio of 5:1 under magnetic stirring at RT for 30 minutes. The nanoparticles formed were obtained by centrifugation and finally dried at -50°C using freeze drier.

2.6.3.1 Evaluation of MTZ loading within CSNPs

Association efficiency (AE) of MTZ-CSNPs were determined by measuring the ultraviolet absorption of the supernatant obtained after centrifugation using UV-visible spectrophotometer at 223.5 nm. The percentage of association efficiency of MTZ-CSNPs were calculated using equation 2.10.

$$AE \% = \frac{T_{MTZ} - T_f}{T_{MTZ}} \times 100 \quad (2.13)$$

Where, T_{MTZ} is the total amount of MTZ used to prepare MTZ-CSNPs and T_f is the free MTZ in the supernatants.

2.6.4 Perindopril Erbumine (PE) Loading into/on Chitosan Nanoparticles (CSNPs)

Perindopril erbumine (PE) was loaded to CSNPs during the preparation of nanoparticles. Approximately 2% of chitosan solution in 1% acetic acid was prepared. For the association of PE into CSNPs, it was added first into the chitosan solution in a PE and chitosan ratio of 1:1 before adding Na-TPP in it. Then, perindopril erbumin loaded chitosan nanoparticles (PE-CSNPs) was formed by drop wise addition of 1% aqueous Na-TPP into chitosan solution containing PE. The reaction was kept under continuous magnetic stirring for 30 minutes at RT and suspension of PE-CSNPs were formed. Then the PE-CSNPs were separated from the suspension by centrifugation and were freeze dried.

2.6.4.1 Evaluation of PE loading within CSNPs

PE-CSNPs suspension was transferred to a centrifugal tube and the nanoparticles were separated from the suspension by centrifugation method for 30 min. PE content in the supernatant was measured by a UV spectrophotometer at 223.5 nm. The association efficiency of PE with CSNPs was calculated using equation 2.9.

$$AE \% = \frac{T_{PE} - T_f}{T_{PE}} \times 100 \quad (2.14)$$

where, T_p is the total amount of PE used to prepare nanoparticles and T_f is the free PE in the supernatants.

2.7 Characterization of Drug Loaded Chitosan Nanoparticles (CSNPs)

2.7.1 SEM Analysis

The scanning electron microscope (SEM) is a microscope which uses electrons instead of light to form an image. Chemical analysis, surface analysis as well as imaging of materials are performed using a SEM. SEM can produce image with magnification from 10 times

(equivalent to a powerful hand-lens) to more than 500,000 times, about 250 times of the best light microscopes.

The surface morphology of unmodified CSNPs and the drug loaded CSNPs were observed using SEM. The samples for SEM analysis were prepared by completely drying the sample and then coating with platinum in vacuum. Then the micrograph of the particles were captured by FESEM (JEOL JSM-7600 F, Field Emission Scanning Electron Microscope) at the Department of Glass and Ceramics, Bangladesh University of Engineering and Technology, Bangladesh.

2.7.2 EDX Analysis

The Energy Dispersive X-ray (EDX) spectroscopy is an analytical technique used for the microanalysis of the composition or chemical characterization of a sample. The fundamental principle of EDX is that each element has a unique atomic structure and creates unique set of peaks on its X-ray spectrum (58). It is used for material characterization by qualitative and semi-quantitative microanalysis on a sample from a relatively low (25×) to high magnification (20,000×).

The elemental analysis of the unmodified CSNPs and CSNPs loaded with drugs was implemented by a FESEM (JEOL JSM-7600 F, Field Emission Scanning Electron Microscope) equipped with an energy dispersive X-Ray spectrum (EDS), which can provide a rapid qualitative and quantitative analysis of the elemental composition.

2.7.3 TEM Analysis

Transmission electron microscopy (TEM) is a technique based on the interaction of electrons with the specimen when the electron beam is transmitted through the specimen. TEM instruments can form an image of significantly higher resolution than the image formed in a light microscopes. The instrument captures the fine detail of the specimen, even as small as individual atoms, which is thousands time smaller than the object seen in a light microscope. Thus TEM can be used to observe crystal structure, to analyze shape, size, quality and density of quantum dot, wells and wires and so on, thus considered as an essential tool for nano science in both materials and biological fields. The morphology and size characteristics of unmodified CSNPs and the CSNPs loaded with different drugs were

observed by a “Transmission Electron Microscope (TEM) (Hitachi, H-7100). The TEM sample was obtained by using a pastor pipette to place a drop of the chitosan nanoparticle suspension onto carbon-coated copper grids. The samples were dried at room temperature and then examined without any further modification or negative staining.

2.7.4 FTIR Analysis

FTIR spectroscopic analysis was done to investigate the interaction of functional groups in CSNPs for drug loading using IRPrestige-21, SHIMADZU at the Department of Chemistry, University of Dhaka, Bangladesh. The samples for FTIR analysis was prepared by mixing about 2 mg of the sample with 200 mg KBr and it was then compressed to form pellets. These pellets were analyzed in FTIR instrument within the range of 400-4000 cm^{-1} .

2.7.5 XRD Analysis

The crystalline phase of the nanoparticles were analyzed by powder X-ray diffraction (XRD) patterns using an XRD 7000 shimadzu (Shimadzu, Kyoto, Japan) diffractometer equipped with Ni-filtered Cu- $K\alpha$ radiation ($\lambda=1.5406\text{\AA}$). The diffractometer was operated at 40 kV and 40 mA. Diffraction patterns were recorded within 2θ range of $5^\circ-70^\circ$ in a continuous mode. The step size was 0.02° .

2.8 Biomedical Application of Drug Loaded Chitosan Nanoparticles

Chitosan nanoparticles (CSNPs) are extensively used nanoparticle systems applied in the biomedical field. For delivery of drugs, it can adsorb or be loaded with multiple drugs and can effectively control the release of drugs. Additionally, it can encapsulate drugs on their surfaces for using in drug delivery as well as act as an antimicrobial.

2.8.1 In Vitro Release of Drugs from chitosan Nanoparticles (CSNPs)

The drug release profiles of chitosan nanoparticles (CSNPs) that were loaded with different drugs in vitro were investigated over time in an appropriate dissolution media. Phosphate-buffered saline (PBS) with the pH of 7.4 was selected as the dissolution medium in this case

as it is isotonic and the pH remains nearly constant with time. Besides, the ion concentrations and osmolality is generally equivalent to those of human fluids. The nanoparticles loaded with different drugs were suspended in 50mL of PBS and then it was put into the water bath shaker under the condition of 37⁰C and 150 rpm. To determine the amount of free drug in the release media at a certain time, 5 mL of the samples were withdrawn at that specific time and were transferred to another test tube. The volume of the main nanoparticles suspension was kept constant by adding another 5 ml of fresh dissolution media to avoid saturation of the media. The process was repeated after scheduled time intervals. The samples that were withdrawn at different time intervals were analyzed by UV-spectrophotometer. The quantity of released drugs in the dissolution media at each scheduled time points was assessed by comparing the uv absorbance of the sample withdrawn at that time with a standard curve of concentration vs. uv absorbance of the series of diluted drug solution in PBS.

Finally, cumulative release (%) of drugs were determined using the following equations:

$$\text{Concentration of drug, } \mu\text{g/ml} = (\text{slope} \times \text{absorbance}) \pm \text{intercept} \quad (2.15)$$

$$\text{Amount of drug released} = \text{Concentration} \times \text{Dissolution bath volume} \times \text{dilution factor} / 1000 \quad (2.16)$$

$$\text{Cumulative release, \%} = \text{Volume of sample withdrawn} \times P_{(t-1)} / \text{Bath volume} + P_t \quad (2.17)$$

where, P_t = percentage of drug release at time t and $P_{(t-1)}$ = percentage of drug release previous to t .

2.8.2 Antibacterial Activity Analysis

The antibiotic drugs (CP and ER) loaded chitosan nanoparticles (CSNPs) were investigated for antibacterial activity against both gram positive and gram- negative bacteria. The bacterial strains were collected from Veterinary Drug Residue Analysis Division (VDRAD), IFRB, AERE, Savar, Dhaka, Bangladesh. All steps of the work were carried out at Molecular Radiobiology and Biodosimetry Division (MRBD) of the same institute. The activities were analyzed by using disc diffusion assay as well as determining the minimum inhibitory concentration (MIC) and minimum bactericidal concentration (MBC).

Preparation of media and plates: Muller-Hinton agar (MHA) media was prepared from the dehydrated medium according to the manufacturer instruction. The accurate weight of Muller-Hinton broth (MHB) powder was dispersed in distilled water was mixed thoroughly

and autoclaved at 121°C for 15 minutes. 1.7% of agar was added to it before autoclaving. After this, the agar medium was cooled and poured into sterile petridishes in a laminar air flow cabinet maintaining aseptic condition before being solidified. 20 ml of media was poured into each petridish to get a uniform thickness and then the medium was allowed to cool to become solidified. After solidification, the plates were dried in laminar air flow cabinet for 30 minutes by keeping lids opened, so that there was no excess surface moisture on the plates.

Preparation of bacterial suspension: The microorganisms to be tested were streaked from pure culture on the MHA plate and was incubated at 37°C for 18-24 h. Then, three isolated colonies from this fresh culture were taken by touching with sterile loop or swab culture plate were taken and transferred into 4 ml of MHB medium and mixed thoroughly by vortexing. The broth was then incubated the broth at in a shaker at 37⁰ c at 225 r.p.m. until it reaches to the visible turbidity equal to or greater than that of a McFarland Standard 0.5. The turbidity was also verified measuring the absorbance of the suspension spectrophotometrically. The absorbance of the suspension should be in the same range as that of the McFarland standard 0.5 (0.08–0.1 at OD625 nm). After adjusting the absorbance of bacterial suspension, it was then diluted in sterile MHB by a factor of 1:100 to prepare the inoculum.

Measurement of zone of inhibition by disc diffusion techniques: The test samples of concentration were applied on a sterile filter paper discs with a micropipette. The solvents from the discs were evaporated by keeping the discs at oven at 40 °C for 1 hour. Then the discs were placed gently on the MHA plates which was previously seeded with 100 µL of fresh culture. The plates were then kept in a refrigerator at 4°C for 2 h to diffuse the test samples from the disc to a considerable portion of the agar media. After that, the plates were incubated at 37°C for 16 h. After the incubation period, the diameter of the zone of inhibition produced by each test samples were measured in mm.

Determination of MIC and MBC by broth macro dilution method: The various dilutions of the test antibiotic drugs and drug loaded chitosan nanoparticles samples in sterile MHB were prepared in the concentration range of 0.06 – 128 mg l⁻¹. Then 1 ml of each dilutions were added to different test tubes for testing the bacterial isolates. One test tube was filled with 1 ml of sterile MHB without antimicrobial agent (negative control) and another with 1 ml of bacterial suspension (growth control) was considered as controlled. Now each of test

test tube containing the sample solution and the growth control test tubes were inoculated with 1 ml of bacterial suspensions and incubated at 37⁰c, shaking at 225 rpm for 16 hrs.

Chapter 3: Results and Discussion

Over the past decades, biomaterials have been extensively developed and utilized in medical devices. Among these materials, chitosan have attracted more attention due to various advantages like biocompatible and biodegradable properties as well as it is a nontoxic material. In this thesis, a method of producing chitosan-based nanoparticles has been introduced as potential medical applications. Chitosan-based nanoparticles, with different antibiotic and antihypertensive drugs, were successfully prepared, showing good performance towards antibacterial activities and as a carrier of drugs.

3.1 Chitosan Yield and Efficiency of Method

The extraction of chitosan from wasted shrimp shells was performed by using a conventional method with some improved efficiency and simplicity. In this extraction process, demineralisation and deproteinisation of shrimp shells were carried out to get chitin, followed by deacetylation of chitin to obtain chitosan from raw shrimp shells. During the extraction process of chitosan, only deacetylation used longer treatment time as it was the only process without complicated requirements such as nitrogen purging, autoclave condition or high temperature reflux (59).

The percentage yield of chitosan was determined based on the dry weight of chitosan derived from the dried shell of shrimp. During the extraction process, at first 14.38 g demineralized shrimp shell were produced from 50 g of dried shell by de-mineralization step. The percentage of yield in this step was 28.76 %. Then the deproteination was carried out and the obtained product is known as chitin. The amount of chitin was 12.5 g. The double de-acetylation of chitin gives chitosan as a final product. The amount was 5.24 g and 4.09 g after first and second deacetylation, respectively. Thus, from 50 g shrimp shell, 4.09 g chitosan was obtained which indicates the percent yield of chitosan from shrimp is only 8.18 % and this result is very similar to various studies. In a study, the percentage yield of chitosan was obtained in the range of 5.6-13.5% (60)

Scheme of the extraction of chitosan from wasted shell of shrimp is shown in [Figure 3.1](#) and [Table 3.1](#) bellow shows the summery of the product yield. Finally, about 615 g of raw shrimp shell were treated according to the same method step by step and about 45 g of

chitosan was obtained and stored for characterization and uses for production of chitosan nanoparticles and other studies.

Table-3.1: Percent yield of products during the extraction of chitosan from shrimp shell.

Dried shrimp shell	De-mineralized shrimp shell	Deproteinized shrimp shell or Chitin	Chitosan
50 g	14.38 g	12.50 g	4.09 g
100 %	28.76 %	25 %	8.18 %

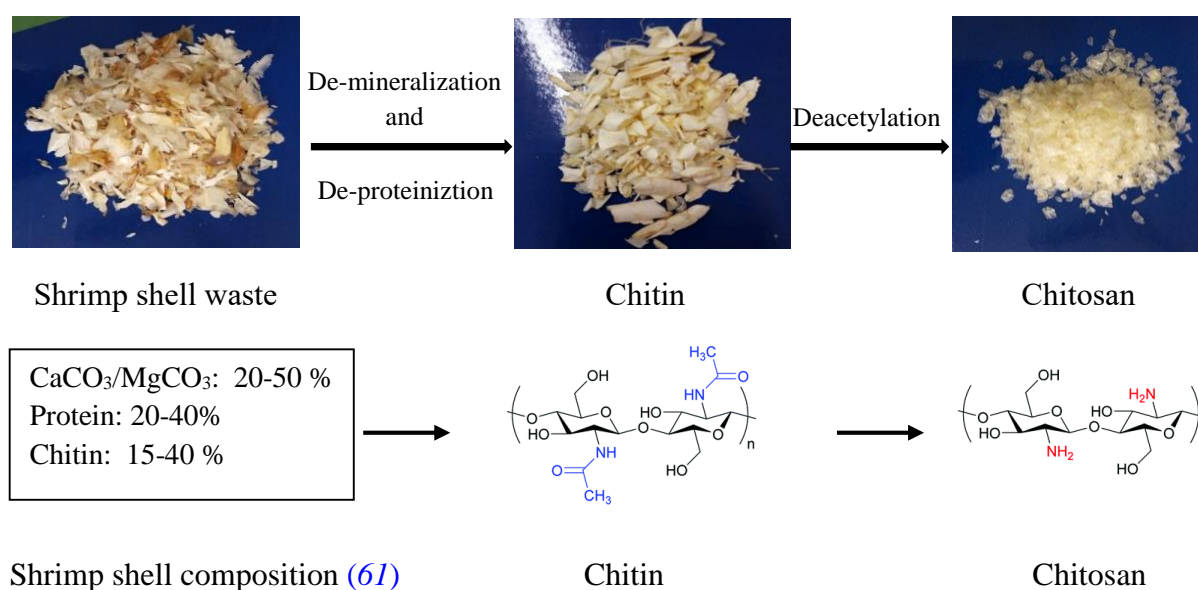


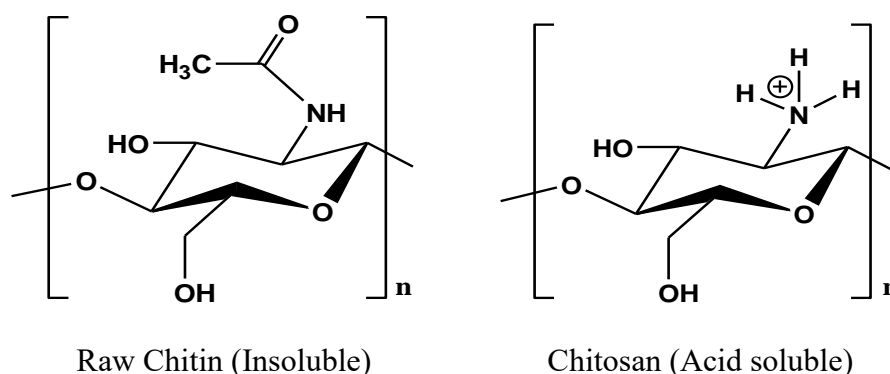
Figure 3.1: Extraction of chitosan from shrimp shell

3.2 Characterization of Chitosan

3.2.1 Solubility

The solubility test of chitosan helps to give a brief idea about the quality of the products produced from the method. The lower solubility is because of the incomplete removal of acetyl group from chitin and also incomplete deproteination during the extraction process (62). Therefore, lower value of degree of deacetylation (DDA) shows negative effect on the solubility of chitosan.

Raw chitin is insoluble in any solvents due to the insufficient protonated amino groups (63, 64). In chitosan, as the DDA increases, contents of amino groups increases and solubility also increases. In this study, the average solubility of chitosan obtained was 82.85%. In comparison to previous study, it may varied from 17.43 to 95.29% with an average of 57.52% (65). The higher solubility obtained in this study indicates that the extracted chitosan contains higher contents of amino groups which is protonated in acidic medium like as equation (3.1) and this allows chitosan to dissolve in acidic solution.



Finally, the higher solubility indicates the higher degree of deacetylation (DDA) of chitin which means that better chitosan has been produced.

3.2.2 Viscosity Average Molecular Weight

The viscometric parameters were measured from the flow time of the solvent (0.2 M $\text{CH}_3\text{COOH}/0.1 \text{ M } \text{CH}_3\text{COONa}$) and the series of diluted chitosan solution using equation (2.4), (2.5) and (2.6). The concentration of chitosan solution was 0.05%, 0.1%, 0.2%, 0.4% and 0.8%.

The value of intrinsic viscosity was obtained 2.001 from the intercept of the plot of reduced viscosity against chitosan concentration (Figure 3.2) by extrapolating it to zero concentration. Viscosity-average molecular weight was derived from $[\eta] = K M_v^\alpha$, where $K = 1.424 \times 10^{-5} \text{ (dm}^3/\text{g)}$ and $\alpha = 0.96$ for chitosan and the solvent 0.2 M $\text{CH}_3\text{COOH}/0.1 \text{ M } \text{CH}_3\text{COONa}$. Thus, molecular weight of chitosan was obtained $2.3 \times 10^5 \text{ Da}$. Depending on the various parameters during production, such as, concentration of alkali, source, temperature, reaction time, dissolved oxygen concentration, the residual aggregates in the

solution, chitin concentration and shear stress, the molecular weight of chitosan may be varied (66).

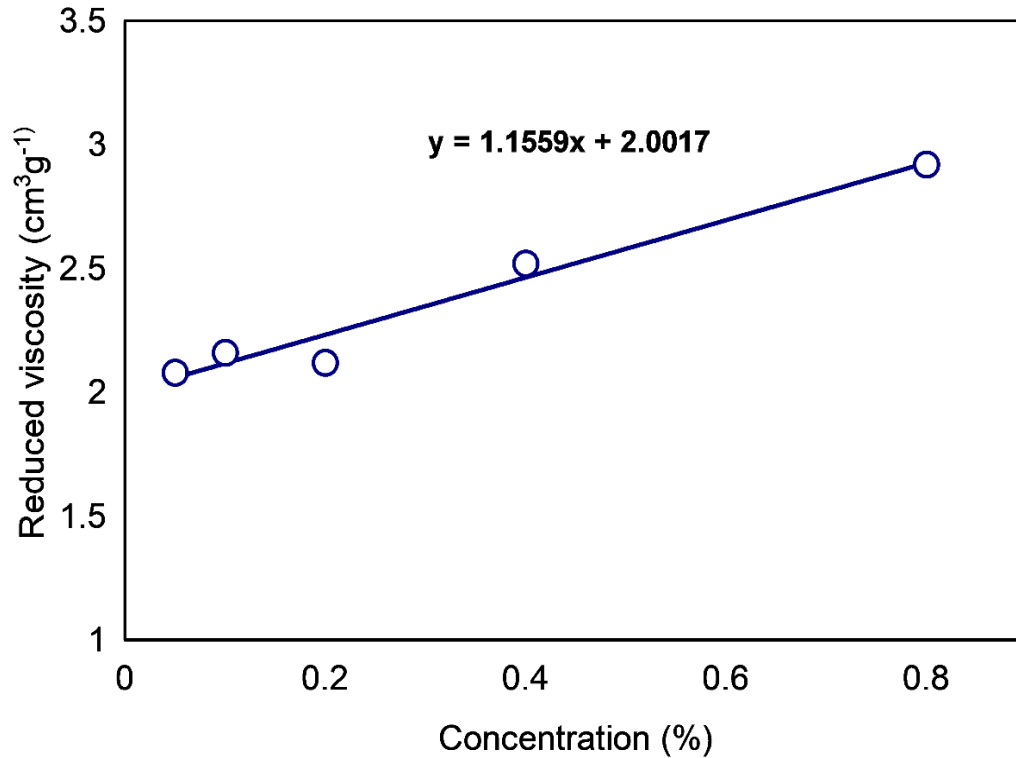


Figure 3.2: Plot of Reduced viscosity against Chitosan concentration

Molecular weight obtained for chitosan is in the range that were found in previous studies. In a study, the molecular weight of shrimp chitosan was between 2.3×10^5 to 2.8×10^5 Da (67). The chitosan of molecular weight ranged from 10,000 Da to 250,000 Da are grouped as low molecular weight chitosan (68). So the extracted chitosan in this study is of low molecular weight chitosan.

The molecular weight of chitosan is considered as one of the standard of quality. Chitosan having a medium molecular weight shows higher anti-cholesterol activity than chitosan containing high molecular weight (69). On the other hand, chitosan possessing low molecular have high biological activities (70) and hence can be appropriately used in biomedical and pharmaceutical fields.

3.2.3 Elemental Analysis of Extracted Chitosan

Elemental analysis of prepared chitosan was performed for the quantitative analysis of elements present in chitin and chitosan. Carbon, hydrogen and nitrogen elemental analysis results for chitin and chitosan are summarized in [Table 3.2](#).

Chitosan is the N-deacetylated derivative of chitin, i.e., the acetamide groups (-NHCOCH₃) of chitin are deacetylated to amine group (-NH₂) and converted into chitosan. As most of the -NHCOCH₃ groups are converted to -NH₂ groups in chitosan, the percentage of carbon will be decreased in chitosan than chitin and similarly C/N ratio will also be decreased. From the result ([Table 3.2](#)), it is seen that chitosan exhibit a significant reduction in the percentage of carbon as well as in C/N ratio compared to chitin which indicates that chitin was deacetylated to produce chitosan.

The C/N ratio of shrimp chitosan was observed to be 7.79% in previous study done by [Kumari, et. al., 2017 \(71\)](#). The low C/N ratio of chitosan in the present study could be due to the impurities present in chitosan ([72](#)).

Table 3.2.: Percentage of carbon, hydrogen, and nitrogen and the C/N ratio for chitin and chitosan

Sample	N (%)	C (%)	H (%)	C/N ratio
Chitin	6.02	42.84	3.916	7.1107
Chitosan	7.57	39.59	4.123	5.2282

3.2.4 Fourier Transform Infrared (FTIR) Spectroscopy Analysis

Fourier Transform Infrared spectroscopic study was performed to characterize the composition of prepared chitosan. [Figure 3.3](#) represents the FT-IR spectra of synthesized chitin and chitosan. The upper spectrum is for chitin and the lower spectrum corresponds to chitosan. The characteristic peaks with their positions are presented in [Table 3.3](#). The FT-IR spectra of chitosan presents a strong absorption band at 3421 cm⁻¹ due to -OH and -NH groups stretching vibrations and intermolecular hydrogen bonding. A peak at 2878 cm⁻¹ is due to symmetric stretching vibration of -CH attributed to pyranose ring. The peaks located at 1657 and 1595 cm⁻¹ are assigned to -C=O stretching vibration (amide I band) and NH bending vibration (amide II band) respectively. The observed sharp peak at 1379 cm⁻¹ is due

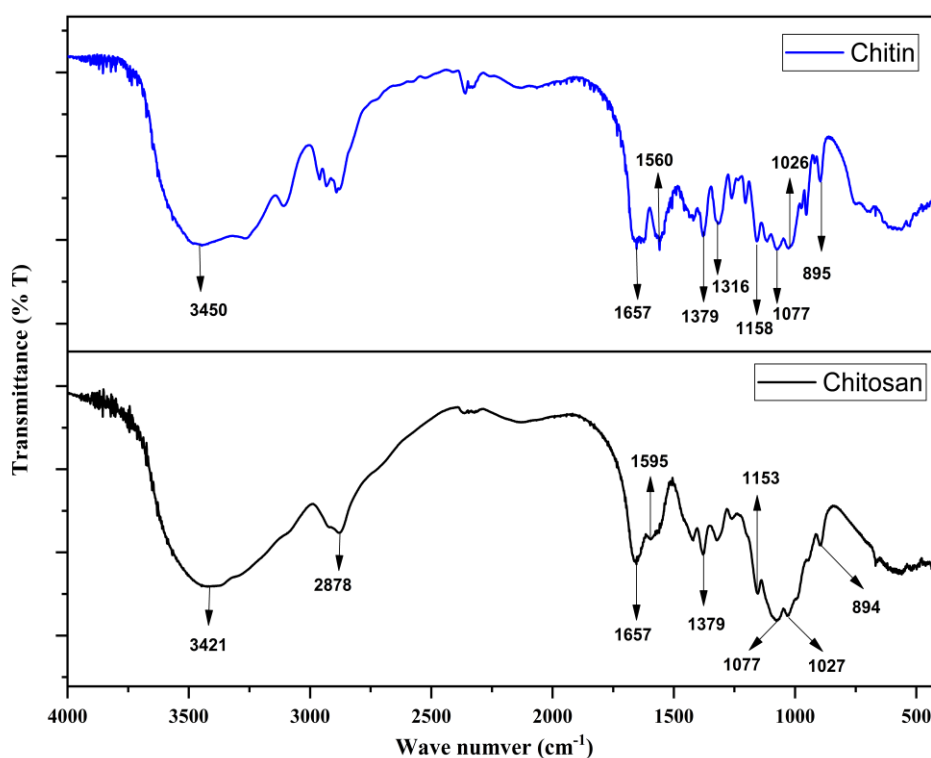


Figure 3.3: FT-IR spectra of extracted chitin and chitosan

Table 3.3: Tentative assessment of IR band of chitin and chitosan

Observed peak (cm ⁻¹)	Tentative band in chitin	Observed peak (cm ⁻¹)	Tentative band in chitosan
3450	O-H and N-H stretching vibration and intermolecular hydrogen bonding	3421	O-H and N-H stretching vibration and intermolecular hydrogen bonding
		2878	C-H stretching attributed to pyranose ring
1656	C = O stretching vibration (amide I band)	1657	C=O stretching vibration (amide I band)
1560	N-H bending vibration (amide II band)	1595	-NH ₂ in amino group
1379	CH ₃ in amide group	1379	CH ₃ in amide group
1316	Complex vibrations due to NHCO group (amide III band)	1323	Complex vibrations due to NHCO group (amide III band)
1077 and 1026	skeletal vibrations involving the C-O stretching	1077 and 1027	skeletal vibrations involving the C-O stretching

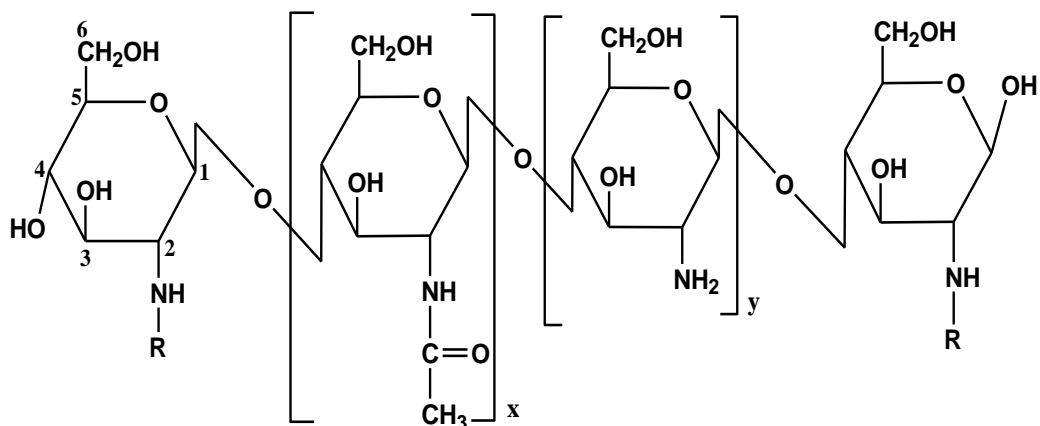
895 and 1158	anhydro glucosidic ring	894 and 1153	anhydro glucosidic ring
---------------------	-------------------------	--------------	-------------------------

to CH₃ in amide group. The peaks located at 1077 and 1027 cm⁻¹ are assigned to the skeletal vibrations involving the C-O stretching.

In the case of chitin, from the upper spectrum of [Figure 3.3](#), we see that the FT-IR spectrum of chitin is quite similar as chitosan. Compared with the spectrum of chitin, the major differences in FT-IR spectra lies in the regions of N-H and C = O vibrations. [Table 3.3](#) represents the tentative assessment of the IR band of chitin and chitosan. From [Table 3.3](#), we see the difference only at the representative peak at 1560 cm⁻¹ and 1316 cm⁻¹. Actually, transformation of chitin to chitosan is occurred through the removal of acetyl group of chitin to amino group and this process reduce the amide content. This reduction of amide group is observed by the reduction of two peaks at 1560 cm⁻¹ and 1316 cm⁻¹. From spectra, the representative peak at 1560 cm⁻¹ which is for -NH bending vibration of NHCOCH₃ group and 1316 cm⁻¹ which is for complex vibration due to -NHCO group are significantly decreased after deacetylation of chitin with a new sharp peak for NH₂ bending vibration that appears at 1595 cm⁻¹. This confirms the conversion chitin to chitosan.

3.2.5 Degree of Deacetylation (DDA) using FTIR Method

The degree of deacetylation (DDA) of chitosan is one of the most important parameter to determine the quality of chitosan as it has significant effect on the chemical, physical as well as biological properties of chitosan such as covalent linking, adsorption and encapsulation ([48](#)). [Figure 3.4](#) shows the structure of chitin and chitosan. The DDA of chitosan sample was determined by applying FTIR method of analysis. The DDA of extracted chitosan was calculated by using equation ([2.6](#)) by matching the identification bands of chitosan in FT-IR spectra. In equation ([2.6](#)), A₁₃₂₀= Absorbance at 1320 cm⁻¹ for complex vibration due to -NHCO group (amide III band) which was found at 1323 cm⁻¹ for extracted chitosan and A₁₄₂₀= Absorbance at 1420 cm⁻¹ which is found at 1417 cm⁻¹ for extracted chitosan.



$R = -\text{COCH}_3$ and $x > 50\%$ \implies chitin

$R = -\text{H}$ and $y > 50\%$ \implies chitosan

Figure 3.4: Structure of chitin and chitosan

The DDA of chitosan according to FT-IR method was found 70% indicating that the extracted product is chitosan. This DDA value is supported by various studies. DDA value of chitosan was found to be in the range of 56 – 99% in a study (73). The DDA value of chitosan extracted by traditional method from wasted shrimp shell in Arabian gulf was found in the range of 88 – 94% (74). In another study, Nouri *et al.*, (2015) observed the DDA value ranged from 71.02 - 82.20 % for deacetylation using traditional method while 79.01 - 88.60 % for deacetylation using microwave method (60). By using higher concentration of alkaline solution which was 50% NaOH for deacetylation process, DDA value obtained was high as well which was 89.79 % (48). Thus, the DDA values can be different for chitosan extracted from different sources and also due to the different parameters or conditions used during the deacetylation process.

3.2.6 X-ray Diffraction (XRD) Analysis

The X-ray diffraction (XRD) pattern of extracted chitosan is presented in Figure 3.5. The two broad diffraction peaks at $2\theta = 10.224^\circ$ and 20.357° in the XRD pattern of chitosan represent the extracted chitosan as semi crystalline in nature (75). According to Yen and Mau, (2007), the fungal chitosan exhibits two crystalline reflections at 9.7° and 19.9° in the XRD pattern. The WAXD pattern of shrimp chitosan contains two major characteristic peaks at $2\theta = 9.9 - 10.7^\circ$ and $19.8 - 20.7^\circ$ (76).

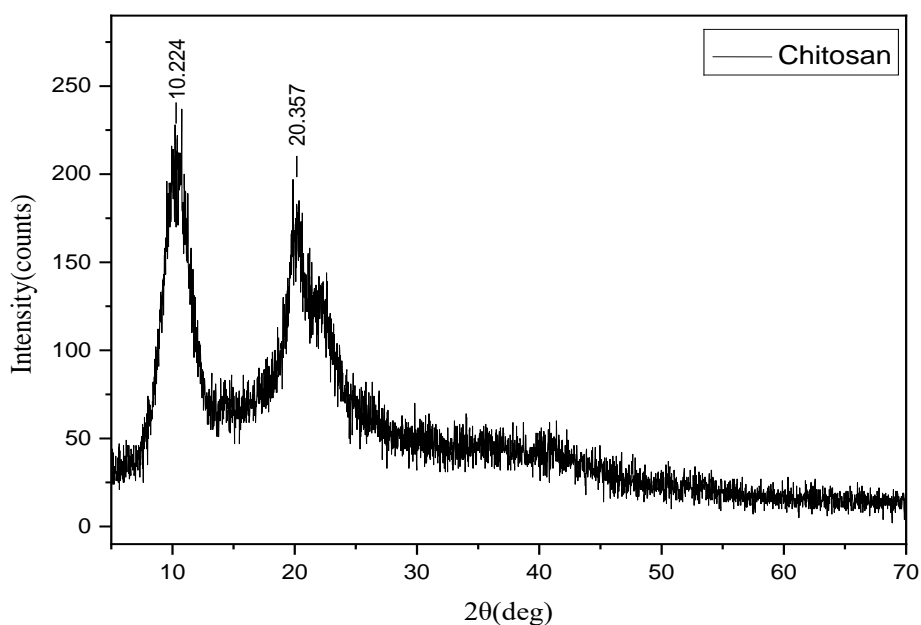


Figure 3.5: XRD pattern of extracted chitosan

From the diffractogram of the extracted chitosan sample, the two characteristic diffraction peaks that are centered at 2θ 10.224° and 20.357° correspond to the crystallographic planes (020) and (110) respectively (77). The crystallinity index of chitosan with respect to (020) plane was calculated from the diffractogram using equation (2.10). The values listed in Table 3.4 indicate that CrI was around 74.12% for extracted chitosan.

Table 3.4: Crystallinity index calculation in refer to 020 reflection for extracted chitosan (I_{am} represents the amorphous diffraction at $2\theta = 16^\circ$)

Sample	I_{020}	I_{am}	CrI ₀₂₀ (%)
Extracted chitosan	228 counts at 10.224°	62 counts at 16°	74.12

3.3 Formation of Chitosan Nanoparticles (CSNPs)

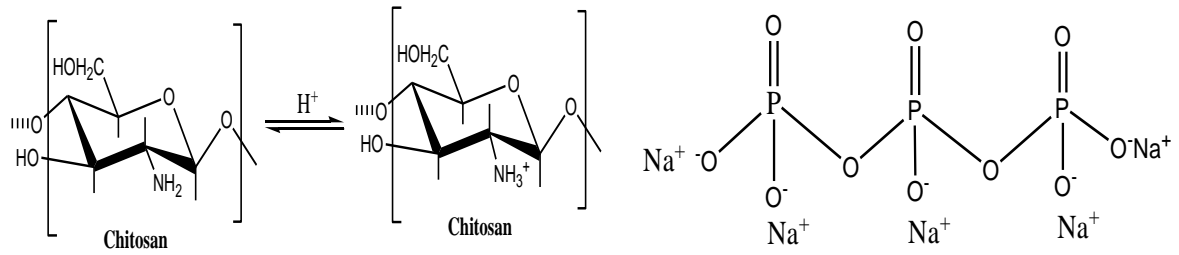
The nanoparticles of chitosan was prepared by using simple method of ionic gelation in which molecular linkage were formed between two oppositely charged macromolecules, chitosan and sodium tripolyphosphate (Na-TPP). Here, Tripolyphosphate (TPP) acts as a polyanion and chitosan is a cationic polymer. They can interact with one another by electrostatic forces. In ionic gelation method, the dissolving of chitosan in aqueous acetic acid solution forms cation of chitosan. The aqueous solution of polyanionic TPP contains negatively charged phosphoric ions. Upon addition of TPP solution into chitosan solution under magnetic stirring, chitosan molecules having abundant NH_3 groups interact with these phosphoric ions and form cross-linked chitosan nanoparticles (78). The size characteristic were found to influence the biological performance of chitosan nanoparticles (79). So, to study the effect of concentration of TPP and chitosan on the nanoparticles formation and on the size of nanoparticles, six different formulations were prepared by varying the chitosan and TPP concentration as shown in Table 3.5. The formation of CSNPs is presented in Figure 3.6.

Finally, three types of phenomena were observed. These were, clear solution, aggregation and opalescent suspension and the latter denotes the completion of the nanoparticle formation process. From Table 3.5, for formulation of CS01 and CS02, the clear solution

Table 3.5: Effect of concentration of chitosan and TPP on chitosan nanoparticles formation

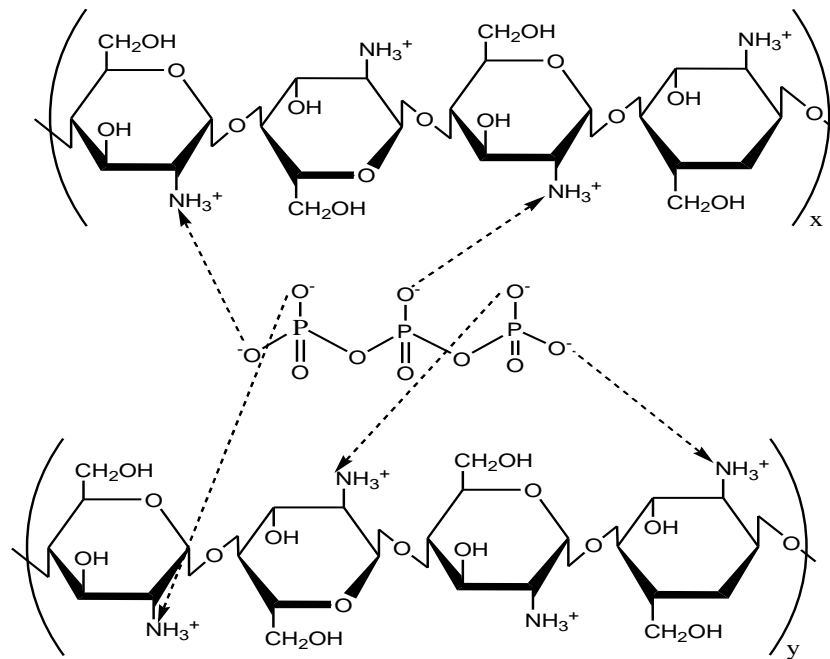
Formulations	Factors			Results	Remarks
	Chitosan concentration (%)	TPP concentration (%)	Chitosan: TPP		
CS01	0.5	0.25		Clear solution	Particle not formed
CS02	0.5	1		Clear solution	Particle not formed
CS03	2	0.25	5:1	Opalescent suspension	Particle formed
CS04	2	1	5:1	Opalescent suspension	Particle formed
CS05	2	2	5:1	Aggregation	Particle not formed

after addition of TPP into chitosan solution indicates that there was no formation of chitosan nanoparticles. This may be due to very low concentration of chitosan. But for CS03 and CS04 formulations, where the concentration of chitosan was relatively high, at a chitosan and TPP mass ratio of 5:1, formation of opalescent suspension indicates that the nanoparticle formation was occurred.



(a) Chitosan in 1% acetic acid (protonation)

(b) Na-TPP



(c) Proposed ionic interaction of chitosan with TPP (adapted from Othman, *et. al.*, 2018) (80)

Figure 3.6: Formation of chitosan nanoparticles

3.4 Characterization of Chitosan Nanoparticles (CSNPs)

3.4.1 SEM and TEM Analysis

The surface morphology of prepared chitosan was characterized by SEM and TEM. Figures 3.7 and 3.8 show the corresponding SEM and TEM images of prepared chitosan-TPP nanoparticles. From the results, it can be said from both SEM and TEM micrographs that there is a decrease in particle size of nanoparticles with an increase in TPP concentration. The nanoparticles have been formed at a 5:1 chitosan/TPP weight ratio. The SEM images of chitosan nanoparticles clearly show a spherical-like structure of 10-20 nm in diameter and particles are in the agglomerated state. But according to the TEM images, the diameter

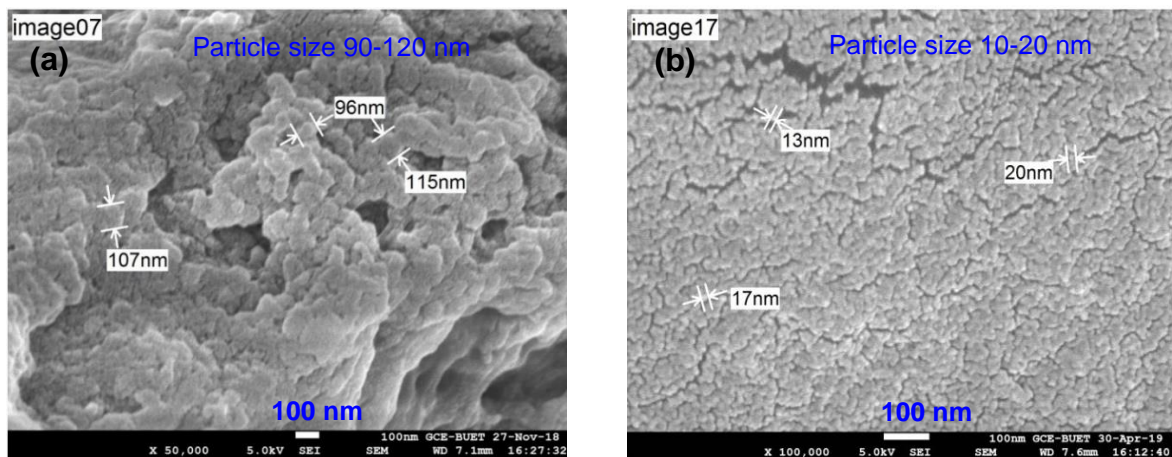


Figure 3.7: SEM micrographs of prepared chitosan nanoparticles for (a) CS03 and (b) CS04 formulations

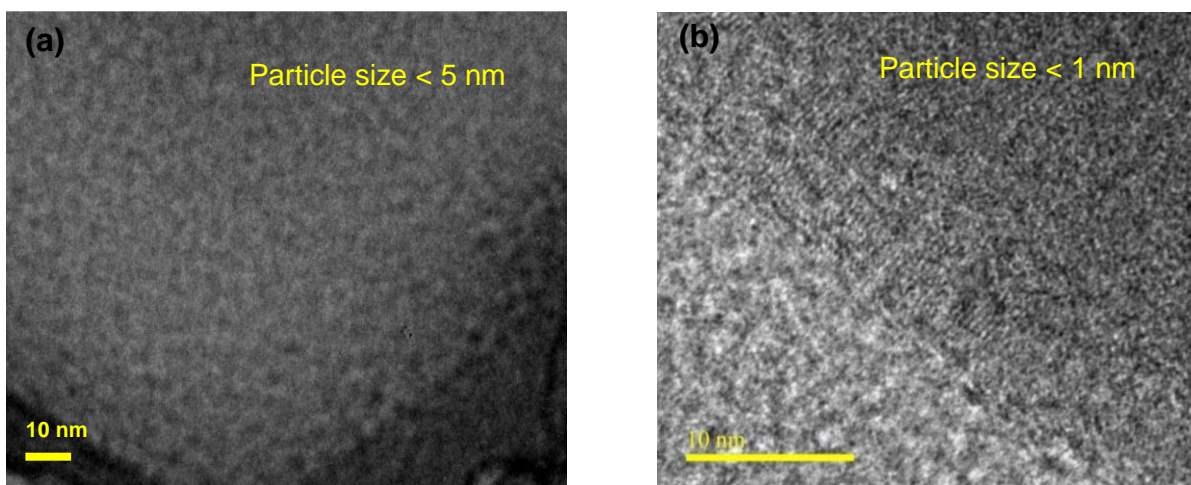


Figure 3.8: TEM micrographs of prepared chitosan nanoparticles for (a) CS03 and (b) CS04 Formulations

of chitosan nanoparticles of CS03 formulation was less than 5 nm. Similarly, in the case of chitosan nanoparticles of CS04 formulation, the TEM images indicated that the particles are uniform with size of below 1 nm in diameter. Thus, the comparison of TEM images of the two nanoparticle formulations reveals that in both cases, the nanoparticle formation has occurred. But the size of nanoparticles was different in two formulations which is the most important issue in biomedical application. The advantage of small size particle is that, when it is used as a carrier in a drug delivery system, shows high cellular uptake and good suspensibility. Besides, due to having larger surface area to volume ratio, smaller particles may have a high drug loading capacity and slow diffusion of drug. Finally, the condition of formation of CS04 is considered as the optimized condition for nanoparticle formation which formed the nanoparticles in the range of 0.1-1.0 nm according to TEM.

It is important to note that, we have got different information about size of the nanoparticles by SEM and TEM analysis. This can be described from the image forming principle of these two techniques. SEM produces images by detection of reflected electrons, while TEM uses the electrons that pass through the sample, that is, transmitted electrons to form an image. As a result, TEM provides information about the internal structure of whereas SEM gives information regarding sample surface and composition. Simply TEM has a higher resolution than SEM by a factor of 10 or more. So, the particles observed by SEM may be the cluster of particles which are identified in TEM images. Finally, we can say that the chitosan particles from optimum conditions contain particles of size less than 1 nm.

Comparing with the results of several previous studies, it was found that the size of the chitosan nanoparticles obtained in this study was significantly lower (67, 81) by using different condition. This reduction in size is very good characteristic of chitosan nanoparticle for use in biomedical and pharmaceutical formulations. Moreover, the nanoparticles obtained in this study were more uniform compared to these studies (67, 81).

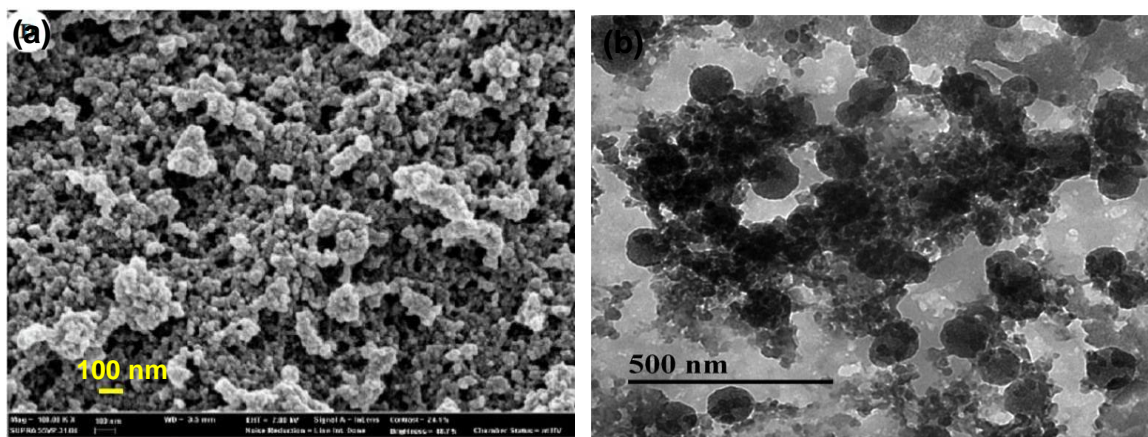


Figure 3.9: The particle size of prepared chitosan nanoparticles observed in different studies (a) using 0.1% chitosan and 0.25% TPP (81) and (b) using chitosan: TPP mass ratio of 12:1 (67)

3.4.2 EDX Analysis

Figure 3.10 shows the EDX spectra from a selected area of chitosan nanoparticles for quantitative elemental analysis. The composition of elements in CSNPs are listed in Table 3.6. The EDX results confirm the presence of the C, N and O with an atomic weight of 78.01%, 3.11% and 16.53% respectively as the element of chitosan. The presence of Na with atomic weight of 0.49% and P with 1.83% confirms the successful formation of chitosan nanoparticles.

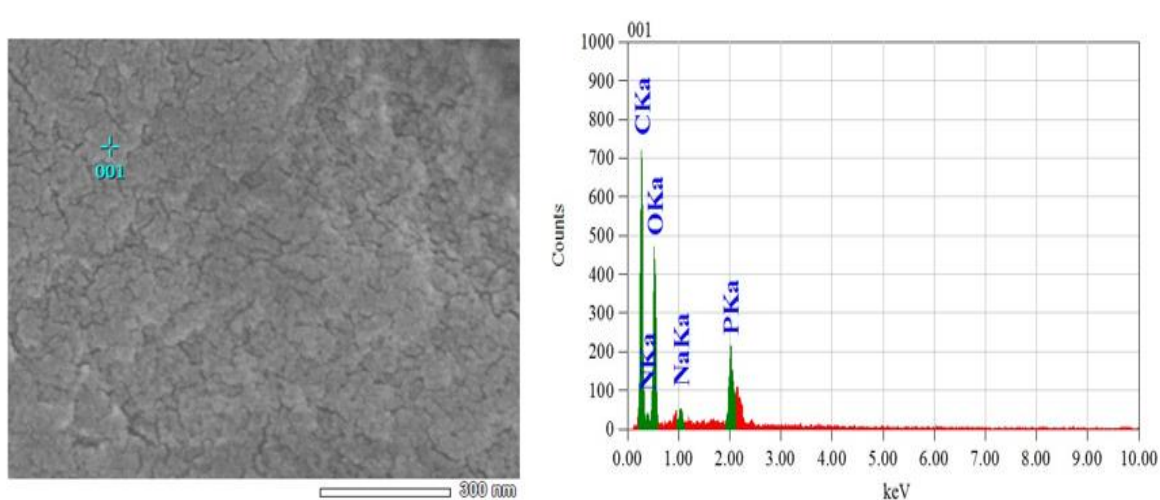


Figure 3.10: EDX spectrum of chitosan nanoparticles

Table 3.6: Distribution of elements in blank chitosan nanoparticles

Element	Mass (%)	Atom (%)
C	71.33	78.01
N	3.31	3.11
O	20.17	16.53
Na	0.86	0.49
P	4.33	1.83

3.4.3 FT-IR Analysis of Chitosan Nanoparticles (CSNPs)

The optimized nanoparticles (CSNPs) prepared at optimized conditions (CS04) was characterized by FTIR analysis. [Figure 3.11](#) represents the FT-IR spectra of extracted chitosan and chitosan nanoparticle obtained from it. It is seen from the FTIR spectra that the spectra of chitosan nanoparticle is very similar to the extracted chitosan. Comparing the FTIR spectra of chitosan and chitosan nanoparticle, we see that pure chitosan was characterized with peaks located at 3421, 1657, 1595, 1417, 1077, 1027 and 894 cm^{-1} as shown in [Table 3.7](#). In chitosan nanoparticle, the characteristic peaks are quite similar except the peaks located at 1657 which relates to C=O stretching in amide group get shifted to 1647 cm^{-1} and the peak at 1595 which relates to NH_2 bending in amino group get shifted 1,540. The reduced stretching frequency may be attributed to the interaction between amino group of chitosan and TPP.

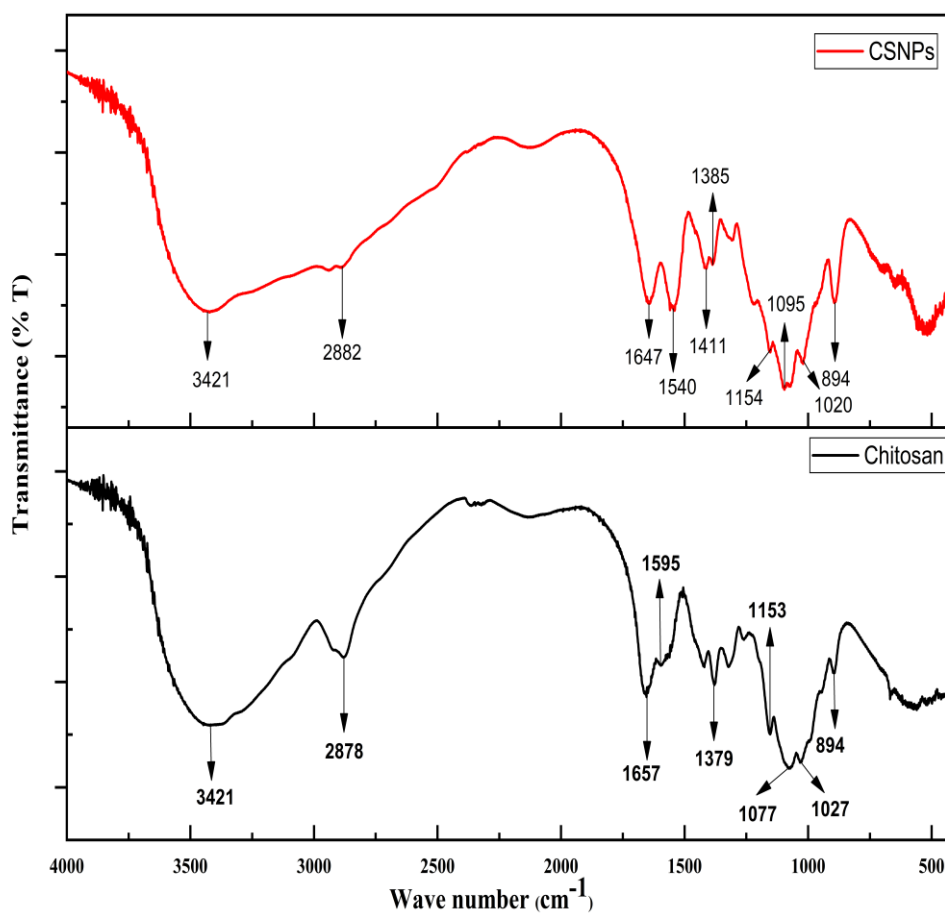


Figure 3.11: FTIR spectra of extracted chitosan and chitosan nanoparticles (CSNPs)

Table 3.7: Tentative assessment of IR band of chitosan nanoparticles (CSNPs)

Observed peak (cm^{-1})	Mode	Tentative band
3421	Symmetric stretching	-NH and -OH
1647	Symmetric stretching	-C=O (amide I)
1540	Bending vibration	-NH ₂ (amide II)
1411		
1095 and 1020	Stretching vibration	C-O (primary alcohol)
894	Anti-symmetric stretching	Glucopyranose ring

3.4.4 XRD Analysis of Chitosan Nanoparticles (CSNPs)

The X-ray diffraction patterns of extracted chitosan and chitosan nanoparticles (CSNPs) are illustrated in Figure 3.12., which shows the presence of two characteristic peaks at 2θ around 10.224° , 20.357° and a shoulder in 22.491° , in agreement with previous reports, which correspond to the (020), (110), and (120) planes, respectively (82, 83).

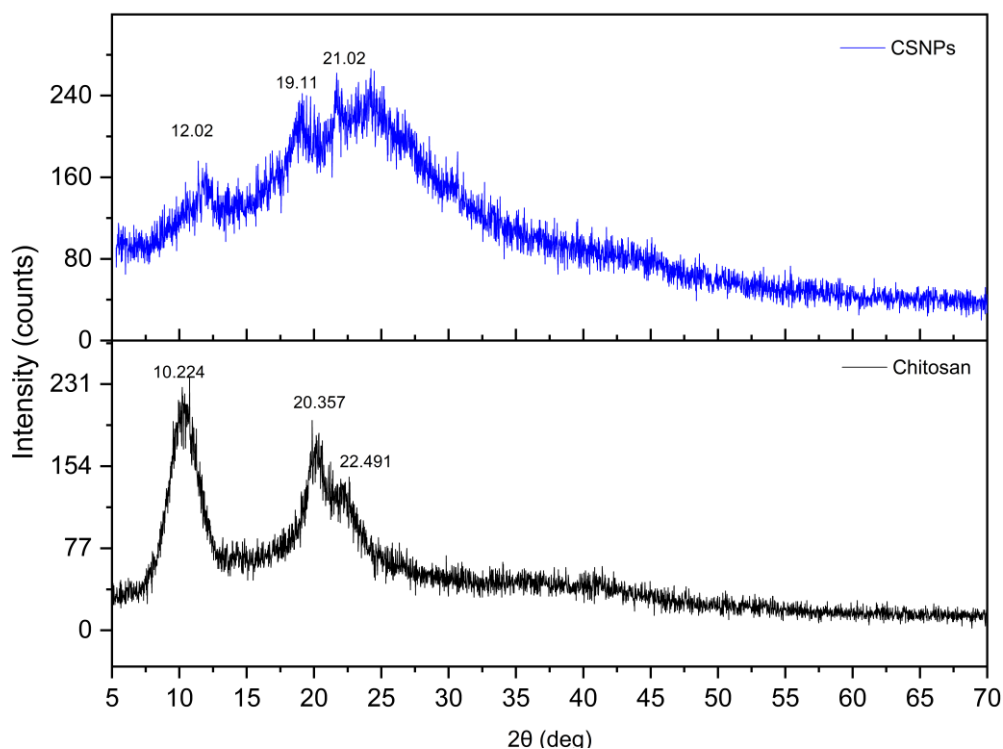


Figure 3.12: X-ray diffraction pattern of chitosan and CSNPs

XRD pattern of chitosan nanoparticles showed broad diffraction peaks at 2θ -scattered angles of 12.02° and 19.11° and 21.62° . The intensity of these crystalline peaks were decreased in comparison with pure chitosan. The decrease in intensity of (110) and (020) planes of CSNPs reflects that native chitosan were successfully transformed into nanoparticles. Thus the crystalline structure of chitosan have been destroyed during nanoparticle formation which indicates the increased amorphous nature in nanoparticle form. The decrease in crystallinity may be due to the fact that CSNPs consist of a dense network structure of interpenetrating counter ions of TPP where the polymer chains are crosslinked with each other by TPP. Thus, the XRD pattern of chitosan nanoparticles is characteristic of an amorphous polymer.

3.5 Ciprofloxacin Loading on Chitosan Nanoparticles (CSNPs)

To evaluate the applicability of chitosan nanoparticles, initially, ciprofloxacin-loaded chitosan nanoparticles (CP-CSNPs) were prepared by using the ionic gelation technique by applying the optimized condition for CSNPs formulation. In this case, ciprofloxacin (CP) was added to chitosan solution at different Chitosan: CP ratio (w:w) before adding TPP solution to it.

3.5.1 Association Efficiency (AE) of Ciprofloxacin (CP)

As the observed particle size of CSNPs is very much lower than obtained in previous studies, it is postulated that the ciprofloxacin can be associated on the surface of CSNPs rather than encapsulation. To determine the effect of the amount of ciprofloxacin on association efficiency, four different Chitosan : CP ratio (w:w), such as, 1:0.5, 1:0.65, 1:0.8 and 1:1 were considered as variable factor. The association efficiency of these formulations were determined using equation (2.11). The average percent of association efficiency of these formulations are shown in Figure 3.13. From Figure, it is seen that the loading process is ciprofloxacin amount dependent but the dependency is not very significant. An increase of ciprofloxacin concentration leads to a slight increase of association efficiency. However, the ratio of 1:0.8 and 1:1 for Chitosan: CP in the loading procedure have resulted in almost no change in association efficiency of the ciprofloxacin (from 83% to 93%). As a consequence, an optimum ratio of Chitosan: CP was obtained to be 1:1 for loading procedure of ciprofloxacin into/on chitosan nanoparticles.

In the current study, the association efficiency of CS4 formulation containing the CP:CS ratio of 1:1 was almost 93% as measured from the remaining CP content in the supernatant after the loading process using a UV-spectrophotometer. This is the highest association efficiency which is due to electrostatic interaction between CS and CP and this formulation of CS4 was selected for further analysis.

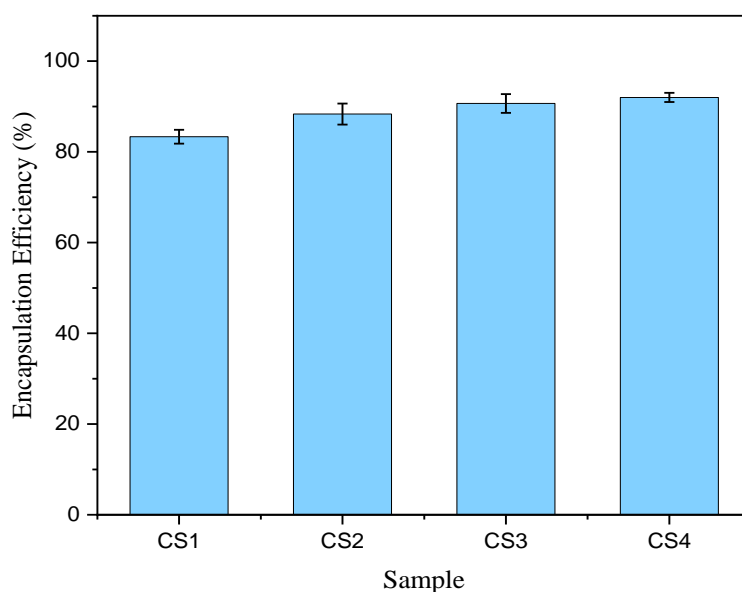


Figure 3.13: The effect of chitosan: CP (w:w) on association efficiency of ciprofloxacin loading on CSNPs. Data are represented as means \pm standard deviations (n = 3)

3.5.2 Characterization of Ciprofloxacin Loaded Chitosan Nanoparticles (CP-CSNPs)

3.5.2.1 SEM analysis

The surface morphology of CP-CSNPs was observed by field emission scanning electron microscope which is shown in [Figure 3.14](#). The SEM image of ciprofloxacin loaded chitosan nanoparticles of 1,00,000 magnification displayed that the particle size was ranging from 20-30 nm. The micrographs of nanoparticles also showed that they were of approximately round in shape. SEM image also showed the physical aggregation of nanoparticles. The corresponding lower magnification of the image at 2,000 revealed the aggregation of nanoparticles.

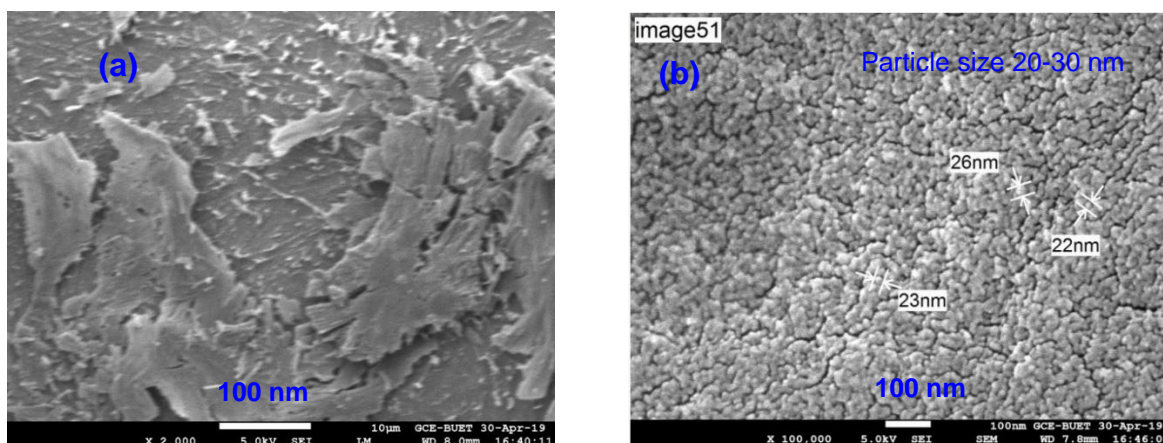


Figure 3.14: SEM micrograph of ciprofloxacin loaded chitosan nanoparticles at (a) $\times 2,000$ and (b) $\times 1,00,000$ magnification.

3.5.2.2 EDX analysis

The elemental composition and loading of CP on CSNPs during nanoparticle formation was investigated by EDX analysis which is shown in [Figure 3.15](#). EDX systems are attached to scanning electron microscopy instruments. An EDX analyzer was used to provide elemental identification and quantitative information using X-ray released from a selected area after interaction with the focused electron beam. The EDX spectra of chitosan nanoparticles after ciprofloxacin loading, presented a new peak corresponding to fluorine. [Table 3.8](#) represents the distribution of elements in CP-CSNPs according to EDX spectrum. From [table 3.8](#), it is seen that the EDX analysis confirmed the presence of sodium and phosphorus with an atomic weight of 0.65% Na and 3.24% phosphorus in the nanoparticles, suggesting the presence of TPP in the nanoparticles. Besides, the EDX spectrum shows signals of F indicating the incorporation of ciprofloxacin into chitosan nanoparticles.

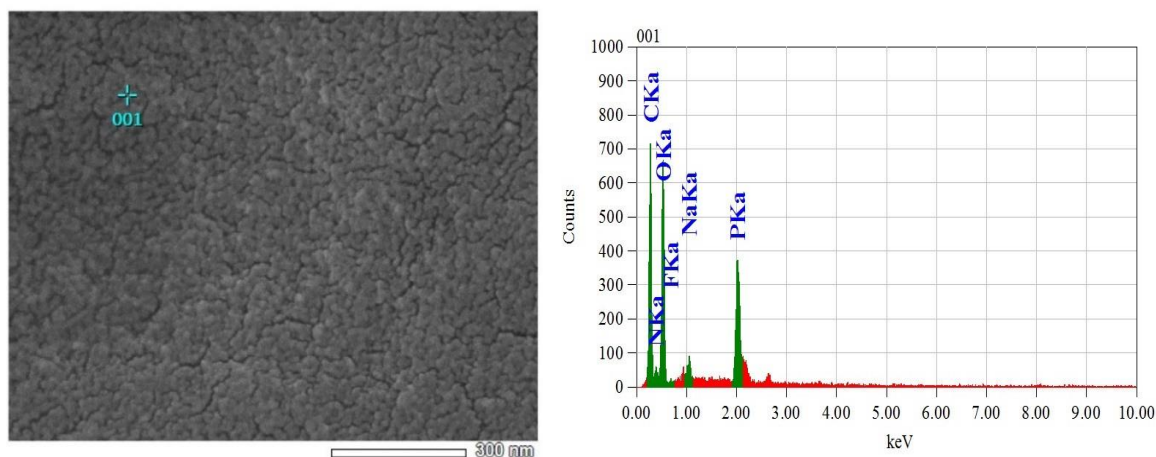


Figure 3.15: EDX spectra of Ciprofloxacin loaded chitosan nanoparticle

Table 3.8: Distribution of elements in ciprofloxacin loaded chitosan nanoparticles

Element	Mass (%)	Atom (%)
C	66.71	74.87
N	3.29	3.17
O	21.43	18.05
F	0.01	0.01
Na	1.11	0.65
P	7.44	3.24

3.5.3.3 TEM analysis

The visualization of the size and morphology of CP-CSNPs were performed in a dried state by TEM which is shown in Figure 3.16. The diameter of the loaded nanoparticles was found to be 1-2 nm. As shown in Figure 3.16(d), the CP-CSNPs possessed a regularly spherical shape. Figure 3.16(a) and 3.16(b) show the possible drug adsorption on the surface of the nanoparticle. From Figure 3.16(d), it is seen that there is some aggregation of the particles with an average particle size of approximately 1-2 nm. The size of the blank chitosan nanoparticles was 0.1-1 nm (Figure 3.8). This increase in size in the case of CP-CSNPs indicates that the drug was successfully associated with CSNPs by adsorption onto the surface of the nanoparticles.

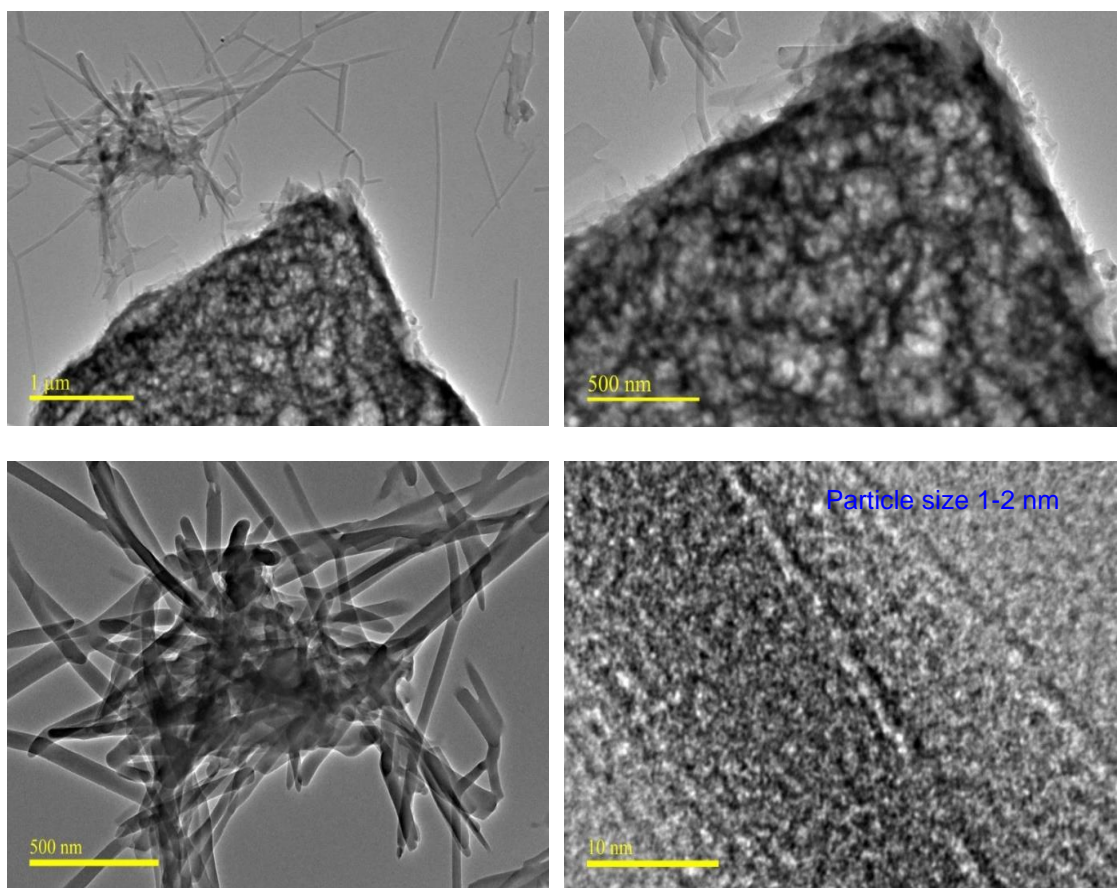


Figure 3.16: TEM micrographs of ciprofloxacin loaded chitosan nanoparticles of CS4 formulation at different magnifications

3.5.4.4 FT-IR analysis

FTIR analysis was performed to confirm the interaction of chitosan, TPP and ciprofloxacin. The FTIR spectra of CP-CSNPs, chitosan and free CP are presented in [Figure 3.17](#) and respective positions are given in [Table 3.9](#). Pure chitosan was characterized by some characteristic peaks located at 3421, 1657, 1595 and 894 cm^{-1} . The band at 3,421 cm^{-1} corresponded to the combined peaks of the NH_2 and OH groups stretching vibrations in the chitosan as shown in [Figure 3.17](#). The broadband between 1,657 and 1,595 cm^{-1} can be attributed to the C=O stretching vibration (amide I band) and the NH_2 group bending vibration (84). The band at 894 cm^{-1} relates to anhydro glucosidic ring. The bands at 2918 and 2878 cm^{-1} are for C-H stretching, 2372 cm^{-1} is due to asymmetric C-N band stretching, 1379 cm^{-1} is because of asymmetric C-H bending of CH_2 group and 1079 cm^{-1} is for skeletal vibration involving C-O stretching.

In the case of CP-CSNPs, the peak at 3,421 corresponded to the hydroxyl groups in pure chitosan was shifted to 3428 cm^{-1} indicating that there could be some hydrogen bonding between ciprofloxacin and chitosan nanoparticles. The band at 1,657 and 1,595 cm^{-1} (amide I and amide II band), which was clearly observed in pure chitosan, decreased in the case of CP-CSNPs, while two new absorption bands appeared at 1,648 and 1,544 cm^{-1} in CP-CSNPs. This result indicated that the NH_3^+ groups of pure chitosan were crosslinked with the TPP groups of sodium polyphosphate, which helped to enhance both the inter- and intra-molecular interactions within the chitosan nanoparticles (85). Besides, the bands at 2945 cm^{-1} (2918 cm^{-1} in chitosan) and 2878 cm^{-1} in CP-CSNPs relate to symmetric and asymmetric CH_3 stretching vibration attributed to pyranose ring of chitosan, and the band at 2358 cm^{-1} is due to asymmetric stretching of C-N band which was found at 2372 cm^{-1} in pure chitosan and 1299-1155 cm^{-1} is for C-F band stretching of ciprofloxacin.

Finally, the FTIR spectra of CP-CSNPs showed that some peaks observed at pure chitosan were shifted, but the shifting was not very significant. So, it can be concluded that CP was loaded to chitosan nanoparticles without functional group interaction but there was electrostatic interaction between ciprofloxacin and chitosan nanoparticles.

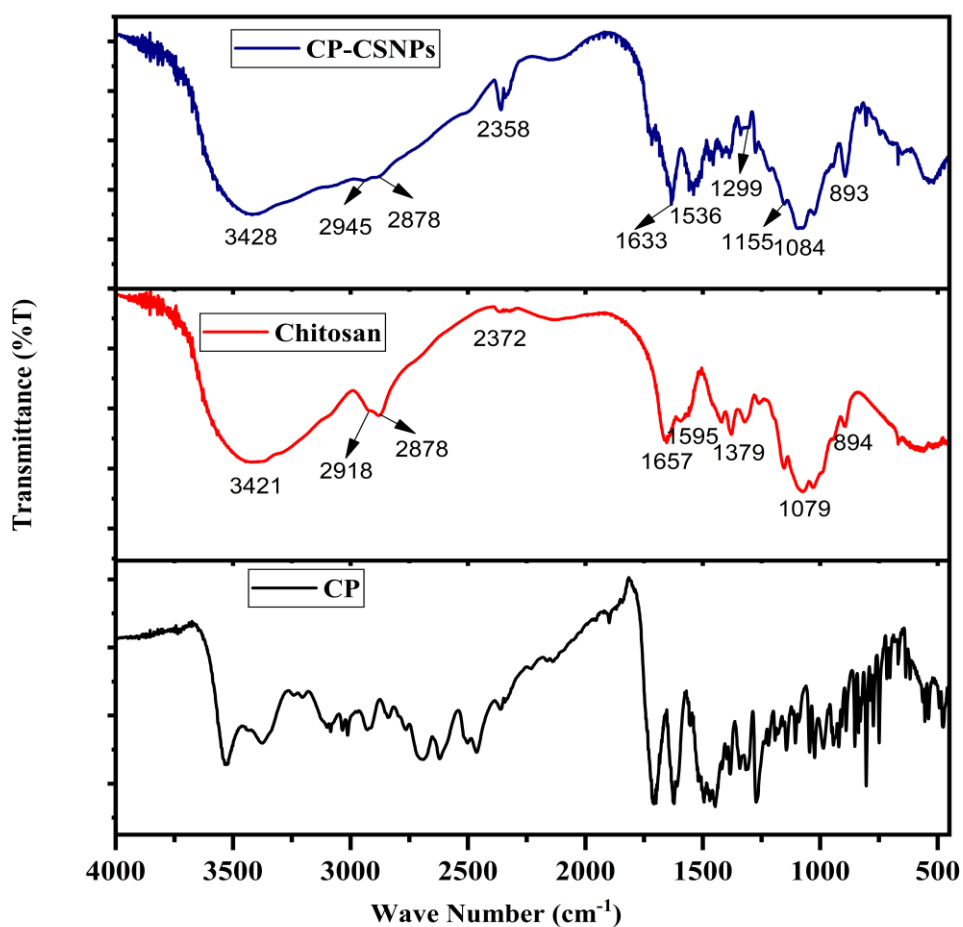


Figure 3.17: FTIR spectra of ciprofloxacin (CP), chitosan, and ciprofloxacin loaded chitosan nanoparticles (CP-CSNPs).

Table 3.9: Tentative assessment of IR band of ciprofloxacin loaded chitosan nanoparticles

Observed peak (cm ⁻¹)	Mode	Tentative band
3428	Symmetric stretching	-NH and -OH
2878 and 2945	Asymmetric and symmetric stretching	-CH ₂ (Pyranose ring)
1640	Symmetric stretching	-C=O (amide I)
1544	Bending vibration	-NH ₂ (amide II)
1096 and 1020	Stretching vibration	-C-O
893 and 1153	Anti-symmetric stretching	Structure of saccharide
2358	asymmetric stretching	C-N
1299-1155	Stretching of ciprofloxacin.	C-F

3.5.5.5 XRD analysis

The XRD pattern of pure ciprofloxacin (CP), chitosan and ciprofloxacin loaded chitosan nanoparticles (CP-CSNPs) and are presented in Figure 3.18. This figure shows that the XRD pattern of chitosan contains the characteristic peaks at 2θ around 10.224° , 20.357° , and a shoulder in 22.491° , in agreement with previous reports, which correspond to the (020), (110), and (120) planes, respectively (82, 83).

In the case of CP-CSNPs, a decrease in % relative intensity of the (110) and (020) planes than the pure chitosan reflects that native chitosan's were successfully transformed into nanoparticles. Besides, these relatively broad and weaker peaks found at $2\theta = 11.57^\circ$ and 19.31° in CP-CSNPs indicate an amorphous state of their structures and a substantial reduction of intramolecular hydrogen bonds (86). It was also seen that the several characteristic peaks of ciprofloxacin did not appear in a diffraction spectrum of ciprofloxacin loaded chitosan nanoparticles. This condition indicates that ciprofloxacin was molecularly dispersed on the nanoparticles.

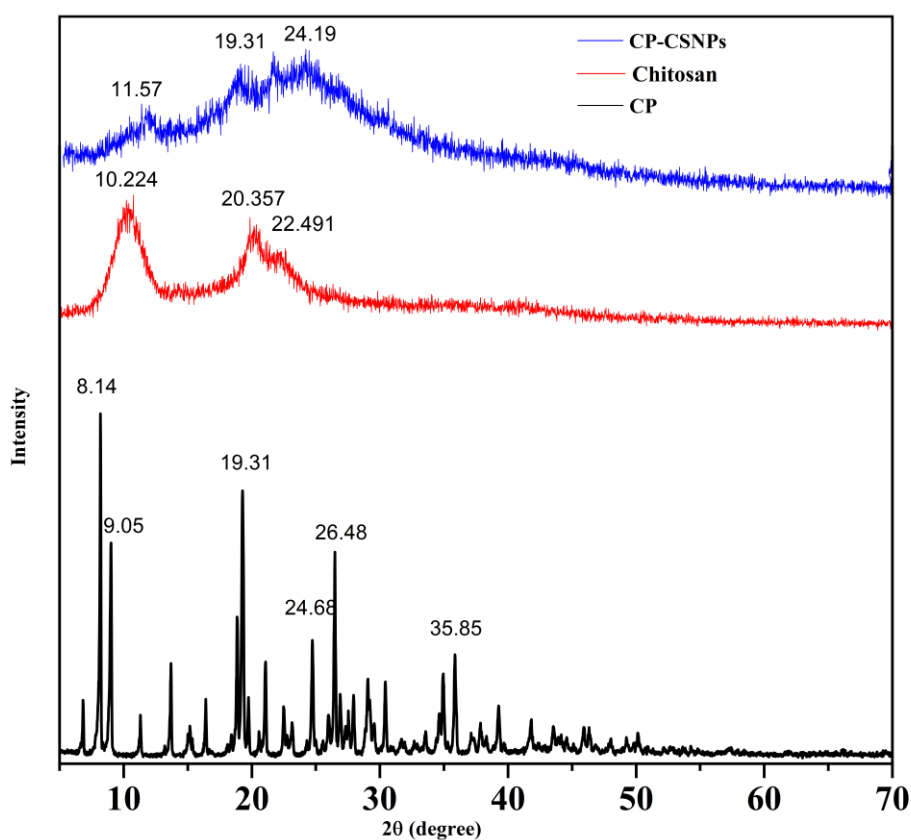


Figure 3.18: The XRD pattern of ciprofloxacin (CP), chitosan and ciprofloxacin loaded chitosan nanoparticles (CP-CSNPs)

3.5.3 Biomedical Application of Ciprofloxacin Loaded Chitosan Nanoparticles (CP-CSNPs)

To study the biomedical application of CP-CSNPs, the *in vitro* antibacterial activity of nanoparticles against various microorganisms was evaluated as well as the *in vitro* drug release profile of CP from the chitosan nanoparticles was observed.

3.5.3.1 *In vitro* release study of ciprofloxacin (CP) from chitosan nanoparticles (CSNPs)

The optimized formulation was CS4 and this formulation was selected for drug release study. [Figure 3.19](#) represents the average cumulative percent release of ciprofloxacin from chitosan nanoparticles at various time intervals. In the *in vitro* release profile, a biphasic pattern was observed. These two phase in the release profile can be occurred due to “Sudden release” and “sustained release”. The sudden release or the initial rapid release can be characterized as the “burst effect”. The burst release from chitosan nanoparticles is may be due to that, some quantities of CP were located on the surface of the CSNPs by a weak electrostatic force which could be easily released by diffusion.

From the release profile, it is very clear that at the sudden release phase, about 34% of ciprofloxacin was released at first ½ h. After this initial rapid release, the second phase is the “sustained release” phase which is slower than previous phase. This slower and sustained release occur throughout the incubation period. As a result, 72% of ciprofloxacin was released after 24 hr. Therefore, the extended release phase lasted from 30 min to 24 h.

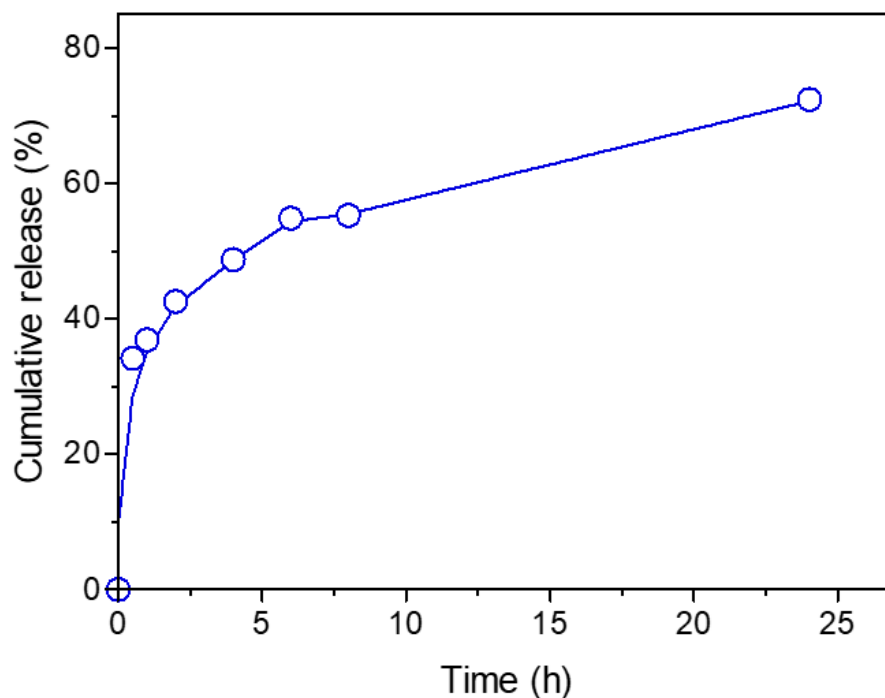


Figure 3.19: Ciprofloxacin release profile from CSNPs in PBS of pH=7.4.

Sustained drug release is the key strategy for reducing the systemic side effects in human body which is associated with the frequency of drug administration and high drug concentrations. One of the most common methods used and studied to control drug release is encapsulation within polymer matrix, which slows diffusion. Chitosan nanoparticle is widely used for encapsulation of drugs because of its biodegradability, biocompatibility and non toxicity. But in the present study, the CSNPs was used for controlled release of drug without encapsulation. Here, adsorption due to electrostatic interactions between the ciprofloxacin and the CSNPs is the governing factor for drug release in this system.

To understand the release mechanism, we first examined the physical characteristics of this release system. The morphology and size of the nanoparticles were characterized by SEM and TEM analysis. The CP-CSNPs were spherical with diameter ranging from 1-2 nm which was higher than blank chitosan nanoparticles (0.1-1nm) which was due to adsorption of CP on the surface of the nanoparticles according to TEM analysis (Figure 3.8). The size of the unmodified chitosan nanoparticles is too small to encapsulate the drug molecules into nanoparticles matrix. However, our results show very similar release profiles as the drugs that are encapsulated into the nanoparticles though it was not encapsulated in chitosan nanoparticles indicating that another mechanism must be involved. To describe the release

mechanism, we postulated that the sustained release that we have observed was primarily caused by adsorption due to electrostatic interactions between CP and CSNPs (87). We also postulate that initially ciprofloxacin was fully adsorbed on the nanoparticle surface. As the nanoparticle begins to degrade, the local pH of the system changes. At a certain threshold, the surface of the nanoparticles becomes neutral, weakening the electrostatic interactions between ciprofloxacin and CSNPs and initiating release.. Release can then be governed by nanoparticle degradation and drug diffusion or desorption, depending on the system. Finally we can describe the mechanism of ciprofloxacin release from chitosan nanoparticles usually involves polymer degradation, erosion, and diffusion of the drugs (87). This sustained drug release from the nanoparticles is important, since it enables the prolonged residence of the drug at the surface of the release site, increases the bioavailability of drug and prolongs the therapeutic effect. Thus, sudden release of drug in the body can quickly reach at effective therapeutic concentration and sustained release can make the drug in the body to stay at the effective therapeutic concentration range. From the above result, it is clear that the chitosan nanoparticles had the effect of prolonging the ciprofloxacin release in the body.

3.5.3.2 Release kinetics of ciprofloxacin (CP) from the nanoparticles

Mathematical models play an essential role in interpreting the drug delivery mechanism from a dosage form. This is an important tool for understanding the kinetics of the release of drugs from a dosage form. A variety of mathematical models are used to understand drug r kinetics, which are explained below:

Zero order model (88): In accordance with the pharmacokinetic principles, the release of drugs from the dosage form may be represented by equation (3.1):

$$C_t = C_0 + K_0 t \quad (3.1)$$

Where, C_t is the quantity of drug released at time t , C_0 is the initial drug concentration at time $t=0$, K_0 is the zero-order rate constant. Thus, the zero-order kinetics define the process of constant drug release from a drug delivery system and the level of drug in the blood remains constant throughout the course of drug administration. Hence, to investigate the drug release kinetics, data obtained from in vitro dissolution study is plotted as a function of time, i.e., cumulative drug release vs. time (Figure 3.20). Hence the slope of the above

plot gives the zero-order rate constant and the correlation coefficient in the graph will indicate whether or not the drug release follows zero order kinetics.

Observation: The graphical representation of cumulative % of drug release in relation to time depicted that the release of CP from CSNPs does not exactly follow the principle of zero order release kinetics. The value of correlation coefficient of data fitness is given in table 3.9.

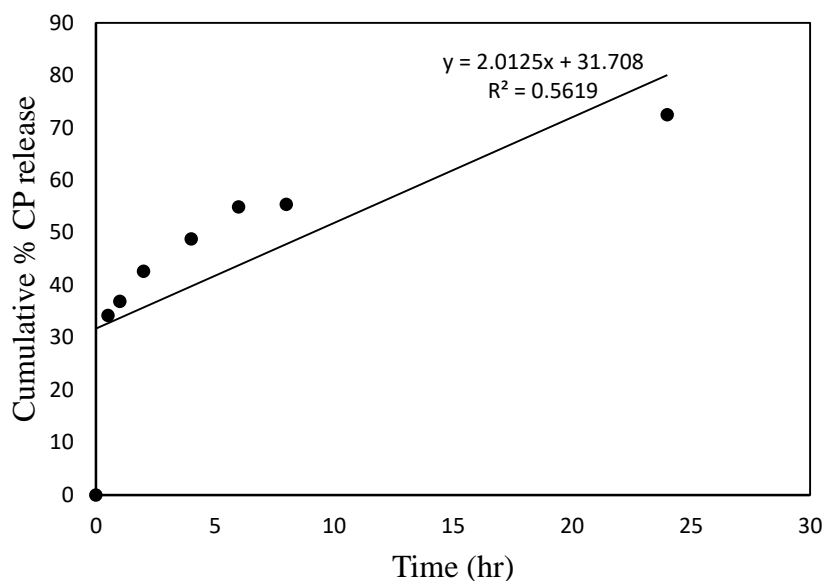


Figure 3.20: Zero order kinetic release of ciprofloxacin.

First order model (88): The drug release following the first order kinetics may be represented by equation (3.2).

$$dC/dt = -K_1 C \quad (3.2)$$

Where K_1 is the first order rate constant. Hence, the first order process is defined as, the rate of which is directly proportional to the concentration of drug undergoing reaction, i.e., greater the concentration, faster the reaction. It therefore follows the linear kinetics. After rearranging and integrating the equation (3.2),

$$\log C = \log C_0 - K_1 t / 2.303 \quad (3.3)$$

Where C_0 is the initial concentration of the drug, C is the percent of drug remaining at time t . To investigate the first order kinetics for drug release, the log % of drug remaining in the

dissolution media obtained from in vitro dissolution study is plotted as a function of time. The slope of the plot indicates the first order rate constant. This model was therefore applied to CP release profile which is represented by [Figure 3.21](#).

Observation: The lower value of correlation coefficient in the graphical representation indicates that CP release from CSNPs does not follow the principle of first order release kinetics.

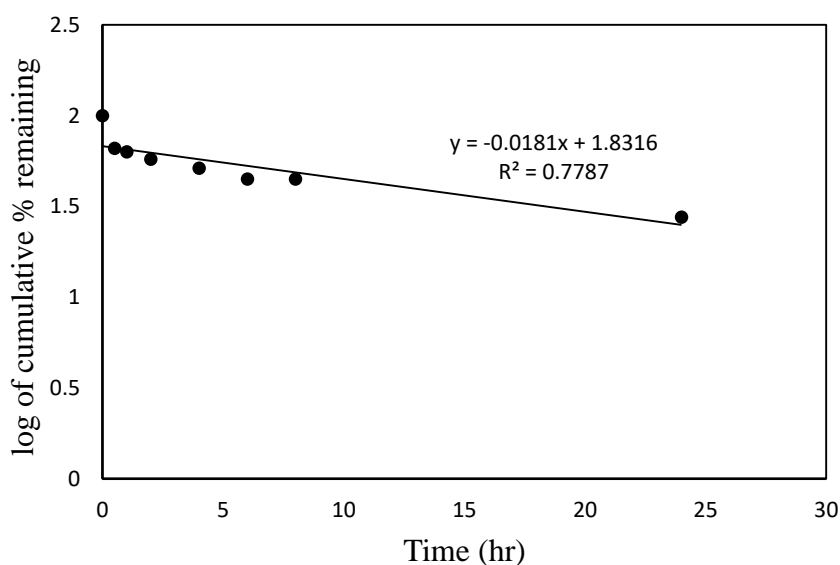


Figure 3.21: First order kinetic release of ciprofloxacin

Higuchi model (89): The release of a drug from a drug delivery system involves both dissolution and diffusion (89). A number of mathematical equations describe drug dissolution and/or release from drug delivery system. In the modern era of controlled-release oral formulations, ‘Higuchi equation’ has become a leading kinetic equation in its own right, as evidenced by studies on the drug dissolution that are recognized as an important factor in the development of drug delivery. The classical basic Higuchi equation is represented by

$$Q = A\sqrt{D(2C_0 - C_s)C_s t} \quad (3.4)$$

Where Q is the cumulative amount of drug released in time t per unit area, C_0 is the initial drug concentration, C_s is the drug solubility in the matrix and D is the diffusion coefficient of the drug molecule in the matrix.

After simplifying o the above equation, Higuchi equation can be represented as,

$$Q = K_H \times t^{1/2} \quad (3.5)$$

Where, K_H is the Higuchi dissolution constant. The data obtained were plotted as cumulative percentage drug release versus square root of time. Therefore, the simple Higuchi model will result a linear Q versus $t^{1/2}$ plot. Hence the slope of the above plot gives the Higuchi rate constant, K_H and the correlation coefficient in the graph will indicate if the drug release follows the Higuchi square root model, i.e., the mechanism of drug release is diffusion controlled or not. Figure 3.22 presents the graphical representation of this model.

Observation: The graphical representation of cumulative % of drug release against square root of time represents that drug release of ciprofloxacin from the matrix is perfectly following Higuchi drug release model as there is highest value of coefficient of correlation.

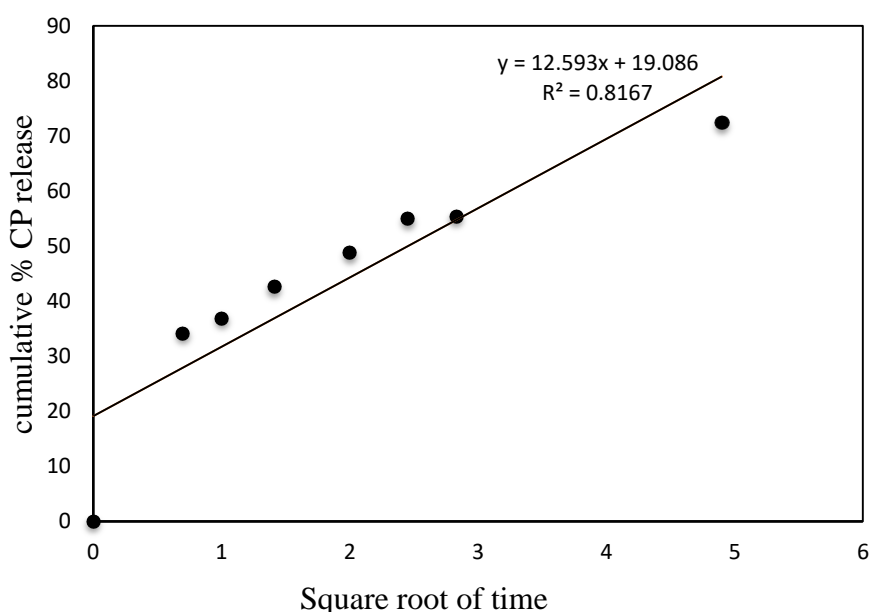


Figure 3.22: Higuchi model kinetic release of ciprofloxacin

Hixson-crowell model (90): The Hixson-Crowell cube root law describes the release from systems where there is a change in the surface area and diameter of particles or tablets. Hence, particles of regular area are proportional to the cubic root of its volume. Equation (3.6) represents a relation between drug release and time established by Hixson-Crowell on the basis of above concept.

$$W_0^{1/3} - W_t^{1/3} = K_{HCT}t \quad (3.6)$$

Where W_0 is the initial amount of drug in the nanocomposite, W_t is the quantity of drug released at time t , K_{HCT} is the Hixson-Crowell constant describing surface volume relation. For the investigation of drug release from a system is following this model or not, the cubic root of drug remaining in dissolution media obtained from in vitro dissolution study is plotted against time. If the value of correlation coefficient of this plot is higher, then we can interpret that change in surface area during the process of dissolution has a significant effect on drug release. Figure 3.23 shows the graphical representation of this model applied on the release profile of CP from CSNPs.

Observation: The lower value of correlation coefficient of this plot indicates that the CP release from CSNPs does not follow the principle of Hixson-Crowell model.

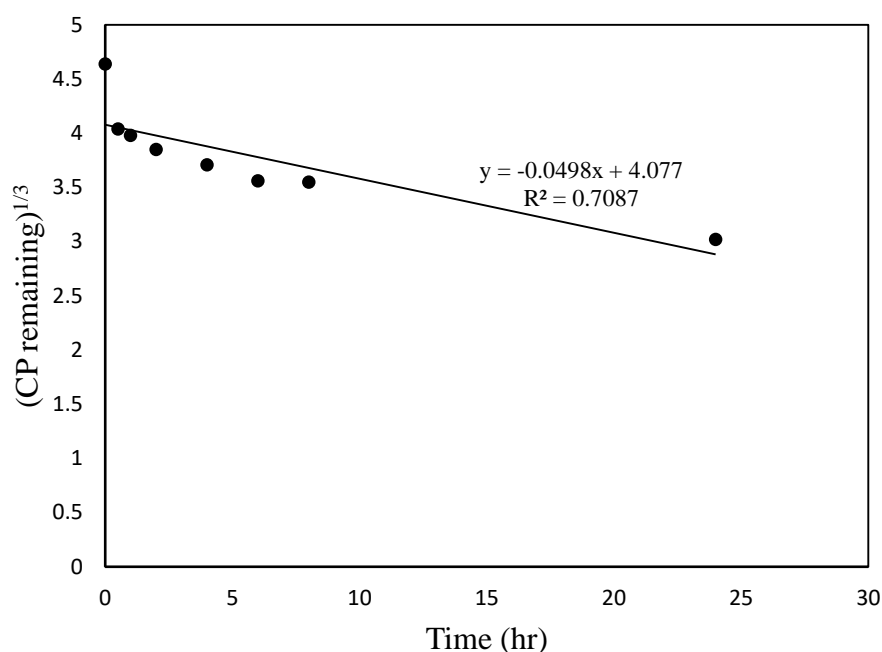


Figure 3.23: Hixson-Crowell model kinetic release of ciprofloxacin

Thus the in-vitro drug release profile was applied in different mathematical models and was interpreted in the form of graphical presentation and evaluated by correlation coefficient (R^2) represented in Table 3.10. The highest degree of correlation coefficient determines the suitable mathematical model that follows drug release kinetics. From the above comparison, it was found that Higuchi square root model showed higher degree of correlation coefficient (R^2) than other models.

Table 3.10: The correlation coefficients (R^2) obtained by fitting the ciprofloxacin release data from the ciprofloxacin loaded chitosan nanoparticles (CP-CSNPs) in PBS solutions at pH 7.4

Samples	Saturation release (%)	R^2			
		Zero order	First order	Higuchi	Hixson-Crowell
CP-CSNPs	72	0.5619	0.7787	0.8167	0.7087

So drug release was found to be best fitted by Higuchi square root model ($R^2 = 0.8167$ for ciprofloxacin) which implies that release of drug from matrix as a square root of time dependent process and diffusion controlled. Hence, drug release profile of ciprofloxacin follows diffusion mechanism.

3.5.3.3 Antibacterial activity analysis

Microbiological studies were observed in the antibacterial activities of the ciprofloxacin loaded chitosan nanoparticles (CP-CSNPs) against two types of bacteria which are, *Escherichia coli* (gram negative) and *Staphylococcus aureus* (gram positive). The antimicrobial activity of were evaluated using different techniques e.g. disc diffusion technique, minimum inhibitory concentration (MIC) test and minimum bactericidal concentration (MBC) test.

Disc diffusion technique: To evaluate the antibacterial activity of CP-CSNPs, different concentrations of free CP and that of CP-CSNPs were tested on microbial pathogens and they were compared. Results from the agar disc diffusion tests for antibacterial activities of CP-CSNPs and the free CP are illustrated in [Figure 3.24](#) Results showed that CP-CSNPs inhibited growth of both gram (+) and gram (-) bacterial strains. The diameters of zone of inhibition (in mm) of free CP and CP-CSNPs against *S. aureus* and *E. coli* are illustrated in [Table 3.11](#).

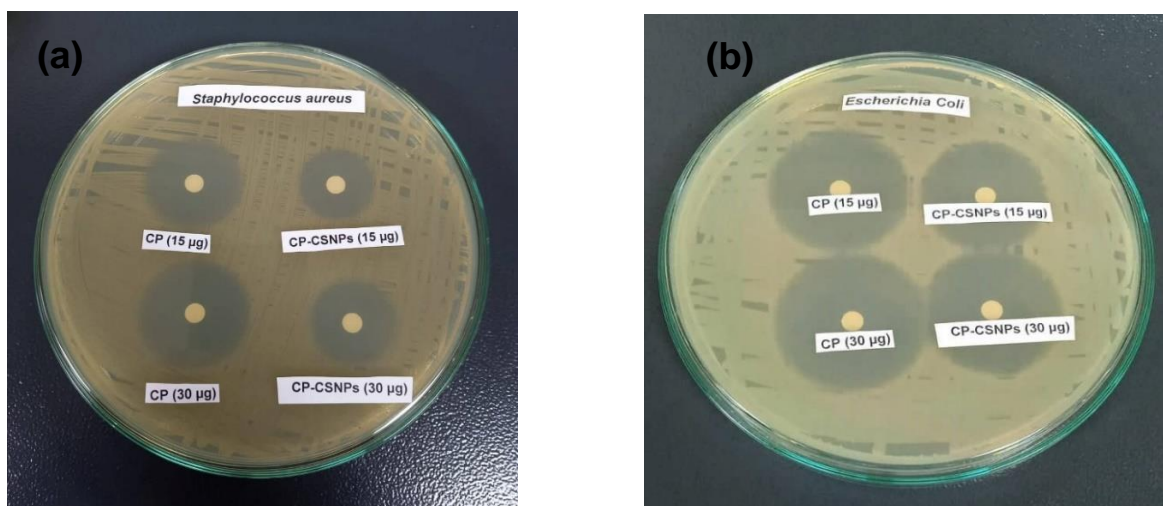


Figure 3.24: Photographic representation of zone of inhibition of free ciprofloxacin (CP) and ciprofloxacin loaded nanoparticles (CP-CSNPs) against *Staphylococcus aureus*.

Table 3.11: Results of the antibacterial activity of free CP and CP-CSNPs

Name of bacteria	Concentration (µg/disc)	Diameter of zone of inhibition (mm)	
		Ciprofloxacin	Ciprofloxacin loaded CSNPs
S. aureus (+ve)	15	29	24
	30	31	25
E. coli (-ve)	15	40	38
	30	44	41

From Figure 3.24, it is seen that in terms surrounding clearing zone, both free CP and CP-CSNPs showed a very clear inhibitory effect against *E. coli* and *S. aureus* indicating that prepared CP-CSNPs are active against both types of bacteria. But under identical conditions, free ciprofloxacin shows little higher zone of inhibition than CP-CSNPs against *S. aureus* and *E. coli*. This might be attributed by the slow diffusion of CP-CSNPs into the agar plate as ciprofloxacin was associated with chitosan nanoparticles of higher molecular weight and the result can be correlated to extended release or slow release of ciprofloxacin in a drug delivery system. In a study, CP-encapsulated PLGA nanoparticles shows lower antimicrobial activity than free CP in the in vitro analysis which is because of sustained release characteristics of nanoparticles (91). But CP-encapsulated PLGA nanoparticles

effectively inhibited the growth of bacteria due to the sustained release characteristics of nanoparticles than free CP in the case of in vivo analysis. These suggest that CP-CSNPs may have superior effectiveness to inhibit the growth of bacteria in vivo due to sustained release property.

MIC and MBC calculation by macro dilution method: The antibacterial activity of CP-CSNPs was further analyzed by MIC and MBC determination by using macro dilution method. Both MIC and MBC value of free CP and CP-CSNPs were same against gram negative bacteria *E. coli* and the value was $<0.03 \mu\text{g/ml}$. However, they showed an MIC value of $4 \mu\text{g/ml}$ and an MBC value of $64 \mu\text{g/ml}$ against gram positive bacteria *S. aureus*.

The results imply that both free CP and CP-CSNPs showed similar effect in liquid media. Sobhani et al., 2017 reported that CP-CSNPs showed better antibacterial activity than free CP (92) whereas Jeong et al., 2008 (91) suggested an opposite indication where in vitro antimicrobial activity of CP-encapsulated PLGA nanoparticles was relatively lower than free CP against *Escherichia coli*. However, our study showed no difference between free antibiotic and antibiotic loaded nano particles in liquid media.

So, we can say that loading of ciprofloxacin on chitosan nanoparticles do not show any negative effect on the antibacterial activity rather it can be highly active to inhibit bacterial growth in vivo.

3.6 Erythromycin Loading on Chitosan Nanoparticles (CSNPs)

Erythromycin (ER) was associated with chitosan nanoparticles (CSNPs) in the optimized condition for CSNPs formation in an ER: chitosan ratio of 1:2 as described in the experimental section and the prepared ER loaded CSNPs was characterized using following techniques.

3.6.1 Characterization of Erythromycin Loaded Chitosan Nanoparticles (ER-CSNPs)

3.6.1.1 SEM analysis

The SEM micrographs of Erythromycin-loaded chitosan nanoparticles in Figure 3.25 shows the morphological characteristics of ER-CSNPs. According to SEM, the particles were found to be uniform and spherical, with agglomerated nano-structures of approximately 35–45 nm in size. The size of the unmodified chitosan nanoparticles was 10-20 nm according to SEM as presented in Figure 3.7. This significant increase in size after the loading process indicates that possible adsorption of erythromycin on the surface of the nanoparticles.

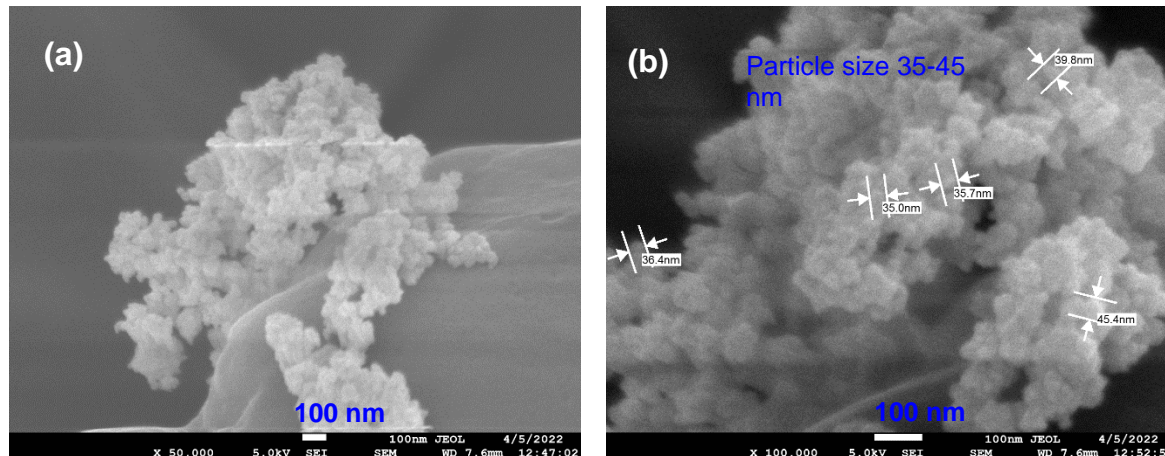


Figure 3.25: SEM micrograph of erythromycin loaded chitosan nanoparticles at (a) $\times 50,000$ and (b) $\times 100,000$ magnification

3.6.1.2 EDX analysis

The EDX results shown in Figure 3.26 confirms the presence of carbon, nitrogen and oxygen which are from chitosan and erythromycin and other elements such as sodium and

phosphorus from sodium tripolyphosphate in minor proportions. The elemental composition of ER-CSNPs according to EDX analysis are listed in Table 3.11.

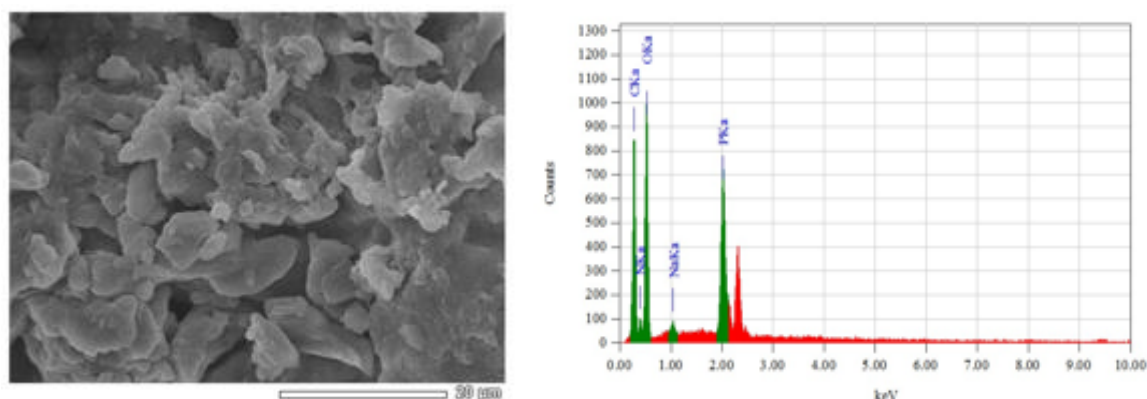


Figure 3.26: EDX spectra of erythromycin loaded chitosan nanoparticles

Table 3.12: Distribution of elements in erythromycin loaded chitosan nanoparticles

Element	Mass (%)	Atom (%)
C	38.38	46.27
N	11.23	11.61
O	42.21	38.21
Na	0.55	0.35
P	7.63	3.57

To compare the elemental composition, it should be noted that the chemical formula of Chitosan is $(C_6H_{11}NO_4)_n$; Sodium tripolyphosphate is $Na_5P_3O_{10}$ and Erythromycin is $C_{37}H_{67}NO_{13}$. A comparison of the elemental composition of ER-CSNPs according to EDX result in Table 3.12 with blank chitosan nanoparticles as presented in Figure 3.7 and Table 3.6 shows that the significant change in the atomic % of C, N and O was observed, indicating the loading of erythromycin on Chitosan nanoparticles.

3.6.1.3 Association efficiency (AE)

The SEM analysis revealed that the size of the ER-CSNPs (Figure 3.25) was significantly higher than the blank CSNPs (Figure 3.7). This increase of particle size indicates that erythromycin was adsorbed on the nanoparticle's surface. Besides, the image of blank

CSNPs obtained by TEM showed that the very small size of CSNPs in the range of 0.1-1nm may not be favorable for drug encapsulation. Thus, the percentage of association efficiency (AE) for the surface adsorbed erythromycin was approximately 92% for the nanoparticle formulation containing the Er : Chitosan ratio of 1:2 which was measured by uv analysis of the remaining erythromycin in the supernatant.

3.6.1.4 FT-IR analysis

The FT-IR spectra of chitosan and ER-CSNPs in [Figure 3.27](#) revealed that the characteristic peaks were almost similar. The FT-IR data in [Table 3.13](#) represents that the peaks for erythromycin loaded chitosan nanoparticles were found at around 3435 cm^{-1} for O–H stretching and N–H stretching vibrations, 1638 cm^{-1} for amide I, 1552 cm^{-1} for amide II and 1077 cm^{-1} for C–O–C stretching vibration. The observed peak at 1386 cm^{-1} , can be assigned due to CH₃ present in amide group of chitosan. The band at 1095 cm^{-1} was found for –C–O stretching vibration and 896 cm^{-1} was for antisymmetric stretching vibration for the structure of saccharide.

The characteristic peaks of chitosan were noticed. The combined peak for –OH stretching and –N–H stretching vibration was found at 3421 cm^{-1} for pure chitosan instead of 3435 cm^{-1} as shown [Figure 3.24](#) which indicates that the hydrogen bonding is enhanced in ER-CSNPs. The peak intensities of amide I band at 1657 cm^{-1} (C=O) and amide II band at 1595 cm^{-1} (NH₂ bending) in pure chitosan decreased in ER-CSNPs and two new sharp peaks at 1638 and 1552 cm^{-1} was observed. These are because of the cross-linking of ammonium groups of chitosan with tripolyphosphate molecules which causes the enhancement of inter- and intra-molecular interaction within ER-CSNPs.

The FTIR spectra of erythromycin ([Figure 3.27](#)) shows many intense, sharp absorption bands due to different functional groups present in molecules but there is no further significant modification of characteristic peaks of erythromycin loaded chitosan nanoparticles from chitosan. This indicates that there was no alteration of chitosan structure suggesting the absence of chemical interaction between ER and CSNPs. But some peaks were slightly shifted as described indicating that the electrostatic interaction is present between adsorbed ER and the CSNPs.

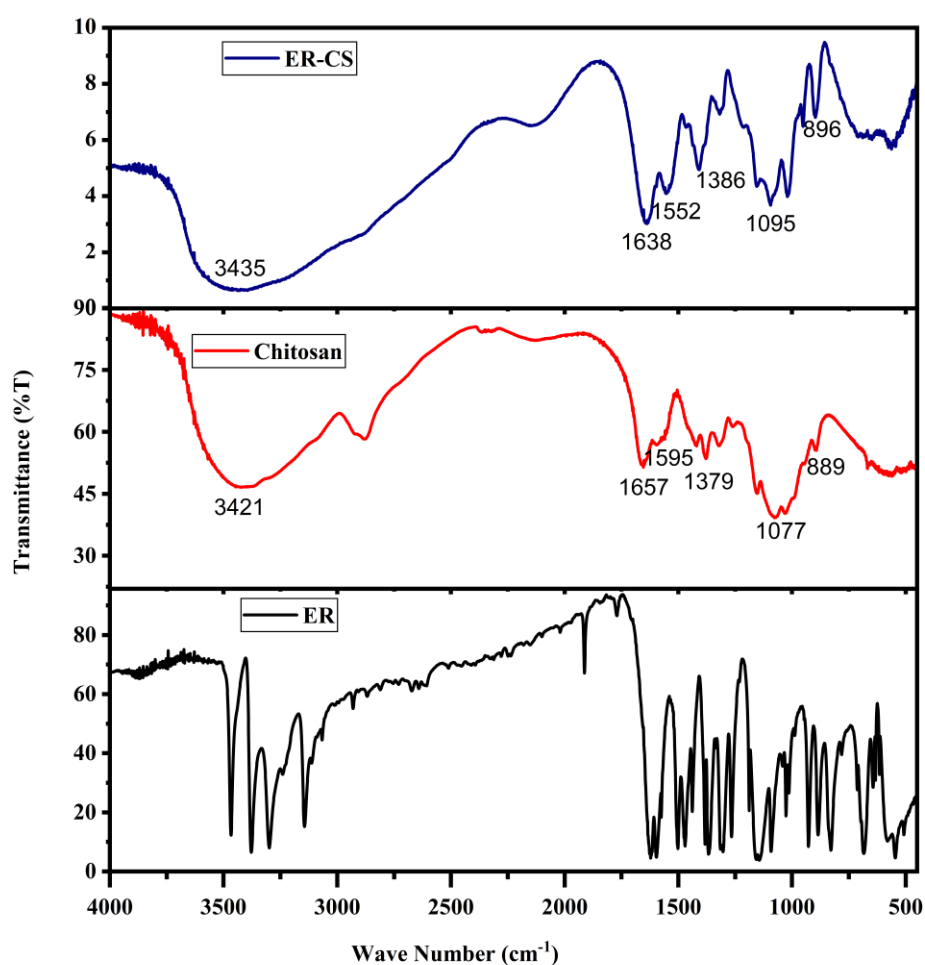


Figure 3.27: FT-IR spectra of pure erythromycin (ER), chitosan and erythromycin loaded Chitosan nanoparticles (ER-CSNPs)

Table 3.13: Tentative assessment of IR band of chitosan and ER-CSNPs

Wavelength (cm ⁻¹)	Mode	Tentative band
3435	Symmetric stretching	- NH and - OH, intermolecular hydrogen bonding
1638	Symmetric stretching	-C=O (amide I)
1552	Bending vibration	-NH ₂ (amide II)
1386	Stretching vibration	CH ₃ in amide group
1095	Stretching vibration	-C-O
896	Anti-symmetric stretching	Anhydro glucosidic ring

3.6.1.5 XRD analysis

The X-ray diffraction (XRD) pattern was analyzed for the identification of crystal phase of ER-CSNPs. The XRD of erythromycin, chitosan and chitosan nanoparticles containing erythromycin is represented in Figure 3.28. The XRD pattern of pure chitosan contains two broad peaks at $2\theta = 10.224$ and 20.357° . These peaks were indicating the semi-crystalline nature of chitosan as described earlier.

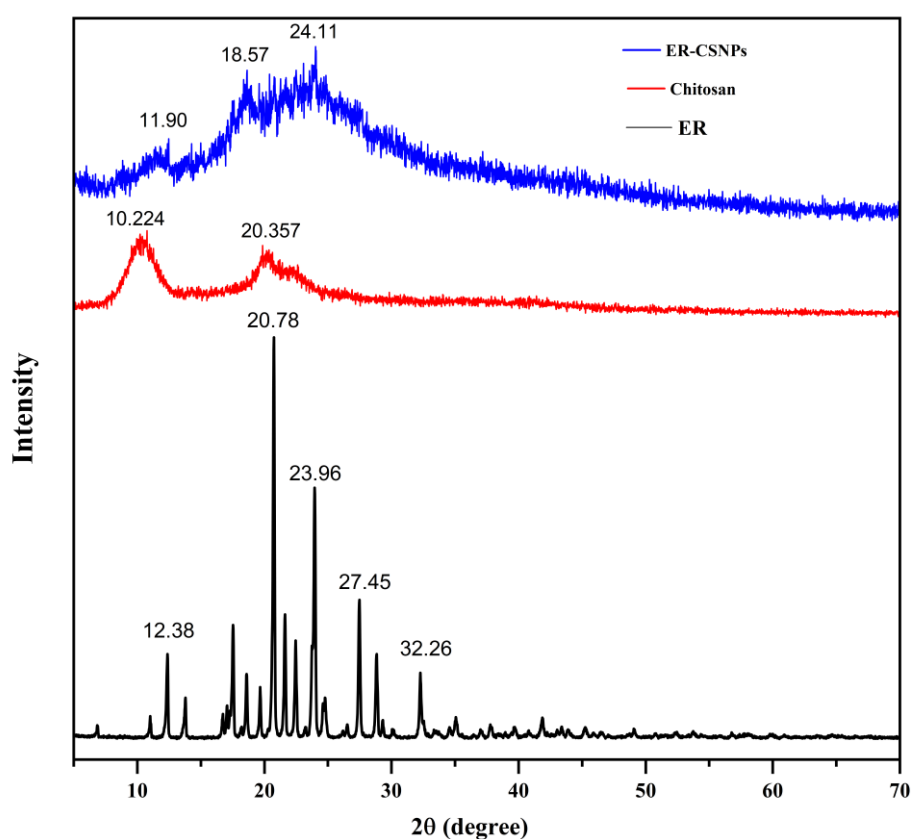


Figure 3.28: Powder XRD pattern of free erythromycin (ER), pure chitosan and erythromycin loaded chitosan nanoparticles (ER-CSNPs).

In the present work, for the erythromycin loaded chitosan nanoparticles, the peaks found at $2\theta = 11.61$ and 18.65 were broader and weaker than unmodified chitosan which indicates the amorphous nature of nanoparticles. Thus, chitosan was converted to an amorphous form during nanoparticle formation after crosslinking with TPP and loading of erythromycin.

The diffraction pattern of pure erythromycin (Figure 3.28) shows many intense sharp which indicates the crystalline nature of drug. These characteristic peaks were absent in XRD

pattern of ER-CSNPs. This disappearance of the characteristic peaks of the ER is because ER was associated with CSNPs and converted into the amorphous state.

3.6.2 Biomedical Application of Erythromycin Loaded Chitosan Nanoparticle (ER-CSNPs)

Biomedical application of ER-CSNPs was studied from the investigation of antibacterial activity of against gram (+ve) and gram (-ve) bacterial strains and the in vitro release profile study of ER from ER-CSNPs.

3.6.2.1 Antibacterial activity analysis

The antimicrobial activity of free ER and ER-CSNPs were evaluated against E.coli which is gram-negative and S.aureus which is gram-positive bacteria by determining the Minimum inhibitory Concentration (MIC) and minimum bactericidal concentration (MBC). [Table 3.14](#) represents the MIC and MBC values of free erythromycin and ER-CSNPs against these two different organisms and [Figure 3.29](#) and [3.30](#) show the photographic representation. MIC values for free ER and ER-CSNPs were same for same category of bacteria and also the MBC values were also same.

Table 3.14: MIC and MBC of erythromycin and ER-CSNPs against two microorganisms

Bacteria	Erythromycin		ER-CSNPs	
	MIC ($\mu\text{g/ml}$)	MBC ($\mu\text{g/ml}$)	MIC ($\mu\text{g/ml}$)	MBC ($\mu\text{g/ml}$)
S. aureus	32	64	32	64
E. coli	16	64	16	64

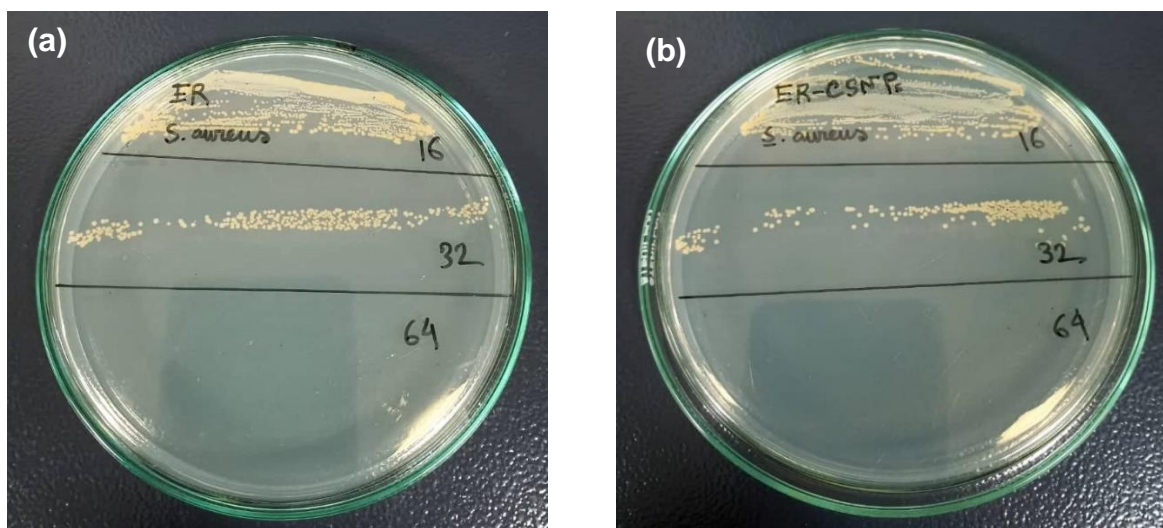


Figure 3.29: MBC of (a) erythromycin (ER) and (b) erythromycin loaded chitosan nanoparticles (ER-CSNPs) against *S. aureus*

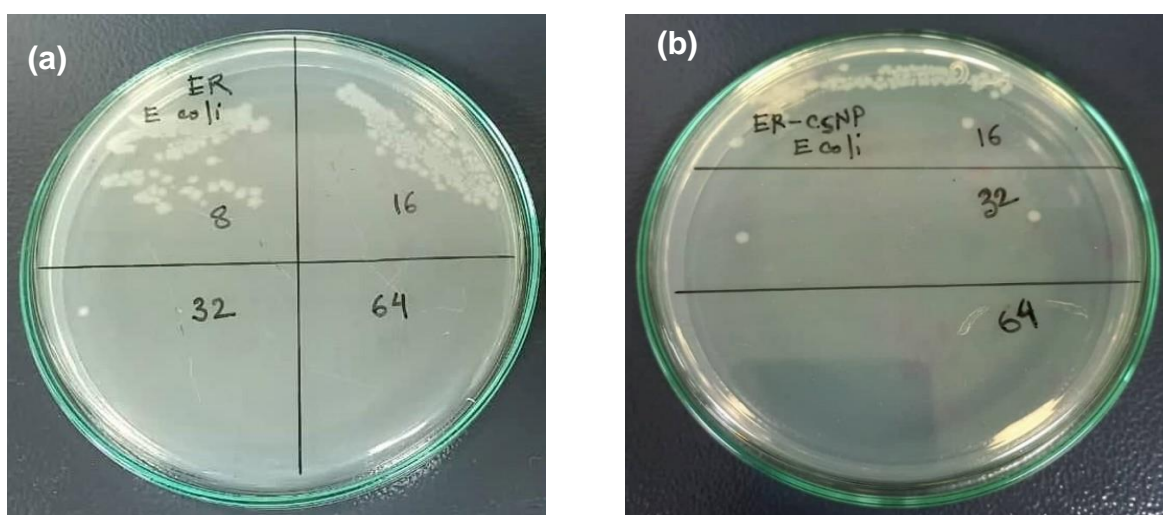


Figure 3.30: MBC of (a) erythromycin (ER) and (b) erythromycin loaded chitosan nanoparticles (ER-CSNPs) against *E. coli*

The results imply that both free erythromycin and chitosan nanoparticle loaded with erythromycin showed similar effect in liquid media. Finally, erythromycin and chitosan nanoparticle loaded with erythromycin were observed to have identical antibacterial properties confirming no negative impact of the chitosan on erythromycin regarding its antibacterial activity.

3.6.2.2 In vitro release study of erythromycin (ER) from chitosan nanoparticles (CSNPs)

In vitro release profile of ER from ER-CSNPs in PBS (pH 7.4) as presented in [Figure 3.31](#) indicates an initial rapid release of about 31% of ER at the first 0.5 h. After the period of rapid release, a slower or sustained release of ER from CSNPs was seen starting from 0.5 h according to the release profile. After 8 h, about 78% of ER was released following the sustained release mechanism. As discussed earlier, this initial rapid release is due to the rapid disintegration and diffusion of ER that are located on the surface of the CSNPs. As this period ended, the release mechanism changes to the degradation of CSNPs by the release medium. According to the SEM observation, the ER was adsorbed on the surface of the CSNPs. Hence, the electrostatic interactions between ER and CSNPs due to the adsorption decreases with the degradation of CSNPs by the release media. This degradation process changes the local pH and at certain threshold, the surface of CSNPs becomes neutral which initiates the drug release weakening the electrostatic interaction between ER and CSNPs.

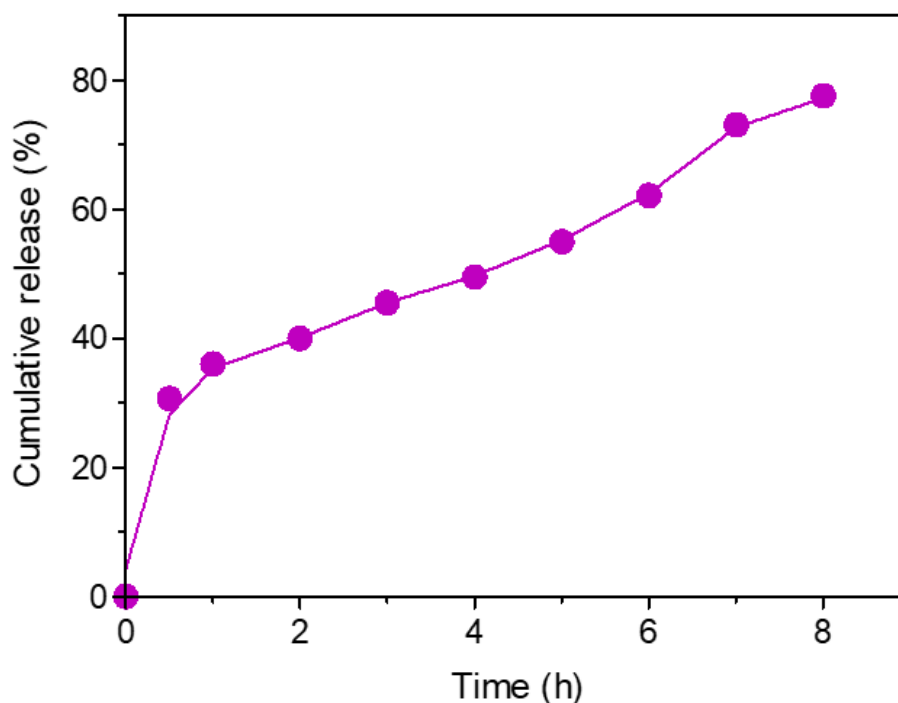


Figure 3.31: In vitro release of ER from CSNPs in PBS of 7.4

3.6.2.3 Release Kinetics of erythromycin (ER) from the nanoparticles

The release behavior of ER from CSNPs was further studied by fitting the data of ER release from CSNPs into phosphate buffered saline (PBS) at pH 7.4 by using zero order, first order, Higuchi and Hixson-Crowell kinetics model representing by the equations (3.1), (3.3), (3.5) and (3.6) respectively. Figure 3.32 represents the fitting of the experimental data of ER release from CSNPs with the linearized form of these kinetic model equations. The value of correlation coefficients for these models are summarized in Table 3.15.

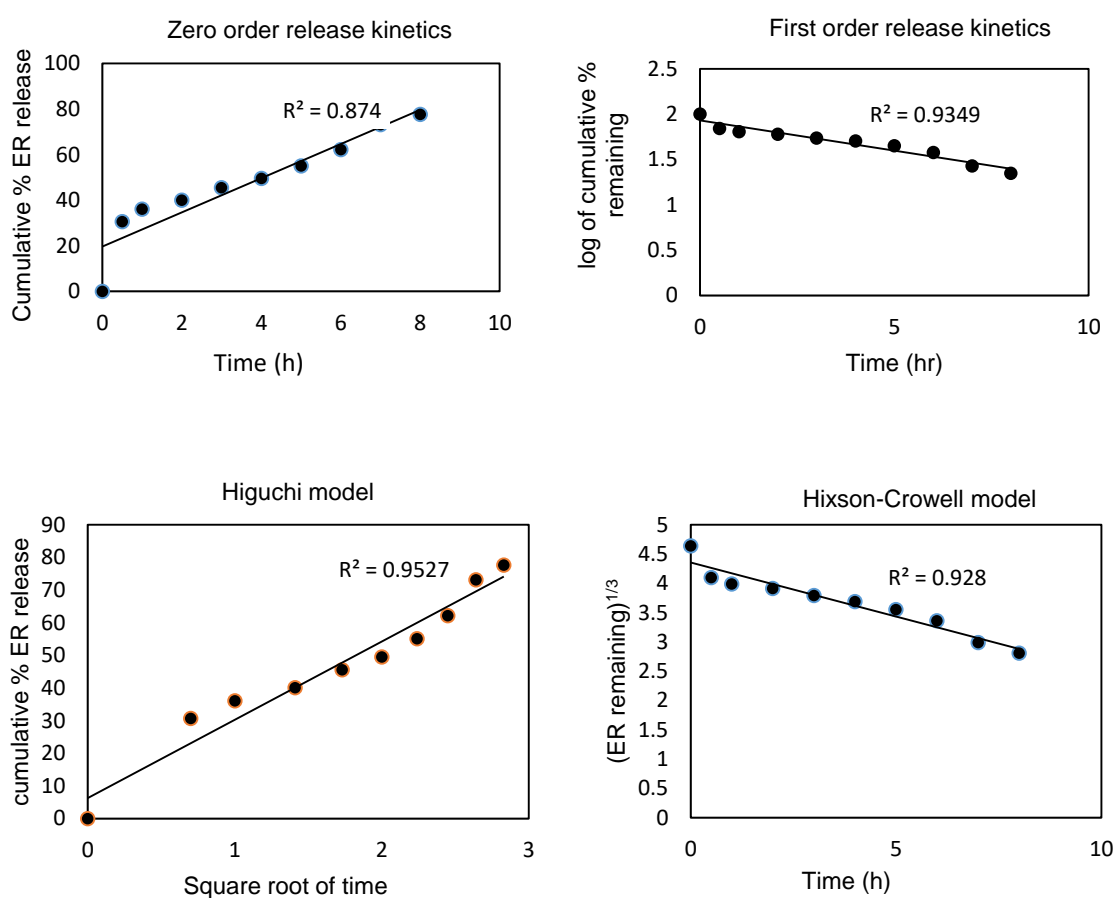


Figure 3.32: Study of release kinetics of ER release from CSNPs into PBS at pH 7.4 using four different kinetic models

Table 3.15: The correlation coefficients (R^2) obtained after data of ER release from ER-CSNPs in PBS of pH 7.4 fitted to different kinetic equations

Samples	Saturation release (%)	R^2			
		Zero-order	First order	Higuchi	Hixson-Crowell
ER-CSNPs	78	0.874	0.9349	0.9527	0.928
Equation		$C_t = C_0 + Kt$	$\log C = \log C_0 - Kt/2.303$	$Q = K \times t^{1/2}$	$W_0^{1/3} - W_t^{1/3} = Kt$

C_t is the amount of drug released at time t , C_0 is the initial concentration of drug, C is the percent of drug remaining at time t , Q is the cumulative amount of drug released in time t , W_0 is the initial amount of drug used, W_t is the remaining amount of drug at time t and K is the rate constant of individual release kinetics.

The highest correlation coefficient (R^2) values of Higuchi square root model (0.9527) represents that the release kinetic data are best fitted to this method. Thus the release profile of ER from CSNPs is following the Higuchi model indicating that the release mechanism of ER from ER-CSNPs follows the diffusion controlled release mechanism.

3.7 Metronidazole (MTZ) Loading on Chitosan Nanoparticles (CSNPs)

Metronidazole (MTZ) was associated with chitosan nanoparticles (CSNPs) in the optimized condition for CSNPs formation in a MTZ to chitosan ratio of 0.5:1. This lower concentration of MTZ in comparison to chitosan was selected for loading of metronidazole within chitosan nanoparticles because of the low solubility of metronidazole in chitosan solution at higher concentration level. In addition, it is evident from results of previous reports that increase of metronidazole concentration leads to a decrease of metronidazole loading on CSNPs (79). Thus MTZ loaded CSNPs was characterized using following techniques.

3.7.1 Characterization of Metronidazole Loaded Chitosan Nanoparticles (MTZ-CSNPs)

3.7.1.1 SEM analysis

The morphological characteristics of MTZ-CSNPs formulation was examined using FESEM. Figure shows the morphology of nanoparticles at different magnifications. It was shown from SEM images that there was cluster of particles and the particles were in the agglomerated state. At higher magnification ($\times 150,000$), the SEM image in Figure 3.33(b) shows that the particle size is in the range of 25-45 nm.

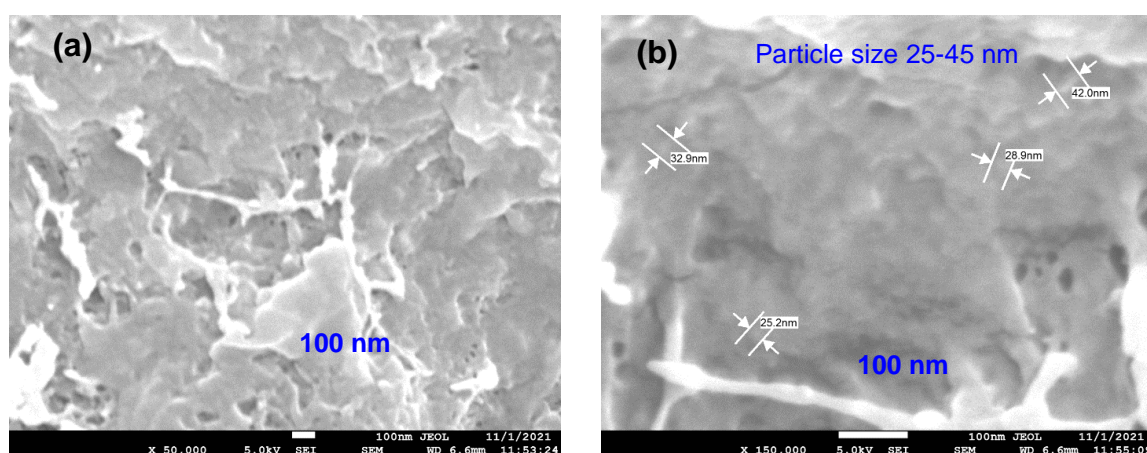


Figure 3.33: SEM micrograph of metronidazole loaded chitosan nanoparticles at (a) $\times 50,000$ and (b) $\times 150,000$ magnification

3.7.1.2 EDX analysis

For the rapid qualitative and quantitative analysis of the composition of elements present in MTZ-CSNPs, an elemental analysis was done using FESEM equipped with an energy dispersive X-ray (EDX) analyzer. The EDX results showed in Figure 3.34 confirms the presence of carbon, nitrogen and oxygen with an atomic weight of 45.14%, 11.04% and 34.02% respectively which are the element of chitosan and metronidazole. The elemental composition of metronidazole loaded chitosan nanoparticles according to EDX analysis are listed in Table 3.16. To compare the composition, it is noted that the chemical formula of chitosan is $(C_6H_{11}NO_4)_n$, Sodium tripolyphosphate is $Na_5P_3O_{10}$, and Metronidazole is $C_6H_9N_3O_3$.

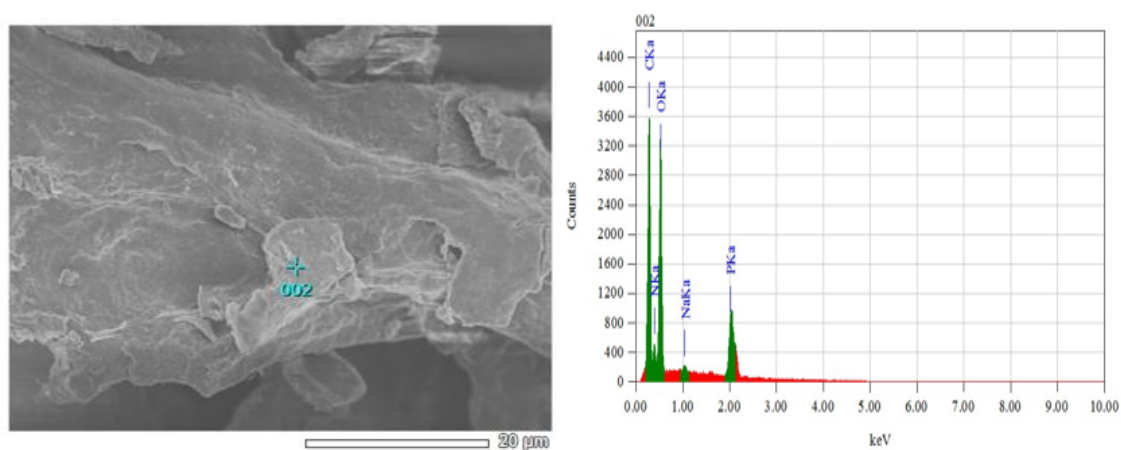


Figure 3.34: EDX spectra of metronidazole loaded chitosan nanoparticles

Table 3.16: Distribution of elements in metronidazole loaded chitosan nanoparticles

Element	Mass (%)	Atom (%)
C	35.21	45.14
N	10.04	11.04
O	35.35	34.02
Na	0.91	0.61
P	18.50	9.20

The EDX results also confirm the presence of Na and P with atomic weight of 0.91% and 9.20% respectively which confirms the presence of sodium tripolyphosphate in the nanoparticles. Comparing the EDX result of MTZ-CSNPs with blank one which is represented in Figure 3.7, it is seen that there is significant change in the atomic % of C, N and O which proves metronidazole loading into chitosan nanoparticles. The EDX qualitative analysis also shows that there is no element present in the nanoparticles as impurity.

3.7.1.3 TEM analysis

The MTZ-CSNPs were examined using the transmission electron microscope (TEM), and the images are shown in Figure 3.35. The selected area electron diffraction (SAED) pattern was also taken using TEM (Figure 3.35) to further confirm the crystalline phase of MTZ-CSNPs. From the Figure 3.35 it is seen that the nanoparticles have spherical shapes with agglomerate behaviors. The size of the individual nanoparticles is around 0.4-1.5 nm whereas the mean diameter of blank chitosan nanoparticles was about 0.1 to 1 nm according to TEM analysis as represented in Figure 3.8. The TEM analysis also represents the increase of particle size after the loading process. Finally, on the basis of SEM and TEM analysis, we can summarize that metronidazole was adsorbed and loaded on the surface of the chitosan nanoparticles. Our further characterization study will give details about this matter. The diffused rings were observed in the SAED pattern of MTZ-CSNPs as shown in Figure 3.35(c) which is due to the amorphous nature of the metronidazole loaded nanoparticles. Meanwhile, in XRD also, amorphous nature of MTZ-CSNPs was reflected by the presence of broad peaks in SAED pattern.

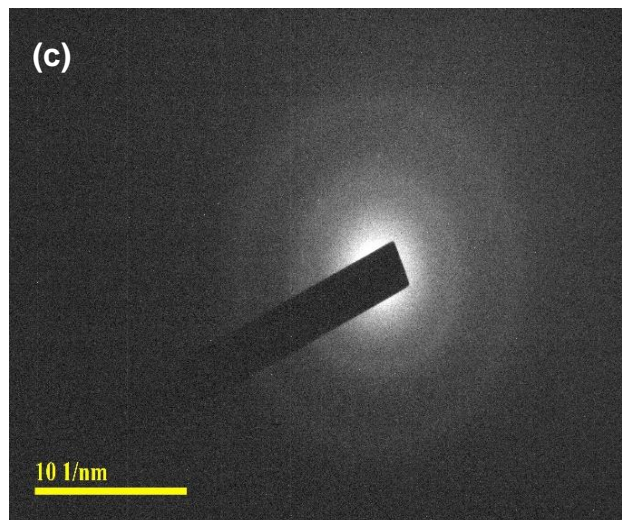
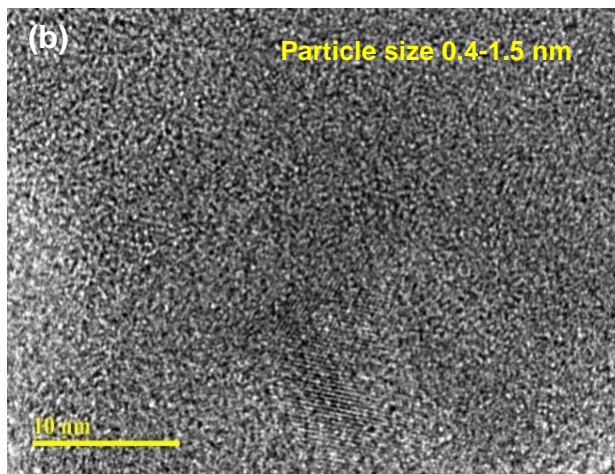
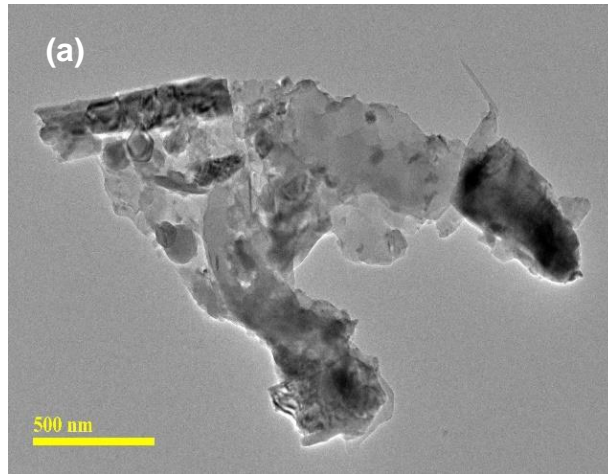


Figure 3.35: (a, b) TEM images of MTZ-CSNPs at two different magnification and (c) the SAED pattern of MTZ-CSNPs

3.7.1.4 Association efficiency (AE)

The association efficiency of metronidazole with chitosan nanoparticles for this selected formulation was determined by equation (2.10). This metronidazole: chitosan ratio of 0.5:1 was selected for loading of metronidazole within chitosan nanoparticles because of the low solubility of metronidazole in chitosan solution at higher concentration level. In addition, it is evident from results of previous reports that increase of metronidazole concentration leads to a decrease of metronidazole loading on CSNPs (79). Finally, the percentage of AE was found to be 89.13 % which is satisfactory and higher than that of previous studies (79).

3.7.1.5 FTIR analysis

To investigate the formation of MTZ-CSNPs, FTIR studies were carried out. Figure 3.36 shows the FTIR spectra of chitosan, metronidazole and MTZ-CSNPs prepared by the ionotropic gelation of chitosan and TPP. The pure chitosan has characteristic peaks for -OH at 3421 cm^{-1} , symmetric and asymmetric stretching of -CH at 2923 and 2878 cm^{-1} respectively, C=O stretching of amide I at 1657 cm^{-1} . The small band of the N-H bending of amide II was found at 1595 cm^{-1} , whereas the presence of the C-N stretching of amide III was found at 1379 cm^{-1} . Furthermore, CH_2 bending and CH_3 stretching were confirmed by the presence of peaks at 1417 and 1323 cm^{-1} , respectively. The absorption bands at 1077 and 1027 cm^{-1} correspond to the C-O stretching. The FTIR of a pure metronidazole is also represented in Figure 3.36. The peaks were obtained at 3223 , 3102 , 1535 , and 1267 cm^{-1} , which can be ascribed to the -OH , -CH , -CN , and -N=O functional groups of the pure metronidazole. In the case of the metronidazole loaded chitosan nanoparticles, the peak for -OH stretching was slightly shifted to 3434 from 3421 cm^{-1} indicating the enhancement of hydrogen bonding in it. The peak for the C=O stretching was found at 1642 cm^{-1} instead of 1657 cm^{-1} . The peak at around 1595 cm^{-1} is assigned to the NH bending vibration of amide II groups which were observed clearly in pure chitosan, decrease dramatically, and a new absorption bands at 1536 cm^{-1} appear, which shows that the ammonium groups are crosslinked with tripolyphosphate molecules. The peak present at 1265 cm^{-1} corresponds to N=O stretching of metronidazole in the nanoparticles. In conclusion, some peaks were slightly shifted. This can be explained due to the hydrogen bonding as well as electrostatic interactions between chitosan and the adsorbed metronidazole on the surface of the nanoparticles.

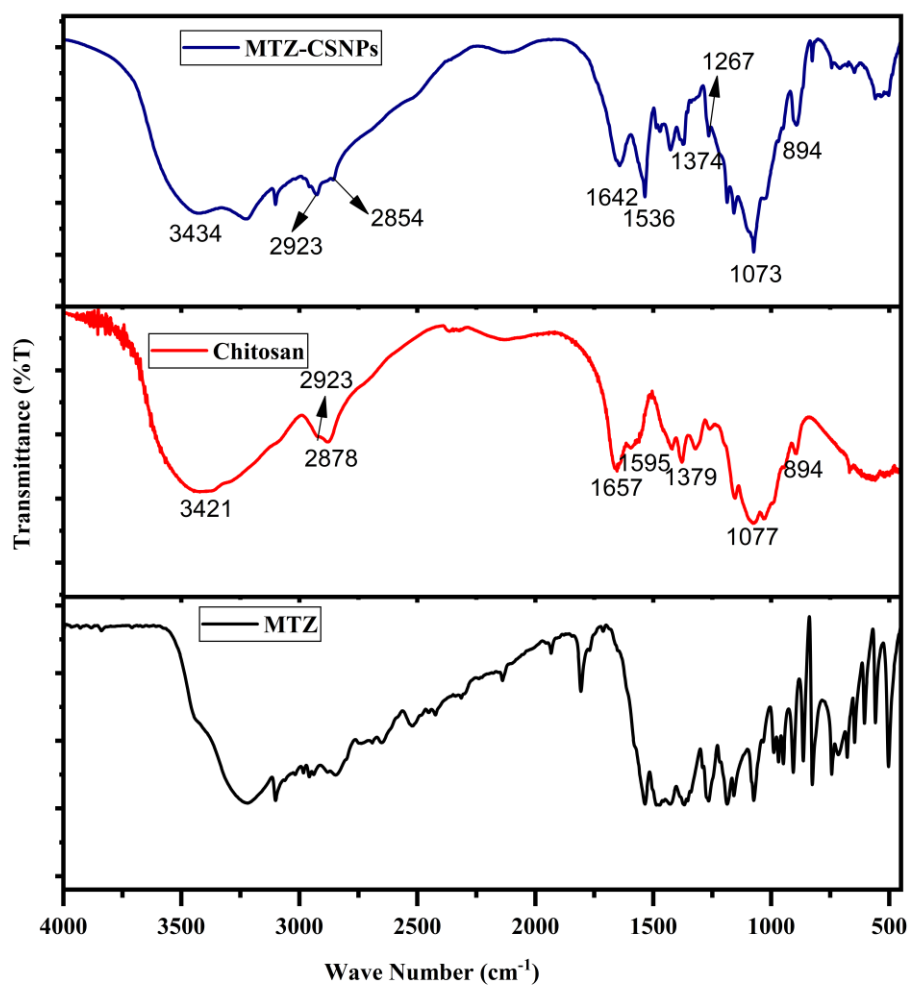


Figure 3.36: FTIR spectra of pure metronidazole (MTZ), chitosan and metronidazole loaded chitosan nanoparticles (MTZ-CSNPs)

Table 3.17: Tentative assessment of IR band of metronidazole loaded chitosan nanoparticles

Observed peak (cm ⁻¹)	Mode	Tentative band
3454	Symmetric stretching	-NH and -OH
2854 and 2923	Asymmetric and symmetric stretching	-CH ₂ (Pyranose ring)
1642	Symmetric stretching	-C=O (amide I)
1536	Bending vibration	-NH ₂ (amide II)
1073	Stretching vibration	-C-O
894	Anti-symmetric stretching	Structure of saccharide
1267	Stretching of MTZ functional group	N=O

3.7.1.6 XRD analysis

Powder X-ray diffraction (XRD) patterns of the pure metronidazole, chitosan and metronidazole loaded chitosan nanoparticles were recorded between 5 and 70° of the 2θ diffraction angle and presented in Figure 3.37. The XRD pattern of pure chitosan shows semi crystalline properties with two peaks at 2θ = 10.224 and 20.357° corresponding to the (020) and (110) planes respectively.

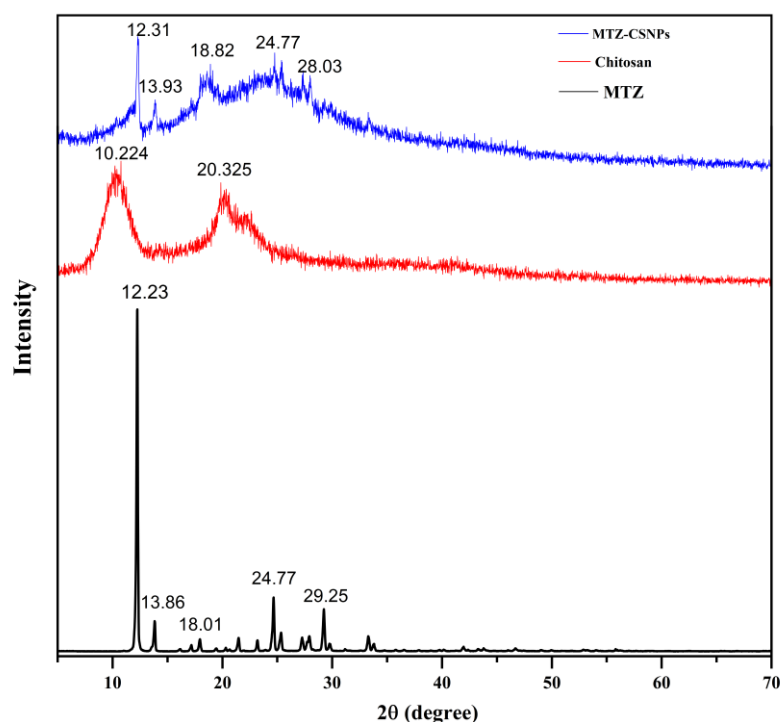


Figure 3.37: Powder XRD pattern of free metronidazole (MTZ), pure chitosan and metronidazole loaded chitosan nanoparticles (MTZ-CSNPs).

In the case of MTZ-CSNPs these diffraction peaks were decreased after metronidazole loading which indicates that crystallinity was completely destroyed in the nanoparticles. At the same time, the metronidazole powder shows several sharp and intense peaks which indicates the crystalline pattern of drug. The XRD pattern of metronidazole loaded chitosan nanoparticles represents some small diffraction peaks for metronidazole at 2θ near 12, 13, 18, 24 and 28° when compared to free metronidazole. But these peaks were very broad and weaker and the other peaks were disappeared in the MTZ-CSNPs. This might be due to the loading of metronidazole on the nanoparticles and the modification procedure destroyed the crystal structure of metronidazole.

3.7.2 Biomedical Application of Metronidazole Loaded Chitosan Nanoparticles (MTZ-CSNPs)

This chitosan-based nanoparticle systems for metronidazole are used to improve the biodistribution properties of MTZ at the released site. To investigate the improvement of biomedical application of MTZ-CSNPs, the in vitro release of MTZ from CSNPs was observed.

3.7.2.1 In vitro release study of metronidazole (MTZ) from chitosan nanoparticles (CSNPs)

Figure 3.38 shows the in vitro release profile of MTZ from CSNPs in phosphate buffer saline of pH 7.4. A rapid release of about 27% of MTZ was observed up to the first 1 h of the release profile which was followed by a slower release of MTZ for the following 25 h. This initial rapid release might be due to the rapid disintegration of MTZ that are located at the surface of the CSNPs or close to the surface of the CSNPs or might be the result of rapid hydration of NPs owing to the hydrophilic nature of chitosan. As the rapid or burst release period ended, the rate of release of MTZ fell which indicates the change in the drug release

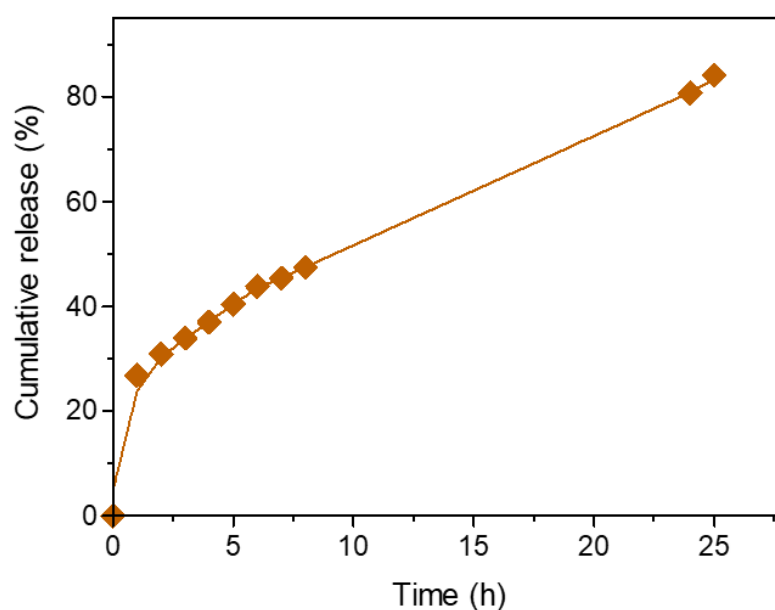


Figure 3.38: Metronidazole release profile from CSNPs in PBS of pH=7.4.

mechanism. The release medium penetrates into the particles and nanoparticles begin to degrade. Therefore, it could be proposed that the major factor that determines the release of MTZ from CSNPs is its solubilization or disintegration rate in the release medium. Initially, according to our previous characterization techniques, we postulated that MTZ was adsorbed onto the nanoparticle surface and there was electrostatic interaction between MTZ molecules and CSNPs due to adsorption. As the nanoparticles begin to degrade, the local pH was changed and at a certain threshold, the surface of CSNPs becomes neutral, which weakens the electrostatic interactions between MTZ and CSNPs and initiates the drug release.

Finally, from the release profile of MTZ-CSNPs, it is clear that the loading of MTZ in the CSNPs can effectively sustain MTZ release.

3.7.2.2 Release kinetics of metronidazole (MTZ) from the nanoparticles

The dissolution or release profile of MTZ can be described by several mathematical models representing several release kinetics. To understand the drug release kinetics of MTZ-CSNPs, the four different mathematical equations which were employed for the dissolution profile of MTZ-CSNPs are represented in [Figure 3.39](#). Data obtained from the in-vitro release studies of MTZ-CSNPs were fitted to zero-order, first-order, Higuchi model, and Hixson-Crowell model. The results for the correlation coefficient (R^2) and percentage of saturation release are presented in [Table 3.18](#). The optimum model was chosen on the basis of the highest correlation coefficient (R^2) value of these models.

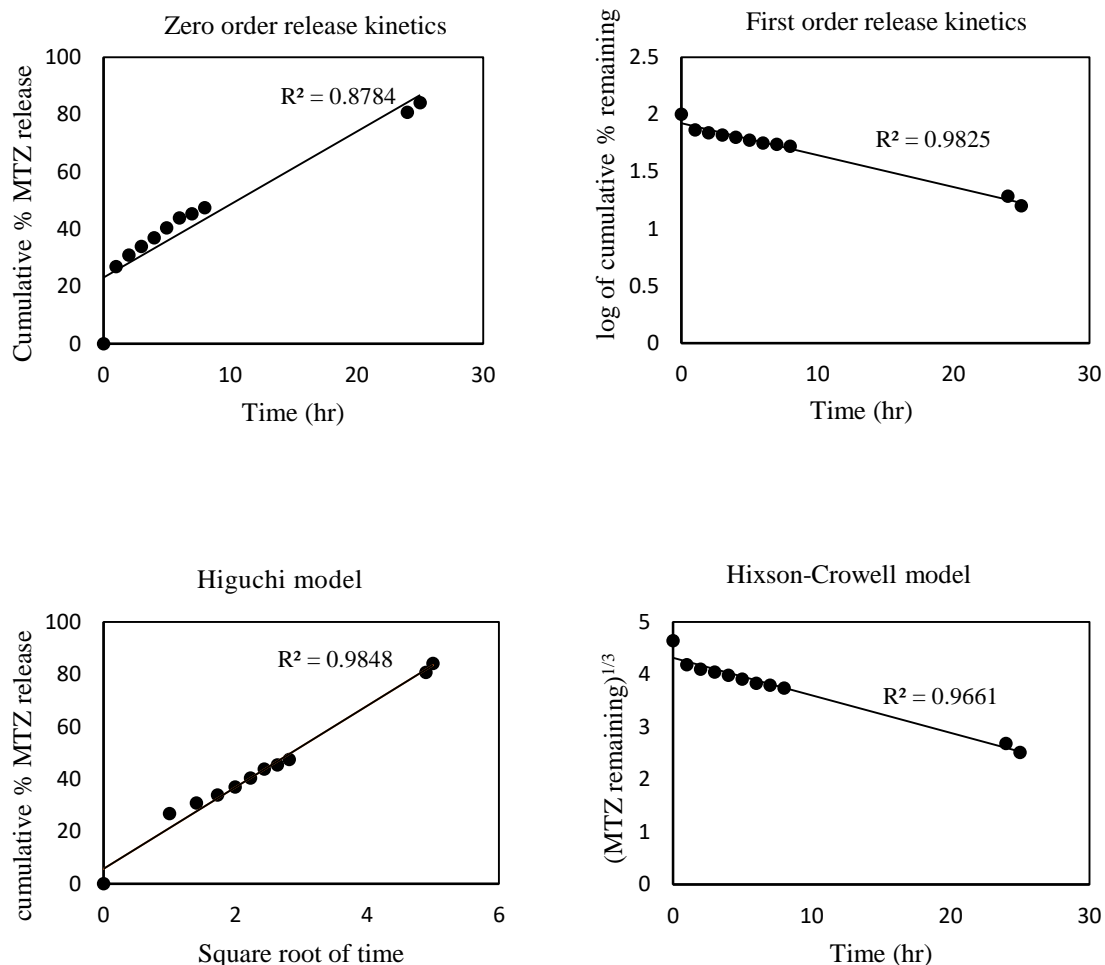


Figure 3.39: Release kinetics study of MTZ release from CSNPs into PBS at pH 7.4 using four different kinetic models.

Table 3.18: The correlation coefficients (R^2) obtained after data of MTZ release from MTZ-CSNPs in PBS of pH fitted to different kinetic equations

Samples	Saturation release (%)	R^2			
		Zero-order	First order	Higuchi	Hixson-Crowell
MTZ-CSNPs	84	0.8784	0.9825	0.9848	0.9661
Equation		$C_t = C_0 + Kt$	$\log C = \log C_0 - Kt/2.303$	$Q = K \times t^{1/2}$	$W_0^{1/3} - W_t^{1/3} = Kt$

C_t is the amount of drug released at time t , C_0 is the initial concentration of drug, C is the percent of drug remaining at time t , Q is the cumulative amount of drug released in time t , W_0 is the initial amount of drug in the pharmaceutical dosage form, W_t is the remaining amount of drug in the pharmaceutical dosage form at time t and K is the rate constant of individual release kinetics.

The graphical representation of these four mathematical represents that the release of MTZ from the CSNPs is perfectly following the Higuchi drug release model as the drug release profile is very closest to the trend line or regression line and the correlation coefficient (R^2) value is the highest. Thus, the Higuchi kinetic model is more satisfactory to describe the release kinetic process of MTZ from the CSNPs compared to other models used in this study. Hence, it can be summarized that the mechanism release profile of MTZ-CSNPs follows the diffusion-controlled release mechanism. Today the Higuchi equation is considered one of the most widely used and the most well-known controlled-release equation.

3.8 Perindopril Erbumine (PE) Loading on Chitosan Nanoparticles (CSNPs)

Perindopril erbumine (PE) was associated with chitosan nanoparticles (CSNPs) in the optimized condition for CSNPs formation in a PE: chitosan ratio of 1:1 and the PE loaded CSNPs was characterized using following techniques.

3.8.1 Characterization of Perindopril Erbumine Loaded Chitosan Nanoparticles (PE-CSNPs)

3.8.1.1 SEM analysis

The visualization of the size and morphology of PE-CSNPs was performed by FESEM. Figure 3.40 shows the FESEM images of PE-CSNPs at different magnifications. The average measured diameter of PE-CSNPs by FESEM was 20-30 nm as shown in Figure 3.40. As compared to the particle size of blank chitosan nanoparticles which is shown in Figure 3.7, the particle size is larger in the case of PE-CSNPs. This difference indicated the possible adsorption of PE on the surface of the nanoparticles increasing the particle size. The images also showed that the particles are spherical in shape, separated from each other, suggesting possible stabilization of the nanoparticles due to the positive surface charges (41).

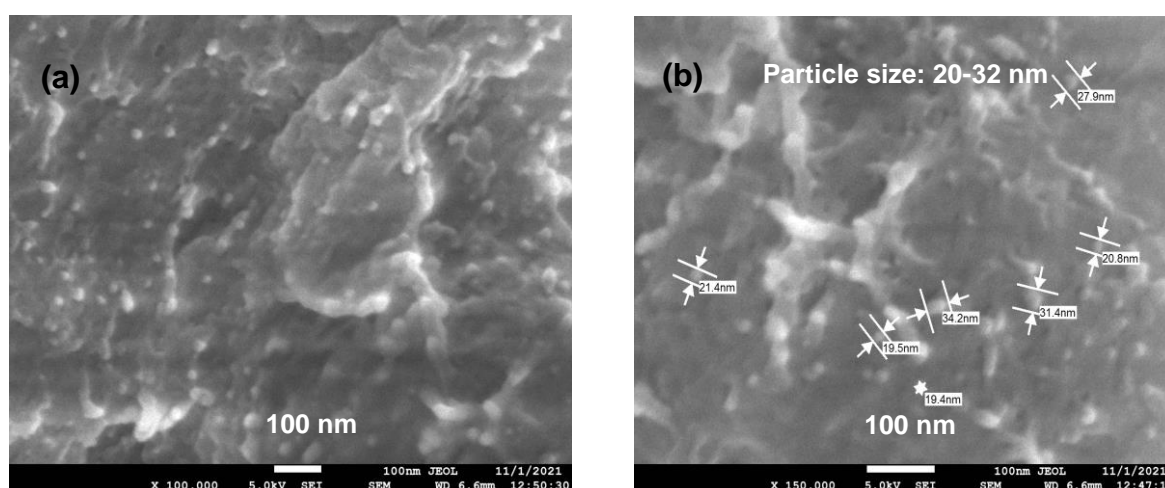


Figure 3.40: SEM micrographs of perindopril erbumine loaded chitosan nanoparticles at (a) $\times 100,000$ magnification and (b) $\times 150,000$ magnification

3.8.1.2 EDX analysis

The qualitative and quantitative analysis of PE-CSNPs were implemented by FESEM equipped with an EDX analyzer which provides the information about the elemental composition in PE-CSNPs. Figure 3.41 shows the EDX spectra from a selected area. The elemental composition of PE-CSNPs according to EDX analysis are listed in Table 3.19. The chemical formula of perindopril erbumine is $C_{23}H_{43}N_3O_5$.

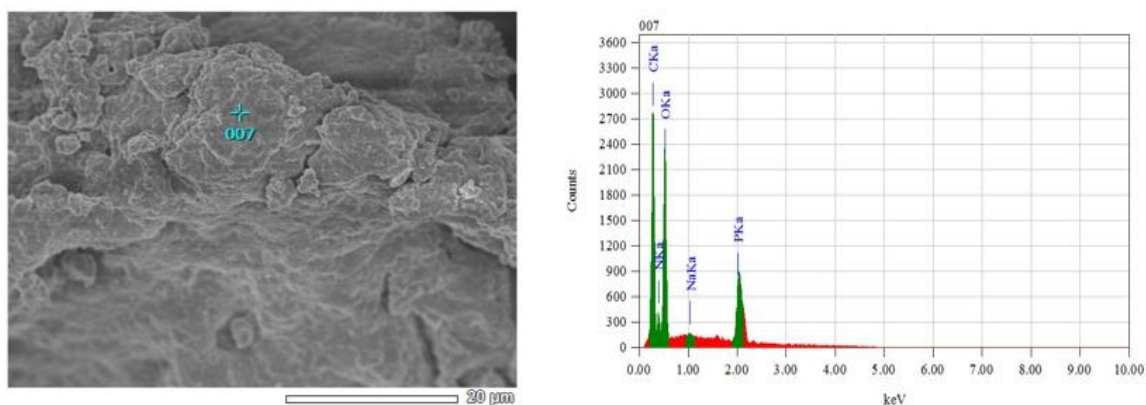


Figure 3.41: Elemental analysis of PE-CSNPs from EDX spectra

Table 3.19: Distribution of elements in perindopril erbumine loaded chitosan nanoparticles

Element	Mass (%)	Atom (%)
C	36.49	46.73
N	9.44	10.37
O	34.28	32.96
Na	0.64	0.43
P	19.15	9.51

The quantitative analysis as confirmed from the EDX spectrum analysis showed that the nanostructure contained C, N, and O with an atomic weight of 46.73%, 10.37%, and 32.96%, respectively which comes for chitosan and perindopril erbumine. Particles also contained Na and P with an atomic weight of 0.43 and 9.51, respectively which confirms the presence of sodium triphosphate in the nanoparticles. Comparison of the EDX quantitative analysis result of PE-CSNPs with blank one (Figure 3.7), it is seen that there is

a significant change in the atomic % of C, N, and O which proves PE was loaded to chitosan nanoparticles.

3.8.1.3 TEM analysis

The high-resolution transmission electron microscope (TEM) and selected area electron diffraction (SAED) pattern using TEM were used to describe the morphology, particle size, and crystal structure of PE-CSNPs. Figure 3.42 illustrated the TEM images and SAED pattern of the prepared PE-CSNPs. The prepared CSNPs loaded with PE were of nanometer size. The TEM images reveal that the prepared nanoparticles display spherical shapes (Figures 3.42 b). The diameter of unmodified chitosan nanoparticles was about 0.1-1 nm in

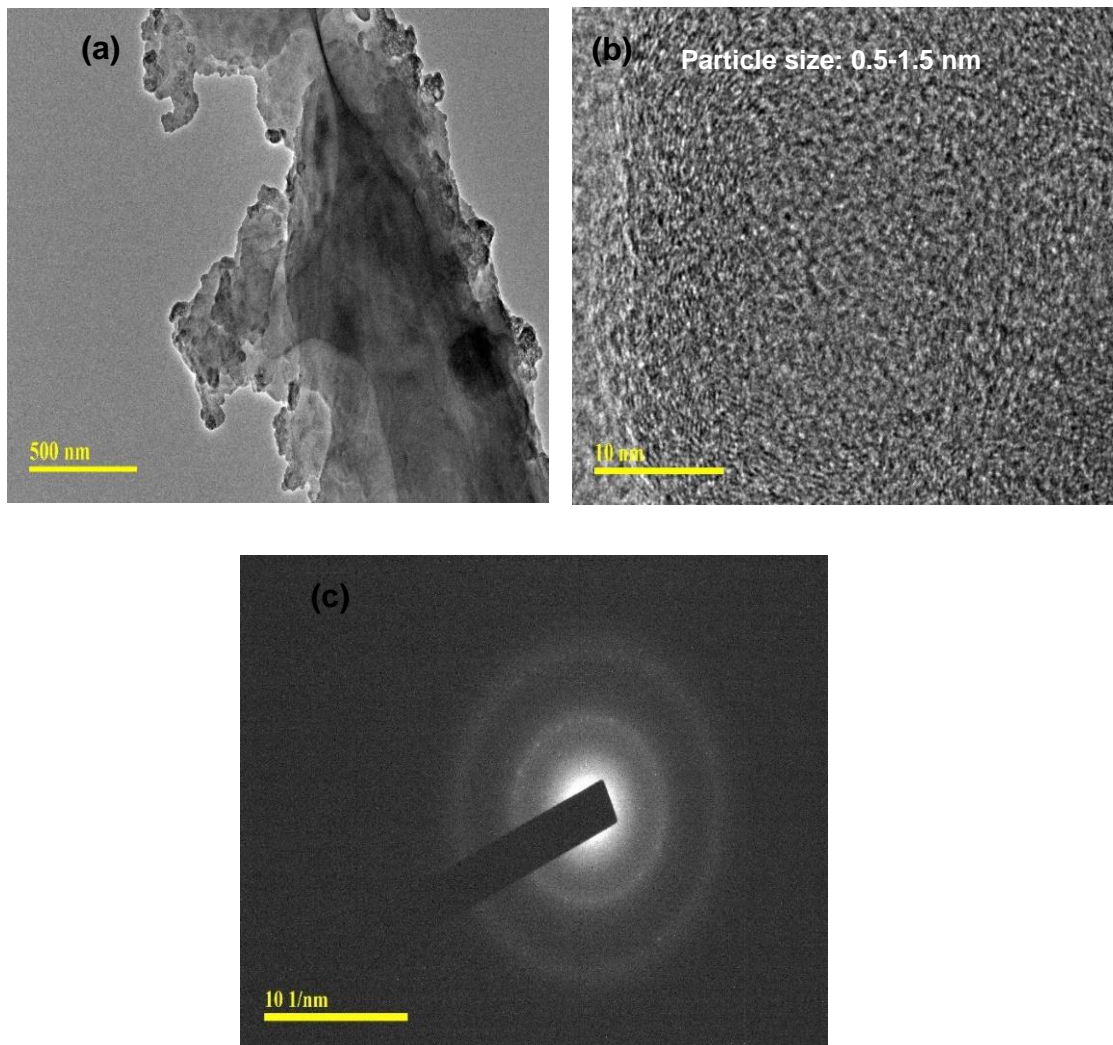


Figure 3.42: TEM micrographs of PE-CSNPs with different magnifications (a and b), and (c) SAED pattern of PE-CSNPs

the range (Figure 3.8), whereas the size range of PE-CSNPs is around 0.5-1.5 nm (Figure 3.42 b). This increase in size after the loading process demonstrated the formation of the chitosan nanoparticles which were loaded with PE and the loading process involves the adsorption of PE on the surface of the CSNPs. The crystalline nature of the particles was confirmed by analyzing the electron diffraction (ED) patterns. According to the ring pattern in SAED of prepared PE-CSNPs, the diffused ring was observed as represented in Figure 3.42 (c) which indicates that the prepared PE loaded nanoparticles is amorphous in nature. Meanwhile, the amorphous phase of PE-CSNPs was also detected with the appearance of broad peaks at the XRD pattern of PE-CSNPs. Thus, the obtained result from SAED pattern is consistent with the results of XRD analysis.

3.8.1.4 Association efficiency (AE)

From the TEM analysis, it was postulated that the loading of PE on the CSNPs occurred by the association of PE within CSNPs by adsorption. Thus, the percentage of association efficiency (AE) of PE with chitosan nanoparticles was determined by equation (2.11). The high concentration of perindopril erbumine with a drug: polymer ratio of 1:1 was efficiently loaded to chitosan nanoparticles with the AE of 88%. This means that about 88% of the perindopril erbumine had successfully been loaded or associated to chitosan nanoparticles.

3.8.1.5 FT-IR analysis

The FTIR analysis of chitosan, perindopril erbumine and perindopril erbumine-loaded chitosan nanoparticles was done to assign the functional groups and the chemical interaction between them. The FTIR spectra of free perindopril erbumine, chitosan, and perindopril erbumine-loaded chitosan nanoparticles are presented in Figure 3.43. The characteristic bands of pure chitosan were observed at around 3421 cm^{-1} for O–H stretching and N–H stretching vibrations, 1657 cm^{-1} for amide I, 1595 cm^{-1} for amide II, and 1077 cm^{-1} for C–O–C stretching vibration. The characteristic peak observed at 1379 cm^{-1} was due to –C–O stretching of the primary alcoholic group in chitosan (Figure 3.43).

The characteristic peaks of perindopril erbumine-loaded chitosan nanoparticles were noticed and they were almost similar. The difference is the shift of band at 3421 cm^{-1} for pure chitosan to 3438 cm^{-1} in the case of perindopril erbumine-loaded chitosan

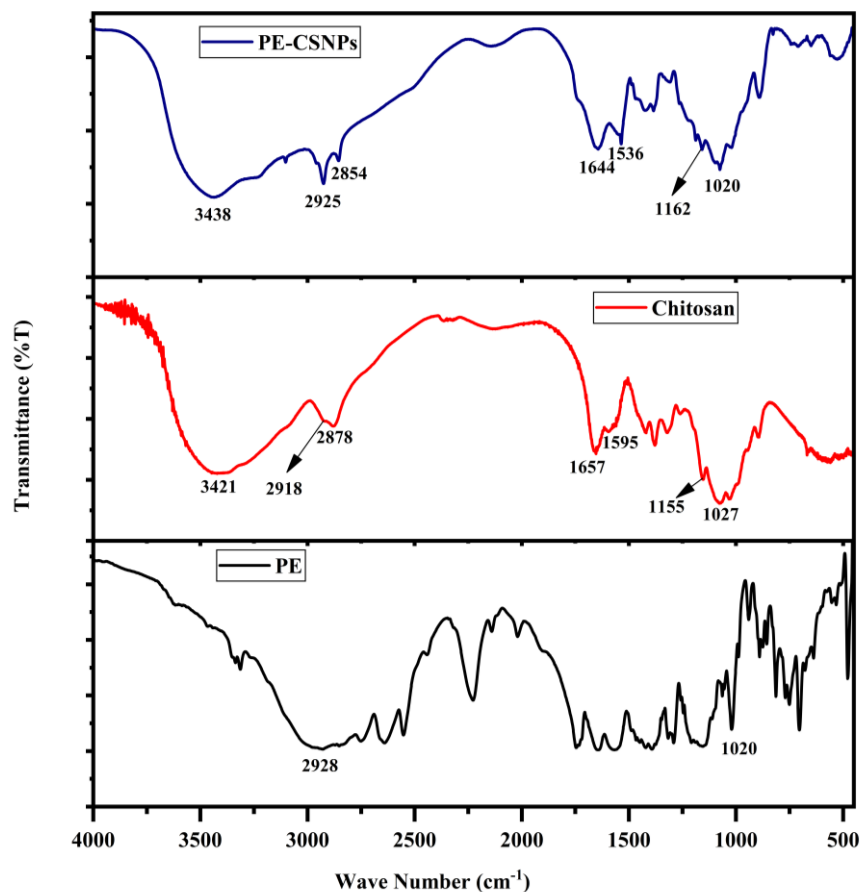


Figure 3.43: FTIR spectra of pure perindopril erbumine, chitosan and perindopril erbumine loaded chitosan nanoparticle.

Table 3.20: Tentative assessment of IR band of PE-loaded chitosan nanoparticles

Wavelength (cm ⁻¹)	Mode	Tentative band
3438	Symmetric stretching	- NH and - OH, intermolecular hydrogen bonding
1644	Symmetric stretching	-C=O (amide I)
1536	Bending vibration	-NH ₂ (amide II)
1074	Stretching vibration	-C-O
889	Anti-symmetric stretching	Structure of saccharide
1020	stretching vibration	C-N in PE
2928	stretching vibration	C-H in NH-CH-propyl in PE
1162	symmetric stretching vibration	C-N-C present in PE

nanoparticles as shown [Figure 3.43](#) which indicates that the hydrogen bonding is enhanced. The intensities of CONH₂ band at 1657 cm⁻¹ and NH₂ band at 1595 cm⁻¹, which was observed clearly in pure chitosan decreased, and two new absorption bands at 1644 and 1536 cm⁻¹ appear, which shows that the ammonium groups are crosslinked with tripolyphosphate molecules. Thus, it is postulated that polyphosphoric groups of sodium polyphosphate interact with the ammonium groups of chitosan, which serves to enhance both the inter- and intramolecular interaction in chitosan nanoparticles.

The FTIR spectra of PE ([Figure 3.43](#)) show many intense, sharp absorption bands due to different functional groups present in molecules such as primary amine, secondary amine, ester, carboxylic acid, and methyl groups. The band at 1020 cm⁻¹ in PE-CSNPs is due to C–N stretching of PE. The band at 2928 cm⁻¹ in PE indicates CH in NH–CH–propyl which was shifted to 2925 cm⁻¹ in PE-CSNPs due to the loading procedure. The band that appeared at 1162 cm⁻¹ in PE-CSNPs is due to the symmetric stretching vibration of C–N–C present in PE. Finally, in PE-CSNPs, some peaks were slightly shifted to higher or lower wave number region when compared to pure chitosan; such as, 2918 to 2925 cm⁻¹, 2878 to 2854 cm⁻¹, 1155 to 1162 cm⁻¹, 1027 to 1020 cm⁻¹. These can be explained due to the electrostatic interaction between adsorbed PE and nanoparticles indicating that PE was loaded to chitosan nanoparticles by adsorption onto the surface.

3.8.1.6 XRD analysis

Powder X-ray diffraction (XRD) patterns of the pure perindopril erbumine, chitosan and perindopril erbumine-loaded chitosan nanoparticles are recorded between 5 and 70° of the 2θ diffraction angle and presented in [Figure 3.44](#). The XRD pattern of pure chitosan contains two peaks at $2\theta = 10.224$ and 20.357° corresponding to the (020) and (110) planes, respectively.

The crystallinity index as calculated before was 74.12 with refer to (020) plane indicates the semi-crystalline structure of chitosan. In the present work, for the perindopril erbumine loaded chitosan nanoparticles, these peaks were relatively weaker than unmodified chitosan which indicates the amorphous nature of nanoparticles. This result is because the chitosan nanoparticles are converted to an amorphous form after crosslinking with tripolyphosphate and PE loading.

The diffraction pattern of pure PE (Figure 3.44) shows many intense sharp peaks in the fingerprint region. The characteristic peaks of pure perindopril erbumine shown in Figure 3.44 were absent from X-ray diffraction pattern of the product (PE loaded chitosan nanoparticles) though the Figure represents some small diffraction peaks for PE $2\theta = 11.51$, 16.55, 18.41, 24.37 when compared to free PE as shown in Figure 3.44. These results suggests that the perindopril erbumine was loaded to the chitosan nanoparticles and the modification procedure destroyed the crystal structure of perindopril erbumine.

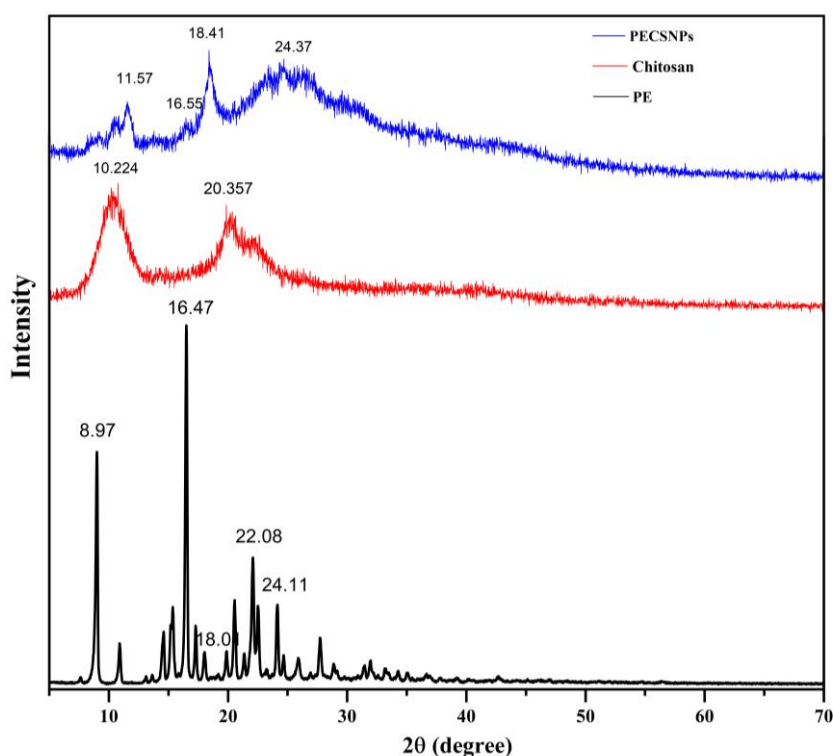


Figure 3.44: Powder XRD pattern of free perindopril erbumine, pure chitosan, and perindopril erbumine-loaded chitosan nanoparticles

3.8.2 Biomedical Application of Perindopril Erbumine Loaded Chitosan Nanoparticles (PR-CSNPs)

Biomedical application of PE-CSNPs was studied by investigating the ability of these delivery systems to release the associated perindopril erbumine over time. For this purpose, the in vitro release studies of the perindopril erbumine from loaded chitosan-TPP nanoparticles were performed

3.8.2.1 In vitro release study of perindopril erbumine (PE) from the nanoparticles

The in vitro release of perindopril erbumine from the nanoparticles was measured over a 7-hour period in PBS at a pH of 7.4. The release profile of PE from PE-CSNPs is shown in Figure 3.45. It was apparent by looking at the trend in the release profiles that perindopril released from the nanoparticles agreed with the postulated initial burst followed by the slower release phase. Thus, the release mechanism of PE from PE-CSNPs can be described as similar to the release mechanism of the previously discussed drug-loaded chitosan nanoparticles as in all cases the drugs were not encapsulated but adsorbed on the nanoparticles due to their small size. Thus, the PE release from PE-CSNPs involves diffusion, polymer degradation, or erosion. The initial burst was a result of the drug diffusion of some adsorbed drugs from the surface to the surrounding media. For the PE-CSNPs, about 32% of PE was released during the first ½ h. After this initial rapid release, the release rate of PE from nanoparticles fell and the release amount reached the maximum at 7 hours through a slower and sustained release. The cumulative release of perindopril from nanoparticles was about 83%. The release results from this study suggest that the nanoparticles could be effective in sustaining the perindopril erbumine release.

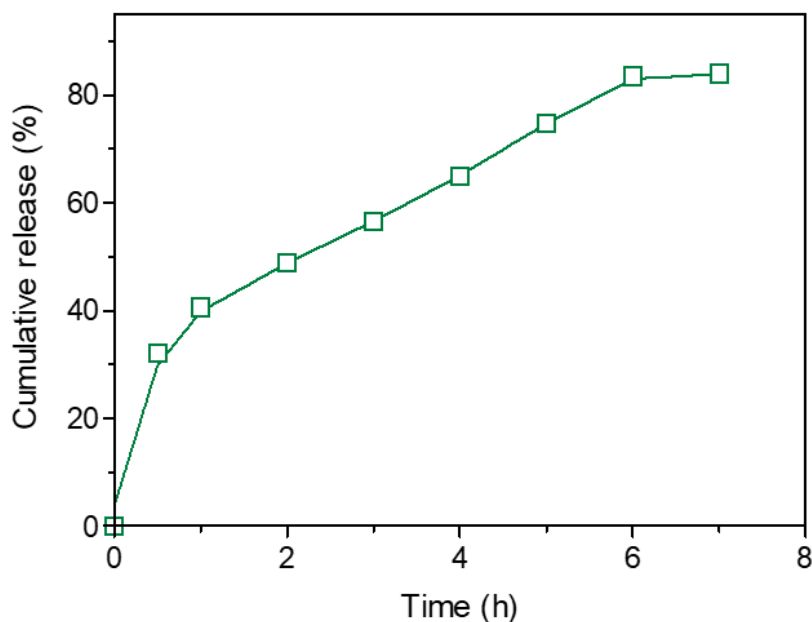


Figure 3.45: Perindopril erbumine release profile from chitosan nanoparticles in phosphate buffered saline of pH=7.4.

3.8.2.2 Release kinetics of perindopril erbumine (PE) from the nanoparticles

In order to study the release behavior of perindopril erbumine from chitosan nanoparticles, the data of the cumulative release of the perindopril erbumine from the nanoparticles were fitted to different kinetic models which are zero order model (3.1), first order model (3.3), Higuchi model (3.5) and Hixson-crowell model (3.6). Figure 3.46 shows plot of the fitting of perindopril erbumine released from chitosan nanoparticles at pH 7.4. The correlation coefficient (R^2) values of different kinetic models obtained by fitting the data of perindopril erbumine release from the chitosan nanoparticles in PBS solutions at pH 7.4 are represented in Table 3.21.

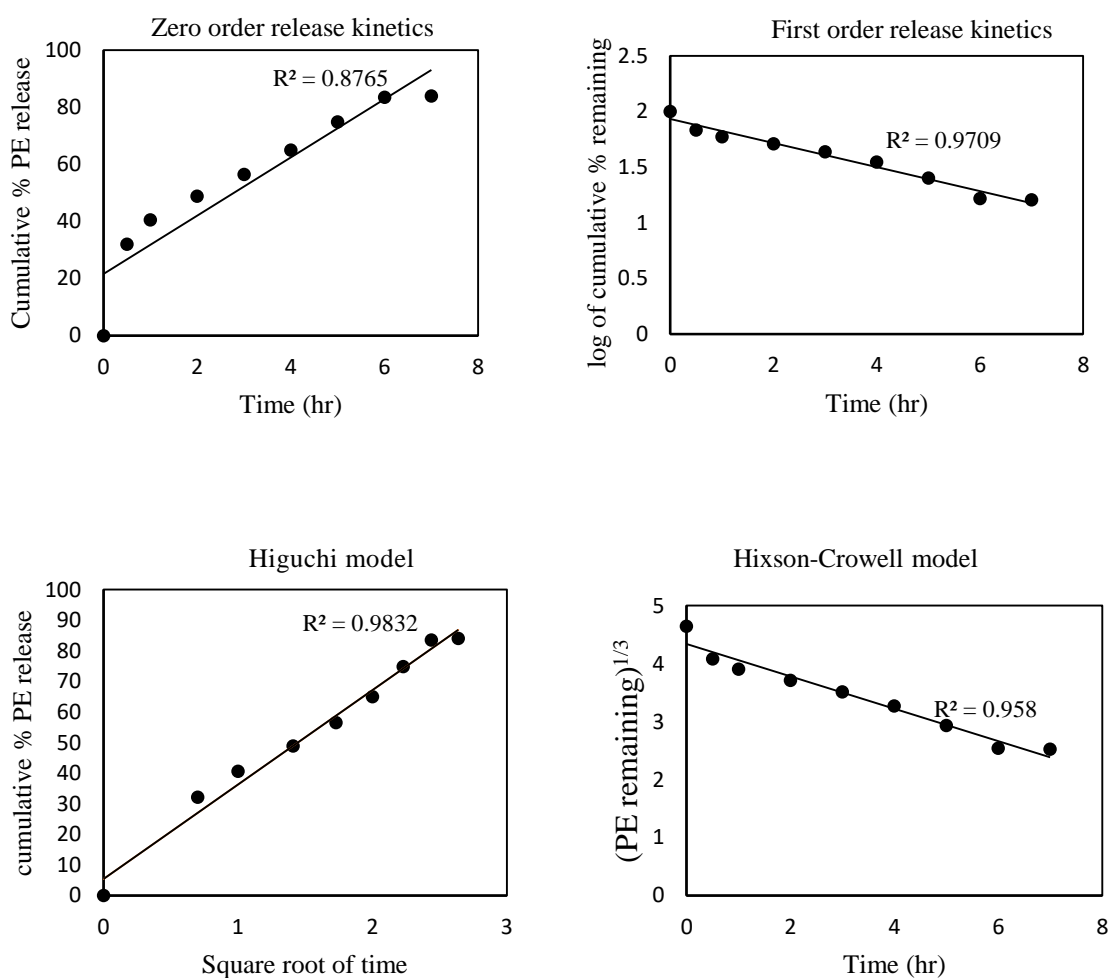


Figure 3.46: Release kinetics study by fitting the data of perindopril erbumine release from chitosan nanoparticles into phosphate-buffered saline at pH 7.4 using four different kinetics model.

Table 3.21: The correlation coefficients (R^2) obtained by fitting the perindopril erbumine release data from the perindopril erbumine loaded chitosan nanoparticles (PE-CSNPs) in PBS solutions at pH 7.4

Samples	Saturation release (%)	R^2			
		Zero order	First order	Higuchi	Hixson-Crowell
PE-CSNPs	83	0.8765	0.9709	0.9832	0.958

Using these four kinetic models in fitting the release kinetic data, it was found that the Higuchi kinetic model is more satisfactory to describe the release kinetic process of perindopril erbumine from the chitosan nanoparticles compared to other models used in this study with a best fit value for the correlation coefficient. So, the results indicated that the release of the drug from the nanoparticles followed the Higuchi square root kinetic model with the highest value of correlation coefficient ($R^2 = 0.958$) which implies that release of drug from matrix as a square root of time dependent process and diffusion controlled. Hence, drug release profile of perindopril erbumine follows diffusion mechanism.

3.9 Proposed Model for Controlled Release Drug Delivery System in This Study

Using the conditions described above, we have successfully prepared a novel drug delivery system of CSNPs of particle size less than 1 nm from extracted shrimp chitosan. The SEM and TEM characterization techniques indicates about the possible adsorption of drugs on its surface. We know that encapsulation of drugs into polymer matrix is a widely used method of controlling drug delivery as it slows diffusion of drugs. Though the very low size of the nanoparticles which has not found in the previous studies and does not allow the encapsulation of drugs in the CSNPs matrix, but drugs were adsorbed on the surface of CSNPs with high association efficiency. Besides, we obtained an extended release profile for all the drugs that were loaded on this CSNPs system without encapsulation and the drug release from all the drug loaded CSNPs are time dependent and diffusion controlled as it follows Higuchi Model. Hence, finally a different mechanism for the controlled release of drugs from CSNPs without encapsulation from the advantage of the adsorption of drugs on CSNPs has been proposed as represented by Figure 3.47.

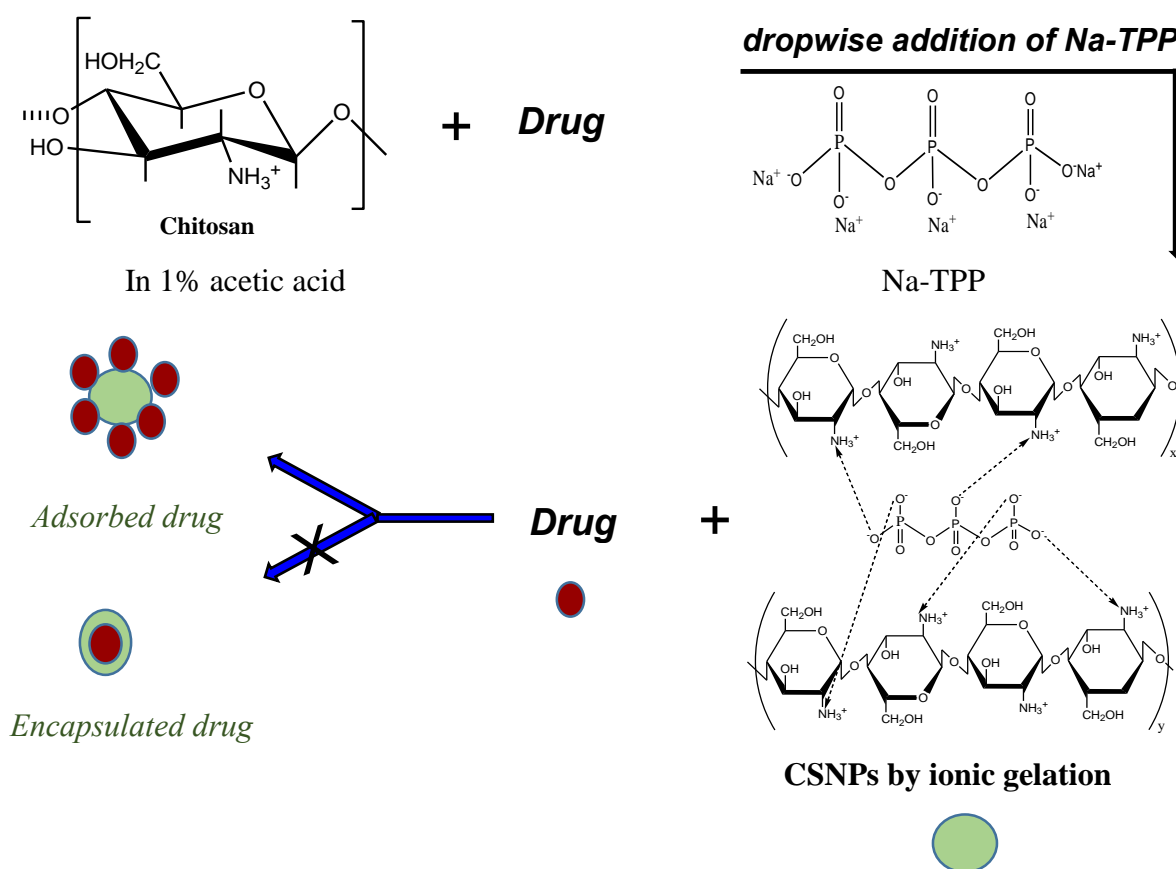


Figure 3.47: Proposed model for drug delivery system

Conclusion

The present research focused on the extraction of chitosan from wasted shell of shrimp and the study of their potential in biomedical application by preparing chitosan nanoparticles that are loaded with different types of drugs such as antibiotic and antihypertensive drugs. Using the traditional method for chitosan extraction which involves deacetylation of chitin obtained from deproteination and demineralization of shrimp shell, a whitish flakes of chitosan was obtained with the average yield of 8.18 %. The various characterization techniques were carried out to describe the quality of extracted chitosan. The percentage of solubility of extracted chitosan was about 83% in 1% acetic acid. This high solubility indicates the high degree of deacetylation of chitosan. The molecular weight was found to be 2.3×10^5 Da which grouped the extracted chitosan as low molecular weight chitosan for appropriately applying in biomedical field. The low C/N ratio of extracted chitosan in elemental analysis and the Fourier transform infrared spectroscopic analysis of chitosan proves the deacetylation of chitin to produce chitosan. The degree of deacetylation of extracted chitosan calculated by FTIR method was found to be 70%. The XRD pattern confirmed the semicrystalline nature of extracted chitosan. Thus, using the preparation procedure described in present study, chitosan samples with suitable physicochemical characteristics for pharmaceutical applications such as, low molecular weight, high solubility and degree of deacetylation value were successfully obtained and can be used in drug delivery.

Thus, a new nano carrier for drugs using this chitosan was prepared by using simple ionic gelation method by varying the preparation conditions like chitosan and TPP concentration. The particle size and morphological characterization done by SEM and TEM analysis showed the effect of chitosan and TPP concentration on the formation of nanoparticles. In accordance with the result obtained, 2% chitosan with 0.25% TPP initiated ionic gelation gives the chitosan nanoparticles with lowest particle size of 0.1 to 1 nm range according to TEM and was considered as the optimized condition for nanoparticle formation. The broad diffraction peaks in the XRD pattern of chitosan nanoparticles indicates the decrease in crystallinity from pure chitosan which results in an improvement of drug adsorption. Finally, four different drugs, ciprofloxacin, erythromycin, metronidazole and perindopril erbumine were successfully loaded to the chitosan nanoparticles in this optimized condition. The drugs were loaded with high association efficiency of 93%, 92%, 90% and 88%

respectively. The little shifting of some characteristic peaks in FTIR spectra of all the drug loaded nanoparticles from pure chitosan indicates about the electrostatic interactions between drugs and chitosan nanoparticles. The morphology of all the drug loaded nanoparticles observed by SEM suggest that the particles were spherical in shape with inhomogeneous surface. The TEM analysis showed that the average diameters were increased in drug loaded nanoparticles as compared to the blank one (0.22nm), such as, for the CP-CSNPs, MTZ-CSNPs and PE-CSNPs, the diameters were 0.37nm, 0.49nm and 0.59nm respectively. This indicates the drug adsorption on the surface of the nanoparticles rather than encapsulation. The in vitro release profile study of CP-CSNPs, ER-CSNPs, MTZ-CSNPs and PE-CSNPs showed 73%, 78%, 84% and 84% release of drugs in a sustained release pattern within 24, 8, 25 and 7h respectively and the release profile is governed by Higuchi model for each cases that implies that the release of drug is diffusion controlled. Though adsorption of drugs on nanoparticles has been observed rather than encapsulation due to the smallest particle size of the nanoparticles, the electrostatic interaction between drugs and nanoparticles became the governing factor in sustaining the drug release effectively. Finally we obtained the extended drug release profile for the four different drugs without encapsulation. Moreover, the antibacterial activity of antibiotic drug loaded chitosan nanoparticles such as CP-CSNPs and ER-CSNPs observed by MIC and MBC determinations shows similar results in case of loaded drug and corresponding free drug. This result implies that loading of drugs on chitosan nanoparticles shows no negative impact on the antibacterial activity. Furthermore, they may show better effectiveness to inhibit bacterial growth in vivo cases due to sustained release property according to several research. Finally it can be concluded that the prepared nanoparticles have promising potentiality in drug delivery.

References

1. Poosapati, A.; Vадnala, S.; Negrete, K.; Lan, Y.; Hutchison, J.; Zupan, M. and Madan, D. Rechargeable Zinc-Electrolytic Manganese Dioxide (EMD) Battery with a Flexible Chitosan-Alkaline Electrolyte. *ACS Appl. Energy Mater.* 2021, **4**(4), 4248–4258.
2. Freitas, R. A. *Nanomedicine*, Volume IIA: Biocompatibility, Landes Bioscience, Georgetown, 2003
3. Dash, M.; Chellini, F.; Ottenbrite, R. M. and Chiellin, E. Chitosan- a Versatile Semisynthetic Polymer in Biomedical Applications. *Prog. Polym. Sci.* 2011, **36**(8), 981- 1014.
4. Kean, T. and Thanou, M. Biodegradation, Biodistribution and Toxicity of Chitosan. *Adv. Drug Deliv. Rev.* 2009, **62**(1), 3-11.
5. Clark, L.T. Safety Profile of Perindopril. *Am. J. Cardiol.* 2001, **88**, 36–40.
6. Agnihotri, A.; Mallikarjuna, N. and Aminabhavi, M. Recent Advances on Chitosan-Based Micro- and Nanoparticles in Drug Delivery. *J. control. Release.* 2004, **100**(1), 5-28.
7. Norouzi, Z.; Abdouss, M.; Shoushtari, A. and Haji, A. Electrospinning of β -Cyclodextrin Grafted Chitosan Nanofibrous Membrane for Dye Removal. *5th Texteh International Conference*, 2012, 275-284.
8. Steinbüchel, A.; De, B. S. and Vandamme, E. J. Polysaccharides II, Polysaccharides from Eukaryotes. *Biopolymers*, **Vol. 6**, Wiley-VCH, Weinheim, Germany, 2002.
9. Khoushab, F. and Yamabhai, M. Chitin Research Revisited. *Mar. Drugs.* 2010, **8**, 1988–2012.
10. Meena, K. P.; Dangi, J. S.; Samal, P. K. and Kumar, M. Nanoparticles technology and recent advances in novel drug delivery systems. *Int. J. Res. Drug Deliv.* 2011, **1**(1), 1-5.
11. Desai, M. P.; Labhasetwar, V.; Walter, E.; Levy, R. J. and Amidon, G. L. The Mechanism of Uptake of Biodegradable Microparticles in Caco-2 Cells is Size Dependent. *Pharm. Res.* 1997, **14**(11), 1568-1573.
12. Salehi, B; Calina, D.; Docea, A. O.; Koirala, N.; Aryal, S.; Lombardo, D.; Pasqua, L.; Taheri, Y.; Castillo, C. M. S.; Martorell, M. Curcumin's Nanomedicine Formulations for Therapeutic Application in Neurological Diseases. *J. Clin. Med.* 2020, **9**(2), 430.
13. Patra, J.; Das, G.; Fraceto, L.; Campos, E. Nano Based Drug Delivery Systems: Recent Developments and Future Prospects. *J. Nanobiotechnol.* 2018, **16**, 71.

14. Haba, Y.; Kojima, C.; Harada, A.; Ura, T.; Horinaka, H. and Kono, K. Preparation of Poly (ethylene glycol)-Modified Poly (amido amine) Dendrimers Encapsulating Gold Nanoparticles and Their Heat-generating Ability. *Langmuir*. 2007, **23**, 5243–5246.
15. Shi, X.; Sun, K. and Baker, J. Spontaneous Formation of Functionalized Dendrimer-Stabilized Gold Nanoparticles. *J. Phys. Chem. C*. 2008, **112**, 8251–8258.
16. López-León, T.; Carvalho, E. L.; Seijo, B.; Ortega-Vinuesa, J. L.; Bastos-González, D.; Ortega-Vinuesa, J. L. and Bastos-González, D. Physicochemical Characterization of Chitosan Nanoparticles Electrokinetic and Stability Behavior. *J. Colloid Interface. Sci.* 2005, **9**, 344–351.
17. Wintstanley, P.; Constable, S. and Walley, T. *Master medicine medical pharmacology*, Churchill Livingstone, 2007.
18. Bhowmik, D.; Gopinath, H.; Kumar, B.; Duraiavel, S. and Kumar, K. Control Release Drug Delivery Systems. *Pharma. Innov.* 2012, **1(10)**, 24-32.
19. Reynolds, T. D.; Gehrke, S. H.; Hussain, A. S. and Shenouda, L. S. Polymer Erosion and Drug Release Characterization of Hydroxypropyl Methylcellulose Matrices. *J. Pharm. Sci.* 1998, **87(9)**, 1115-1123.
20. Muzzarelli, R.; Jeuniaux, C. and Gooday, G.W. Chitin in Nature and Technology, *Proceedings of the Third International Conference on Chitin and Chitosan*, Plenum Press, New York, 1986.
21. Brine, C. J.; Sandford, P. A. and Zikakis, J. P. *Advances in Chitin and Chitosan*, Elsevier Science Publishers Ltd., London, 1992.
22. Omidian, H. and Park, K. Swelling Agents and Devices in Oral Drug Delivery. *J. Drug Deliv. Sci. Technol.* 2008, **18(2)**, 83-89.
23. Bairwa, N. K.; Sethiya N. K. and Mishra S. H. Protective Effect of Stem Bark of *Ceiba pentandra* linn. against Paracetamol-induced Hepatotoxicity in Rats. *Pharmacognosy Res.* 2010, **2(1)**, 26-30.
24. Calvo, P.; Remunan-Lopez, C.; Vila-Jato, J. L. and Alonso, M. J. Novel Hydrophilic Chitosan-Polyethylene Oxide Nanoparticles as Protein Carriers. *J. Appl. Polym. Sci.* 1997, **63(1)**, 125-132.
25. British Pharmacopia (BP), The stationary office, London, 2009, 493.
26. Latha, S; Selvamani, P.; Kumar, C. S.; Sharavanan, P.; Suganya, G.; Beniwal, V. S. and Rao P. R. Formulation Development and Evaluation of Metronidazole Magnetic Nanosuspension as a Magnetic-Targeted and Polymeric-Controlled Drug Delivery System. *J. Magnetism Magnetic Materials.* 2009, **321**, 1580-1585.

27. Patel, G.; Patel R. B. and Patel, H. R. Formulation and In-Vitro Evaluation of Microbially Triggered Colon Specific Drug Delivery Using Sesbania Gum. *e-J Sci Tech.* 2011, **6(2)**, 33-45.
28. Wong, J.; Patel, R. A. and Kowey, P. R. The Clinical Use of Angiotensin-Converting Enzyme Inhibitors. *Prog. Cardiovasc. Dis.* 2004, **47**, 116–130.
29. Almaaytah, A.; Qaoud, M.; Khalil Mohammed, G.; Abualhajjaa, A.; Knappe, D. and Hoffmann, R. Antimicrobial And Antibiofilm Activity of UP-5, an Ultrashort Antimicrobial Peptide Designed Using only Arginine and Biphenylalanine. *Pharmaceuticals.* 2018, **11(1)**, 3.
30. Baghdan, E.; Pinnapireddy, S. R.; Strehlow, B.; Engelhardt, K. H.; Schäfer, J.; and Bakowsky, U. Lipid Coated Chitosan-DNA Nanoparticles for Enhanced Gene Delivery. *Int. J. Pharmaceut.* 2018, **535**, 473–479.
31. Kiilll, C. P.; Barud, H. D. S.; Santagneli, S. H.; Ribeiro, S. J. L.; Silva, A. M.; Tercjak, A. Synthesis and Factorial Design Applied to a Novel Chitosan/Sodium Polyphosphate Nanoparticles via Ionotropic Gelation as an RGD Delivery System. *Carbohydr. Polym.* 2017, **157**, 1695–1702.
32. Rassu, G.; Porcu, E. P.; Fancello, S.; Obinu, A.; Senes, N.; and Galleri, G. Intranasal Delivery of Genistein-Loaded Nanoparticles as a Potential Preventive System against Neurodegenerative Disorders. *Pharmaceutics.* 2019, **11**, 8.
33. Vitali, A.; Stringaro, A.; Colone, M.; Muntiu, A. and Angiolella, L. Antifungal Carvacrol Loaded Chitosan Nanoparticles. *Antibiotics.* 2022, **11(1)**, 11.
34. Yadav, P. and Yadav, A. B. Preparation and Characterization of BSA as a Model Protein Loaded Chitosan Nanoparticles for the Development of Protein-/Peptide-Based Drug Delivery System. *Futur J. pharm. Sci.* 2021, **7**, 200.
35. Sohail, A.; Khan, R.U.; Khan, M.; Khokhar, M.; Ullah, S.; Ali, A.; Bilal, H.; Khattak, S.; Khan, M. and Ahmed, B. Comparative Efficacy of Amphotericin B-Loaded Chitosan Nanoparticles and Free Amphotericin B Drug Against Leishmania Tropica. *Bull. Natl. Res. Cent.* 2021, **45**, 187.
36. Ekhlas, A. El., Manal, K. El.; Ghada, M.T. and Hassan, M.I. Preparation of Biocompatible Chitosan Nanoparticles Loaded by Tetracycline, Gentamycin and Ciprofloxacin as Novel Drug Delivery System for Improvement the Antibacterial Properties of Cellulose Based Fabrics. *Int. J. Biol. Macromol.* 2020, **161**, 1247-1260.
37. Ciro, Y.; Rojas, J.; Oñate-Garzon, J. and Salamanca C. H. Synthesis, Characterisation and Biological Evaluation of Ampicillin–Chitosan–Polyanion Nanoparticles Produced by Ionic Gelation and Polyelectrolyte Complexation Assisted by High-Intensity Sonication. *Polymers.* 2019, **11(11)**, 1758.

38. Alqahtani, F. Y.; Aleanizy, F. S.; Tahir, E. E.; Alquadeib, B. T.; Alsarra, I. A.; Alanazi, J. S. and Abdelhady, H. G. Preparation, characterization, and antibacterial activity of diclofenac-loaded chitosan nanoparticles. *Saudi Pharm. J.* 2019, **27**, 82–87.
39. Duceac, L. D.; Calin, G.; Eva, L.; Marcu, C.; Goroftei, E. R. B.; Dabija, M. G.; Mitrea, G.; Luca, A. C.; Hanganu, E.; Gutu, C.; Stafie, L.; Banu, E. A.; Grierosu, C. and Iordache, A. C. Third-Generation Cephalosporin-Loaded Chitosan Used to Limit Microorganisms Resistance. *Materials.* 2020, **13**, 4792.
40. Bin-Jumah, M.; Gilani, S. J.; Jahangir, M. A. , Zafar, A.; Alshehri, S. , Yasir, M.; Kala, C.; Taleuzzaman, M. and Imam, S. S. Clarithromycin-Loaded Ocular Chitosan Nanoparticle Formulation, Optimization, Characterization, Ocular Irritation, and Antimicrobial Activity. *Int. J. Nanomedicine.* 2020, **15**, 7861-7875.
41. Ashvini, H. M.; Balla, A. and Mutta, S. K. Clarithromycin-loaded Chitosan Nanoparticles Preparation, Characterisation and Antibacterial Activity on Streptococcus pneumonia. *Indian J. Pharm. Sci.* 2019, **81(2)**, 302-308.
42. Abdel-Moneim, A.; El-Shahawy, A.; Yousef, A. I.; El-Twab, S.M.A.; Elden Z.E. and Taha, M. Novel Polydatin-Loaded Chitosan Nanoparticles for Safe and Efficient Type 2 Diabetes Therapy In Silico, In Vitro and In Vivo Approaches. *Int. J. Biol. Macromol.* 2020, **154**, 1496-1504.
43. Patel, G. and Yadav, B.K.N. Study of 5-Fluorouracil Loaded Chitosan Nanoparticles for Treatment of Skin Cancer. *Recent Pat. Nanotechnol.* 2020, **14(3)**, 210-224.
44. Razei, A.; Cheraghali, A. M.; Saadati, M.; Ramandi, M. F.; Panahi, Y.; Hajizade, A.; Siadat, S. D. and Behrouzi A. Gentamicin-Loaded Chitosan Nanoparticles Improve Its Therapeutic Effects on Brucella-Infected J774A.1 Murine Cells. *Galen Med. J.* 2019, **8**, e1296.
45. Kirimlioğlu, G. Y. and Oztürk, A. A. Levocetirizine Dihydrochloride-Loaded Chitosan Nanoparticles Formulation and In Vitro Evaluation. *Turk. J. Pharm. Sci.* 2020, **17(1)**, 27-35.
46. El-Assal, M. I. and El Menofy, N. G. Chitosan Nanoparticles as Drug Delivery System for Cephalexin and its Antimicrobial Activity against Multiidrug Resistant Bacteria. *Int. J. Pharm. Pharm. Sci.* 2019, **11(7)**, 14-27.
47. Rhazi, M.; Desbrières, J; Tolaimate, A.; Alagui, A.; Vincendon, M. and Vottéro, P. Investigation of Different Natural Sources of Chitin Influence of the Source and the Deacetylation Process on the Physicochemical Characteristics of Chitosan. *Polym. Int.* 2000, **49**, 337-344.

48. Puvvada, Y. S.; Vankayalapati, S. and Sukhavasi, S. Extraction of Chitin from Chitosan Exoskeleton of Shrimp for Application in the Pharmaceutical Industry. *Int. Curr. Pharm. J.* 2012, **1(9)**, 258-263.
49. Brugnerotto J.; Lizardi J.; Goyoolea F.; Arguelles-Monal W.; Desbrieres J. and Rinaudo M. An Infrared Investigation in Relation with Chitin and Chitosan Characterization. *Polymer.* 2001, **42**, 3569–3580.
50. Zhang, Y.; Xue, C.; Li, Z.; Zhang, Y. and Fu, X. Preparation of Half-Deacetylated Chitosan by Forced Penetration and its Properties. *Carbohydr. Polym.* 2006, **65**, 229-234.
51. Garg, U.; Chauhan, S.; Nagaich, U. and Jain, N. Current Advances in Chitosan Nanoparticles Based Drug Delivery and Targeting. *Adv. Pharm. Bull.* 2019, **9(2)**, 195-204.
52. Zhang, E.; Xing, R.; Liu, S.; Qin, Y.; Li, K. and Li, P. Advances in Chitosan-Based Nanoparticles for Oncotherapy. *Carbohydr. Polym.* 2019, **222**, 115004.
53. Ansari, R.; Sadati, S. M.; Mozafari, N.; Ashrafi, H. and Azadi, A. Carbohydrate Polymer-Based Nanoparticle Application in Drug Delivery for CNS-Related Disorders. *Eur. Polym. J.* 2020, **128**, 109607.
54. Divya, K. and Jisha, M. S. Chitosan Nanoparticles Preparation and Applications. *Environ. Chem. Lett.* 2018, **16**, 101–112.
55. Al Ali, S. H. H.; Al-Qubaisi, M; Hussein, M. Z.; Ismail, M.; Zainal, Z. and Hakim, M. N. Controlled Release and Angiotensin-Converting Enzyme Inhibition Properties of an Antihypertensive Drug Based on a Perindopril Erbumine-Layered Double Hydroxide Nanocomposite. *Int. J. Nanomed.* 2012, **7**, 2129.
56. Arias, J.; Lopez-Viota, M.; Gallardo, V. and Ruiz, M. Chitosan Nanoparticles as a New Delivery System for the Chemotherapy Agent Tegafur. *Drug Deliv. Ind. Pharm.* 2010, **36(6)**, 744-750.
57. Du, Y.; Ying, X.; Wang, L.; Zhai, Y.; Yuan, H.; Yu, R. and Hu, F. Sustained Release of ATP Encapsulated in Chitosan Oligosaccharide Nanoparticles. *Int. J. Pharm.* 2010, **392(1-2)**, 164-169.
58. Goldstein, J.; Newbury, D. E.; Joy D. C.; Lyman, C. E.; Echlin, P.; Lifshin, E. and Sawyer, L. *Scanning Electron Microscopy and X-ray Microanalysis*, Third edition, Plenum Press, New York, 2003, 689.
59. Mirzadeh, H., Yaghoobi, N., Amanpour, S., Ahmadi, H., Mohagheghi, A. and Hormo, F. Preparation of Chitosan Derived from Shrimp's Shell of Persian Gulf as a Blood Hemostasis Agent. *Iran. Polym. J.* 2002, **11(1)**, 63-68.

60. Nouri, M.; Khodaiyan, F.; Razavi, S. H. and Mousavi, M. Improvement of Chitosan Production from Persian Gulf Shrimp Waste by Response Surface Technology. *Food Hydrocoll.* 2015, **3**, 1-9.
61. Kurita, K. Chitin and Chitosan: Functional Biopolymers from Marine Crustaceans. *Mar. Biotechnol.* 2006, **8**, 203-226.
62. Brine, C. J. and Austin, P. R. Chitin Variability with Species and Method of Preparation. *Comp. Biochem. Physiol.* 1981, **69B**, 283-286.
63. Mohammed, M. H.; Williams, P. A. and Tverezovskaya, O. Extraction of Chitin from Prawn Shells and Conversion to Low Molecular Mass Chitosan. *Food Hydrocoll.* 2013, **31**, 166-171.
64. Islam, M. M.; Masum, S. M.; Molla, M. A. I.; Rahman, M. M.; Shaikh, A. A. and Roy, S. K. Preparation of Chitosan from Shrimp Shell and Investigation of Its Properties. *Int. J. Basic Appl. Sci.* 2011, **11(1)**, 116-130.
65. Patria, A. Production and Characterization of Chitosan from Shrimp Shells Waste. *AAFL Bioflux.* 2013, **6(4)**, 339-344.
66. Younes, I.; Hajji, S.; Frachet, V.; Rinaudo, M.; Jellouli, K. and Nasri, M. Chitin Extraction from Shrimp Shell using Enzymatic Treatment. Antitumor, Antioxidant and Antimicrobial Activities of Chitosan. *Int. J. Biol. Macromol.* 2014, **69(0)**, 489–498.
67. Antoniou, J.; Liu, F.; Majeed, H.; Qi, J.; Yokoyama, W. and Zhong, F. Physicochemical and morphological properties of size-controlled chitosan–tripolyphosphate nanoparticles. *Colloids and Surfaces A: Physicochem. Eng. Aspects.* 2015, **465**, 137–146.
68. Pavinatto, A.; Pavinatto, F. J.; Deleuzuk, J.; Nobre, T. M.; Souza, A. L.; Campana-Filho, S. P. and Oliveira, O. N. Low molecular-weight chitosans are stronger biomembrane model perturbants. *Colloids and Surfaces B: Biointerfaces.* 2013, **104(1)**, 48-53.
69. Brzezinski, R.; Lehoux, J. G. and Kelly A. Clinical Studies on the Innocuousness of Chitosan and its Short-Chain Derivative Generated by Enzymatic Hydrolysis. *Asia Pac. J. Clin. Nutr.* 2004, **13**, S96.
70. Minh, N. C.; Hoa, N. V. and Trung, T. S. Preparation, Properties and Application of Low-Molecular-Weight Chitosan. *Handbook of Chitin and Chitosan.* 2020, **1**, 453-471.
71. Kumari, S.; Annamareddy, S. H. K.; Abanti, S. and Rath, P. R. Physicochemical Properties and Characterization of Chitosan Synthesized from Fish Scales, Crab and Shrimp Shells. *Int. J. Biol. Macromol.* 2017, **104**, 1697-1705.

72. Yen, M.-T.; Yang, J-H and Mau, J.-L. Physicochemical Characterization of Chitin and Chitosan from Crab Shells. *Carbohydr. Polym.* 2009, **75(1)**, 15-21.
73. No, H. K. and Meyers, S. P. Preparation and Characterization of Chitin and Chitosan-A Review. *J. Aquatic Food Prod. Technol.* 1995, **4(2)**, 27-52.
74. Al-Sagheer, F. A.; Al-Sughayer, M. A.; Muslim, S. and Elsabee, M. Z. Extraction and Characterization of Chitin and Chitosan from Marine Sources in Arabian Gulf. *Carbohydr. Polym.* 2009, **77**, 410-419.
75. Bangyekan, C.; Aht-Ong, D. and Srikulkit K. Preparation and Properties Evaluation of Chitosan Coated Cassava Starch Film. *Carbohydr. Polym.* 2006, **63(1)**, 61-71.
76. Prashanth, K. V. H.; Kittur, F. S. and Tharanathan, R. N. Solid State Structure of Chitosan Prepared under Different N-Deacetylating Conditions. *Carbohydr. Polym.* 2002, **50**, 27–33.
77. Zhang, Y.; Xue, C.; Xue, Y.; Gao, R. and Zhang, X. Determination of the Degree of Deacetylation of Chitin and Chitosan by X-Ray Powder Diffraction. *Carbohydr. Res.* 2005, **340(11)**, 1914-1917.
78. Debnath, S.; Kumar, R. S. and Babu, M. N. Ionotropic Gelation – A Novel Method to Prepare Chitosan Nanoparticles. *Res. J. Pharm. Technol.* 2011, **4(4)**, 492-495.
79. Ruchika and Himanshi. Formulation and Evaluation of Metronidazole Loaded Chitosan Nanoparticles. *Int. J. Sci. Res. Methodol.* 2016, **4(4)**, 1-17.
80. Othman, N.; Masarudin, M. J.; Kuen, C. Y.; Dasuan, N. A.; Abdullah, L. C.; Md. Jamil, S. N. A. Synthesis and Optimization of Chitosan Nanoparticles Loaded with L-Ascorbic Acid and Thymoquinone. *Nanomaterials.* 2018, **8**, 920.
81. Oh, J. W.; Chun, S. C. and Murugesan, C. Preparation and In Vitro Characterization of Chitosan Nanoparticles and Their Broad-Spectrum Antifungal Action Compared to Antibacterial Activities against Phytopathogens of Tomato. *Agronomy.* 2019, **9(1)**, 21.
82. Anusha, J. R.; Fleming, A. T.; Valan, A. M.; Chul, K. B.; Al-Dhabi, N. A.; Yu ,K. H. and Justin, R. C. Mechanochemical Synthesis of Chitosan Submicron Particles from the Gladius of *Todarodes Pacificus*. *J. Adv. Res.* 2016, **7**, 863–871.
83. Hejjaji, E. M. A.; Smith, A. M. and Morris, G. A. Designing Chitosan-Tripolyphosphate Microparticles with Desired Size for Specific Pharmaceutical or Forensic Applications. *Int. J. Biol. Macromol.* 2017, **95**, 564–573.
84. Nagarwal, R. C.; Singh P. N.; Kant, S.; Maiti, P. and Pandit , J. K. Chitosan Nanoparticles of 5-Fluorouracil for Ophthalmic Delivery: Characterization, *in-Vitro* and *in-Vivo* Study. *Chem. Pharm. Bull.* 2011, **59**, 272-278.

85. Qi, L.; Xu, Z.; Jiang, X.; Hu, C. and Zou, X. Preparation and Antibacterial Activity of Chitosan Nanoparticles. *Carbohydr. Res.* 2004, **339(16)**, 2693-2700.
86. Barbosa, H. F. G.; Francisco, D. S.; Ferreira, A. P. G. and Cavaleiro, É. T. G. A New Look Towards the Thermal Decomposition of Chitins and Chitosans with Different Degrees of Deacetylation by Coupled TG-FTIR. *Carbohydr. Polym.* 2019, **225**, 115232.
87. Pakulska, M. M.; Donaghue, I. E.; Obermeyer, J. M.; Tuladhar, A.; McLaughlin, C. K.; Shendruk, T. N. and Shoichet, M. S. Encapsulation-free Controlled Release: Electrostatic Adsorption Eliminates the Need for Protein Encapsulation in PLGA Nanoparticles. *Sci. Adv.* 2016, **2(5)**, e1600519.
88. Dash, S.; Murthy, P. N.; Nath, L. and Chowdhury, P. Kinetic Modeling on Drug Release from Controlled Drug Delivery Systems. *Acta. Pol. Pharm.* 2010, **67**, 217-223.
89. Subal, C. B. Modelling of Drug release: The Higuchi equation and its application. *Pharmabiz. com.* 2006.
90. Singhvi, G. and Singh, M. In-Vitro Drug Release Characterization Models. *Int. J. Pharm. Stud. Res.* 2011, 77-84.
91. Jeong, Y. I.; Na, H. S.; Seo, D. H.; Kim, D. G.; Lee, H. C. and Jang, M.K. Ciprofloxacin-Encapsulated Poly(Dllactide-Co-Glycolide) Nanoparticles and Its Antibacterial Activity. *Int. J. Pharm.* 2008, **352(1-2)**, 317- 23.
92. Sobhani, Z.; Samani, S. M.; Montaseri, H. and Khezri, E. Nanoparticles of Chitosan Loaded Ciprofloxacin: Fabrication and Antimicrobial Activity. *Adv Pharm Bull.* 2017, **7(3)**, 427-432.